BIOMIMETIC SYNTHESIS OF POLY(PROPYLENE-FUMARATE)-CALCIUM PHOSPHATE COMPOSITES FOR TISSUE ENGINEERING

By

Dorna Hakimi Mehr

B.Sc., Iran University of Science and Technology, 1999
M.A.Sc., University of British Columbia, 2001

THESIS SUBMITTED IN PARTIAL FULFILMENT OF
THE REQUIREMENTS FOR THE DEGREE OF

DOCTOR OF PHILOSOPHY

In

THE FACULTY OF GRADUATE STUDIES

(Materials Engineering)

THE UNIVERSITY OF BRITISH COLUMBIA

April 2006

Abstract

A novel in-situ co-precipitation process for the synthesis of poly(propylene-fumarate)-calcium phosphate composites was developed. In this process the calcium phosphate phase nucleates and grows in the presence of poly(propylene-fumarate) (PPF), in a novel two-solvent system including tetrahydrofuran (THF) and water. It was found that the presence of the organic solvent (THF) does not affect the phase evolution of the calcium phosphate. Both in the presence and absence of THF crystalline dicalcium phosphate dihydrate (DCPD, brushite) and poorly crystalline hydroxyapatite (HAp) form, and transform to crystalline HAp after 24 hours of synthesis time. Contrary to the organic solvent, PPF has a significant influence on the calcium phosphate phase that forms in its presence. It is found that PPF provides a template for the formation of the calcium phosphate phase through a coordination bond between the calcium ion and the carbonyl group of the polymer. As a result of this templating, hydroxyapatite can form in a significantly shorter period of time (~1 hr) compared to the system where PPF is not present (24 hrs). The nature of the calcium phosphate phase that forms in the presence of PPF depends on the molecular weight and concentration of PPF. High concentration of PPF in the composite (e.g. 80%) stabilizes an amorphous calcium phosphate (ACP) phase and hinders its transformation to crystalline apatite, while low concentration of PPF (e.g. 5%) promotes the formation of crystalline apatite. Higher molecular weight PPF (Mw = 4500) is found to be more efficient in stabilizing the amorphous phase compared to lower molecular weight PPF (Mw = 1800). While high molecular weight PPF stabilizes ACP, low molecular weight PPF promotes its conversion to crystalline apatite. TEM observations revealed that flake-like hydroxyapatite crystals form in the absence of PPF while spherical ACP particles form in a composite containing 80% PPF. The ACP nano-particles (50-100 nm in diameter) are homogeneously distributed within the PPF matrix. The PPF-calcium phosphate composite can crosslink into a 3D structure by UV irradiation.

Table of Content

List of Tables

List of Figures

Nomenclature

ACP	Amorphous calcium phosphate
BAPO	Bis(2,4,6 - trimethylbenzoyl) phenyl phosphine oxide
BP	Benzoyl peroxide
BSA	Bovine serum albumin
CN	Calcium nitrate
DCPA	Anhydrous dicalcium phosphate
DCPD	Dicalcium phosphate dihydrate
DEF	Diethyl fumarate
DMP	Dentin matrix protein
DMT	N,N-dimethyl-toluidine
EHDP	Ethane-1-hydroxyl-1, 1-diphosphonate
ESA	Electrokinetic sonic amplitude
FTIR	Fourier transform infrared
HAp	Hydroxyapatite
NVP	N-vinyl pyrrolidinone
OCP	Octacalcium phosphate
PAA	Poly (acrylic acid)
PEG	Polyethylene glycol
PGA	Poly (glycolic acid)
PLA	Poly (lactic acid)
PLGA	Poly (lactic-co-glycolic acid)
PPF	Poly(propylene fumarate)
PVA	Poly (vinyl alcohol)
SAD	Selected area diffraction
SAMs	Self-assembled monolayers
SEM	Scanning electron microscopy
TCP	Tricalcium phosphate
TE	Tissue engineering
TEM	Transmission electron microscopy
TGA	Thermal gravimetric analysis
THF	Tetrahydrofuran
UV	Ultra violet
XRD	X-ray diffraction

List of symbols

μ_d	Dynamic mobility
c	Speed of sound
C_{ACP}	Concentration of the reactant ACP
E	Activation energy
a	Particle size
Ksp	Thermodynamic solubility product
R	Gas constant
T_{ca}	Initial calcium concentration
T_P	Initial phosphate concentration
Δ_p	Density difference
ε	Dielectric permittivity
η	Viscosity
Φ	Volume fraction of particles
ω	Angular frequency
ζ	Zeta potential

Acknowledgments

I would like to express sincere gratitude to my supervisor, Dr. Tom Troczynski, for his support and guidance throughout my long years in his lab. I would especially like to thank Dr. Derek Gates for his outstanding support for my work and also Dr. Chi-Wing Tsang for his help in synthesis of the polymer. I am also grateful to Dr. Rizhi Wang for his advice and support throughout this work.

I specially like to thank all the staff at the department of Materials Engineering for their assistance and for making this long journey more enjoyable.

To my parents,
To the memory of my grandparents,
And especially to my loving husband, Alireza, without whose support, love, and understanding none of this would have been possible

1 Introduction

Materials science has made significant contribution to the field of bone substitution by introducing new materials with improved mechanical properties, biocompatibility, bioactivity, and degradability. During the 1960's and 70's materials for bone replacement, such as metallic implants, were chosen with the goal of matching the mechanical properties, e.g. stiffness, of the tissue together with minimal toxicity [1]. By the mid 1980's a new generation of biomaterials, such as bioactive glasses, glass ceramics and synthetic hydroxyapatite (HAp), were developed that were capable of eliciting a positive reaction in the physiological environment rather than passively replacing the tissue [1]. However, replacing the living tissues with synthetic materials is reaching its limit of effectiveness as these materials, in contrast to living tissues, are not capable of adjusting to the changing physiological conditions. Therefore the new generation of biomaterials is aiming at restoring or improving the tissue function rather than substituting the damaged tissue. In view of this context, Tissue Engineering (TE) has emerged in the past 10 years. Langer and Vacanti [2] have defined TE as "an interdisciplinary field of research that applies the principles of engineering and life sciences toward the development of biological substitutes that restore, maintain, or improve tissue function". In this field, a donor tissue is harvested and is dissociated into individual cells; the cells further attach and grow on the substrate. The tissue engineered construct (i.e. the cells attached to the substrate) is implanted to replace the damaged tissue and the biodegradable substrate is further resorbed [3-7]. The growth of the harvested cells is anchorage-dependant; therefore the success of any cell transplantation therapy relies on a suitable substrate [3]. The substrate must provide a suitable 3D architecture for cell proliferation and extracellular matrix deposition until the new tissue is regenerated [3-7]. It can also actively participate in the new tissue formation process by releasing growth factors or differentiation factors encapsulated in its structure [8-11].

The first commercial applications of TE products include bioartificial skin, cartilage repair, hematopoietic progenitor cell isolation, and immunomodulatory therapy for cancer [12]. Although only few TE products have received FDA approval, it is estimated about 70 companies are investing a sum of $600 million per year in research and development of new products [13, 14]. The worldwide market for tissue engineered products is conservatively estimated to reach $500 billion by year 2010, and many governments including US, Japan, European Union, and Australia have begun significant national initiatives to support the TE (regenerative medicine) research and development [15]. Recurring diseases resulting from tissue failure such as diabetes, osteoporosis, and cardiovascular diseases cause major suffering for senior citizens and significantly affect the health care systems [15]. Tissue engineering and regenerative therapies provide the hope for the most effective medical treatment and therefore higher quality of living for people suffering from these diseases. In addition to restoring the function of damaged tissues, the greatest impact of TE in the future would be its ability to produce physiological models, such as tissues, outside the body for examining disease pathogenesis and experimenting with new therapies [14].

In order to translate scientific discoveries into effective treatment for patients, many technical difficulties have to be overcome. Adequate access to healthy cells, optimization of scaffolds, and advanced bioreactors capable of reproducing physiological environments, are the major challenges faced by TE researchers. Scaffolds used in TE today are far from ideal due to their lack of suitable mechanical properties, dictated by specific application site, as well as lack of interconnecting pores [16]. The porous structure is necessary in order for the cells to grow into the three dimensional matrices [16]. Requirements for scaffolds such as biocompatibility in bulk and degraded form, suitable mechanical strength (these properties vary depending on the

application site), porosity for the transportation of cells and nutrients, controlled degradation, and appropriate surface structure and chemistry for cell attachment need to be properly addressed in order to produce a suitable scaffold for TE [3]. Designing a scaffold that can release growth factors, genes and proteins upon degradation also present another challenge. Therefore, new materials and material synthesis technologies need to be developed and optimized to adequately address these challenges.

One of the promising new technologies for the synthesis of biomaterials with advanced functionalities is biomimetic synthesis. In a biomimetic process the knowledge acquired by examining natural processes is applied in the fabrication of synthetic materials. Synthesis of biomimetic materials, on one hand, produces synthetic materials with required properties and on the other hand provides valuable information regarding the mechanisms of these natural processes [17, 18, 19]. Biomineralization is a natural process in which living organisms produce inorganic materials. Through the biomineralization process organic macromolecules control the crystal size, morphology, distribution and orientation of inorganic molecules, producing biocomposites with extraordinary properties such as bone and teeth [18]. Materials scientists are increasingly looking into biomineralization process to fabricate new hybrid organic-inorganic materials. Through these studies valuable information regarding the organic-inorganic interfaces, types of molecular interactions, and evaluation of the stability of these linkages are obtained.

This work investigates a biomimetic process for the synthesis of poly(propylene fumarate)–hydroxyapatite composite for fabrication of a biocompatible and biodegradable TE scaffold. Through this process, calcium phosphate crystals nucleate and grow in the presence of the organic molecules (PPF). Similar process happens in the formation of natural bone where

calcium phosphate mineralizes in the presence of organic molecules such as collagen and proteins. PPF is a biocompatible and biodegradable synthetic polymer which has recently shown promising results in in-vivo studies [20, 21]. One of the most interesting features of PPF is its ability to cross-link by UV-irradiation [20]. This property makes PPF an attractive candidate for the fabrication of 3D TE scaffolds through modern stereolithography techniques. Using this technique, 3D structures with complex architecture can be designed and fabricated. This technique also has the ability to incorporate biosensors in the scaffold during the fabrication process and therefore improve its functionality. On the other hand, PPF lacks bioactivity and its mechanical properties need to be improved [20, 22, 23]. Calcium phosphates and in particular hydroxyapatite, natural constituent of bone, are bioactive and biocompatible materials [24] and can therefore act as reinforcement to PPF while adding bioactivity to the polymer. The biomimetic approach produces a composite of PPF and calcium phosphate that can not be produced through the more traditional methods for making composites such as mechanical mixing of the components. For example in making composites with the dispersed phase having particles size in the nano-scale, aggregation of the nano particles into larger agglomerates is a significant challenge which can now be overcome through the biomimetic processing. Proposed interaction of PPF molecules with the calcium phosphate particles ensures a better bonding between the components of the composite and can therefore enhance the mechanical performance of the composite. This process also provides better control on the phase evolution and crystallinity of calcium phosphate. The crystallinity of the calcium phosphate phase can significantly affect its degradation and therefore its bioactivity [24, 25].

The most significant outcome of this work is understanding the mechanism of the interaction of the organic molecules (PPF) with the inorganic particles (HAp). Such understanding opens up

the possibility for biomimetic processing of other polymer-ceramic composites, especially those with water insoluble polymers. This can also lead to new processing of drug-ceramic composites for controlled delivery applications. Understanding the interactions between organic molecules with inorganic particles can also provide us with tools to tailor the properties of the composites and on the other hand can contribute to the efforts of understanding natural mineralization. The mechanism by which PPF molecules interact with calcium phosphate particles offers an insight regarding one possible pathway for similar interactions that occur in vivo.

2 Literature review

2.1 Materials for tissue engineering scaffolds

Materials used for TE should be biocompatible (i.e. do not provoke unwanted tissue response), biodegradable (i.e. degrade into nontoxic products), and should possess suitable surface chemistry, promoting cell attachment and function [26]. Metals, ceramics, natural and synthetic polymers, and composites have been used as matrix for TE scaffolds [26, 27, 28, 29]. In the following sections the materials used for TE purposes which are relevant to this research will be discussed.

2.1.1 Synthetic polymers

An important class of synthetic degradable polymers includes poly(α-hydroxy ester)s and co-polyesters of the lactic acid and glycolic acid [3, 30]. Poly lactic acid (PLA), polyglycolic acid (PGA), and their combinations have been extensively used in biomedical devices. A wide range of degradation rates can be achieved through varying the monomer ratio or changing the crystallinity of these polymers [3]. Some limitations regarding synthetic polymers are; (i) all polyesters release acidic degradation products that can adversely affect biocompatibility, (ii) these polyesters are relatively stiff which is a disadvantage in regards to compliance with soft tissues and blood vessels, and (iii) most of the polyesters do not have a suitable surface for the attachments of drugs, crosslinkers, or other biologically active agents [31]. Other synthetic degradable polymers include polyanhydrides, polyorthoesters, and polyphosphazens [3].

2.1.1.1 Poly(propylene fumarate)

Fisher et al. [20] developed a TE scaffold based on poly(propylene fumarate) (PPF). PPF's repeating unit contains one carbon-carbon double bond that allows for covalent cross-linking as well as two ester groups that allow hydrolytic degradation of the polymer (Figure 2-1). PPF is a viscous liquid at room temperature and needs cross-linking of its fumarate groups to become a solid. A cross-linked PPF is both biocompatible and biodegradable [20].

Photoinitiated polymerization process is a very effective and attractive way for scaffold processing. These processes are advantageous as they proceed at relatively high rates at low temperatures, their reaction initiation and termination is controllable, and the geometry of the final product may be easily defined [20]. In addition, photoinitiated processes may use many available light sources which in turn expand the number of possible products [20]. In vivo studies have shown that PPF is advantageous compared to other synthetic polymers used in TE (such as PLA or PGA) due to its slower degradation rate as well as the minimal fibrous tissue encapsulation observed after implantation [21]. In future photocrosslinking of PPF may allow for the construction of precisely defined implants through the use of direct or stereolithographic UV laser [32]. The structure produced by the latter could be designed to possess defined architecture, in terms of both external dimensions and internal porosity, which may considerably improve its performance [32].

Crosslinking of PPF is possible using a crosslinking monomer *N*-vinyl pyrrolidinone (NVP), the thermal initiator benzoyl peroxide (BP), and the accelerator *N,N*-dimethyl-toluidine (DMT) [33]. Fisher et al. [20] showed that the crosslinking is also possible using only the photoinitiator bis(2,4,6-trimethylbenzoyl) phenylphosphine oxide (BAPO) and long wavelength ultraviolet

(UV) light, eliminating the need for a crosslinking monomer and an accelerator. Same authors [20] have also shown that a three dimensional, porous scaffold with interconnecting pores can be produced using PPF with a salt leaching strategy. The presence of the leachable porogen (salt) did not affect the initiation of the PPF crosslinking. The authors produced a scaffold with interconnected porosity when the porogen concentration was 80% or higher. However, the release of the remnants of the porogen in the scaffold during the degradation of the scaffold reduced the pH of the environment and therefore facilitated the degradation process. An inflammatory response in the tissue was also observed at the early stages of implantation which the authors attributed to the electrolyte imbalance caused by the leaching of the sodium chloride salt [33].

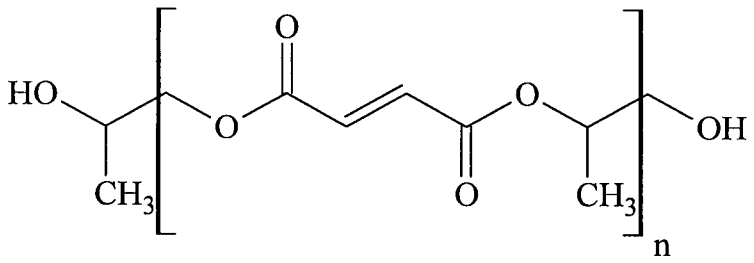

Figure 2-1 Poly(propylene fumarate)

In order to decrease the viscosity of PPF and therefore to improve the handling of the polymer it is possible to dilute the polymer in its crosslinking precursor, diethyl fumarate (DEF) [20]. The effect of DEF is dependent on its concentration. At low concentrations, DEF chains bridge the crosslinked PPF chains more closely together and therefore increase the efficiency of the crosslinking process. This produces a denser network and improves the mechanical properties. In high concentrations of DEF, the PPF chains dissolve in DEF and therefore are separated from

each other. As a result, an open structure with deteriorated mechanical properties is produced. Addition of 25% of DEF to PPF is recommended in order to improve the mechanical properties and lower the viscosity of PPF [20].

In-vitro degradation studies of a composite material based on PPF and β-tricalcium phosphate have shown that the compressive strength and the elastic modulus of the degrading composite material increases to a maximum and then decreases to lower values [34]. The value of the maximum depends on the initial PPF crosslinking density and β-TCP content. PPF-based composite material is the first degradable material whose mechanical properties increase with degradation time. This trend of strength and modulus increase in the degrading composite is attributed to the complexation of the carboxyl groups, formed as PPF degraded, by divalent calcium cations released from degrading β-TCP, although a definite explanation is yet to be found [34]. Addition of tricalcium phosphate to PPF serves two purposes: first, it adds to the osteoconductivity of the polymer and second, it serves to improve the mechanical properties of the scaffold.

Due to the insufficient mechanical properties of PPF, attempts have been made to reinforce the PPF matrix with various reinforcing agents such as calcium phosphates and alumina nanoparticles. Horch et al. [23] incorporated surface-modified nano-alumina (Al_2O_3) in the poly(propylene fumarate)/ poly(propylene fumarate)-diacrylate (PPF/PPF-DA) networks in order to improve the modulus of the polymer. They observed a three-fold increase in Young's modulus. These composites also showed improved bioactivity i.e. better osteoblast adhesion and reduced fibroblast attachment. A fall-off in modulus of the composites at alumina concentrations above 30 wt% was attributed to the light scattering effect of the incorporated alumina which

affected the efficiency of the crosslinking process. Aggregation of alumina nanoparticles at higher concentrations also contributed to the observed decrease in Young's modulus of the composite. The improved mechanical properties can be explained by good dispersion of the alumina particles as well as better covalent bonding between the alumina particles and the polymer matrix due to functionalization of the alumina surfaces [23].

In-vivo study of photocrosslinked PPF has confirmed its biocompatibility and its suitability as a scaffold for bone TE applications [21]. Minimal fibrous encapsulation suggests that PPF is acceptable by the host. A trend of increasing porosity with time was also observed which suggested that the surface of the PPF material was degrading. The mild tissue response associated with the degrading scaffold implies that the degradation products (mainly propylene glycol and fumaric acid) of the photocrosslinked polymer are themselves acceptable to the host tissue [21]. However, the effect of porosity and pore size was not evident in this study probably due to the short period of implantation.

2.1.2 Ceramics

While polymers are ductile and not sufficiently rigid, ceramics are generally too stiff and brittle. The main challenge facing ceramics is to function under multi-axial load and under corrosive environment in the body [24]. These challenges had been overcome by specially designed ceramics that can perform under such extreme conditions. In order for a bioceramic to be successful a bond should form between the implant and the surrounding tissue. Depending on the reaction that a ceramic elicits in the surrounding tissue the mechanism of tissue attachment varies [24]. Therefore, bioceramics are categorized into: non-toxic and biologically inert (alumina and zirconia), nontoxic and biologically active (hydroxyapatite and bioglass), and

finally nontoxic and resorbable (hydroxyapatite and β-tricalcium phosphate) [24, 35]. Most of the implant failures occur at the implant-tissue interface. Therefore, the bonding between the implant and the surrounding tissue has a critical role in the success of the implant. The extent of the interfacial bonding between the implant and the tissue is determined by the type of implant and whether or not the material is bioactive. Bioactive ceramics are by definition [24] those that can "elicit a specific biological response at the interface of the material which results in the formation of a bond between the tissue and the material".

Producing porous biomaterials also improves interfacial bonding by exposing a larger surface area of the implant to the surrounding tissue. In-growth of the tissue into the pores of the biomaterial provides a "biological fixation" and minimizes the loosening and therefore micro-movement of the implant [24].

Calcium phosphates are excellent candidates for bone repair and regeneration as their chemical compositions are similar to the mineral phase of natural bone [36]. They have also been shown to be osteoconductive [37] and have been extensively used in medicine and dentistry as coating on implants, for alveolar ridge augmentation, maxillofacial surgery, and scaffold for bone growth [24, 35, 38, 39].

At the body temperature, in contact with water, and in pH<4.5, brushite (DCPD, $CaHPO_4 . 2H_2O$) and in pH>4.5 hydroxyapatite ($Ca_{10}(PO_4)_6(OH)_2$, HAp) are stable phases of calcium phosphate while tricalcium phosphate ($Ca_3(PO_4)_2$, TCP) and tetracalcium phosphate ($Ca_4P_2O_9$) are stable at higher temperatures [24]. Higher temperature calcium phosphate phases react with

water at body temperature to form HAp; therefore their solubility reaches that of the HAp [24]. Many of the calcium phosphate implants are made by compaction of HAp powder and sintering at high temperatures [24]. The starting HAp powder can be made by mixing calcium and phosphorous precursors with the right Ca:P ratios in aqueous systems while other ions such as carbonate and fluoride can be incorporated into the growing crystals. The degradation rate of ceramic biomaterials depends on surface area, crystallinity, crystal perfection, grain or crystal size, and ionic substitution in the crystals which can be tailored for different applications [3]. Due to the low mechanical reliability of the HAp implants (the Weibull modulus of HAp is low in physiological solutions; m=12) their applications have been limited to low-load bearing applications, coatings on medical implants and in composites with polymers [24].

2.1.2.1 HAp precipitation from solutions

Precipitation of calcium phosphates from solutions has been extensively studied due to its importance in industrial [40] and environmental applications, such as waste water treatment [41, 42], as well as its biological relevance [43-46]. In precipitation of calcium phosphates from aqueous solutions, the nature of the phases that deposit at the early stages of precipitation is dependant on pH, supersaturation, and temperature [43-58]. At the same time environmental factors such as the presence of other ions or substances and the presence of foreign surfaces that would induce heterogeneous precipitation further complicate this system [59-72].

Calcium phosphate solutions in which precipitation occurs are supersaturated with respect to five different calcium phosphate phases. These calcium phosphate phases in order of increased solubility are HAp (K_{sp}* = 4.7 x 10^{-59} (mol/L)[9]), tricalcium phosphate ($Ca_3(PO_4)_2$, TCP,

* K_{sp} is the thermodynamic solubility product at 25°C.

K_{sp}= 1.2 x 10^{-29} $(mol/L)^5$), octacalcium phosphate ($Ca_8H_2(PO_4)_6.5H_2O$, OCP, K_{sp}= 1.25 x 10^{-47} $(mol/L)^8$), anhydrous dicalcium phosphate ($CaHPO_4$, DCPA, K_{sp}= 1.26 x 10^{-7} $(mol/L)^2$), and dicalcium phosphate dihydrate ($CaHPO_4.2H_2O$, DCPD, brushite, K_{sp}= 2.49 x 10^{-7} $(mol/L)^2$) [57, 58]. HAp is the most thermodynamically stable calcium phosphate which should form upon precipitation [57, 58]. Figure 2-2 shows the calcium concentration and pH values of solutions supersaturated with various calcium phosphate phases. The points at which two calcium phosphate phases are at equilibrium are dependent on the pH and the ionic strength of the solution [57]. The pH dependency is due to the fact that the orthophosphoric is a weak and polybasic acid and the concentrations of the HPO_4^{2-}, $H_2PO_4^{-1}$, and PO_4^{3-} change with pH [58]. As can be seen from Figure 2-2, at pH above 6, a precipitating solution is metastable in respect to several calcium phosphate phases depending on its initial concentration. Therefore, initially the least stable phases form and further dissolve as the supersaturation of the solution decreases to form a more thermodynamically stable phase [57]. Figure 2-3 shows the calculated product log (T_{Ca}* T_P) for equilibrium with respect to each calcium phosphate phase as a function of pH, calculated from the solution containing calcium chloride and potassium phosphate [52]. It can be observed that at a constant pH condition the initial phase that forms upon precipitation is dependant on the initial calcium and phosphate concentrations. In conditions similar to that of point A (T_{Ca}=T_P= 1.4 mM, pH=7.4) in Fig 2-2 Koutsoukos et al. [52] have observed DCPD to be the first participated phase while a condition similar to that of point B (T_{Ca}= 1.2 mM, T_{Ca}/T_P=1.33, pH=7.4) results in OCP as a precursor to the formation of the apatite phase.

It has been well established that kinetic factors play a critical role in the nature of the precipitated phases [55-57]. Liu et al. [73] investigated the kinetics of hydroxyapatite precipitation at pH 10 to 11 in aqueous solutions with the initial T_{Ca}=0.5 M and the Ca/P=1.67.

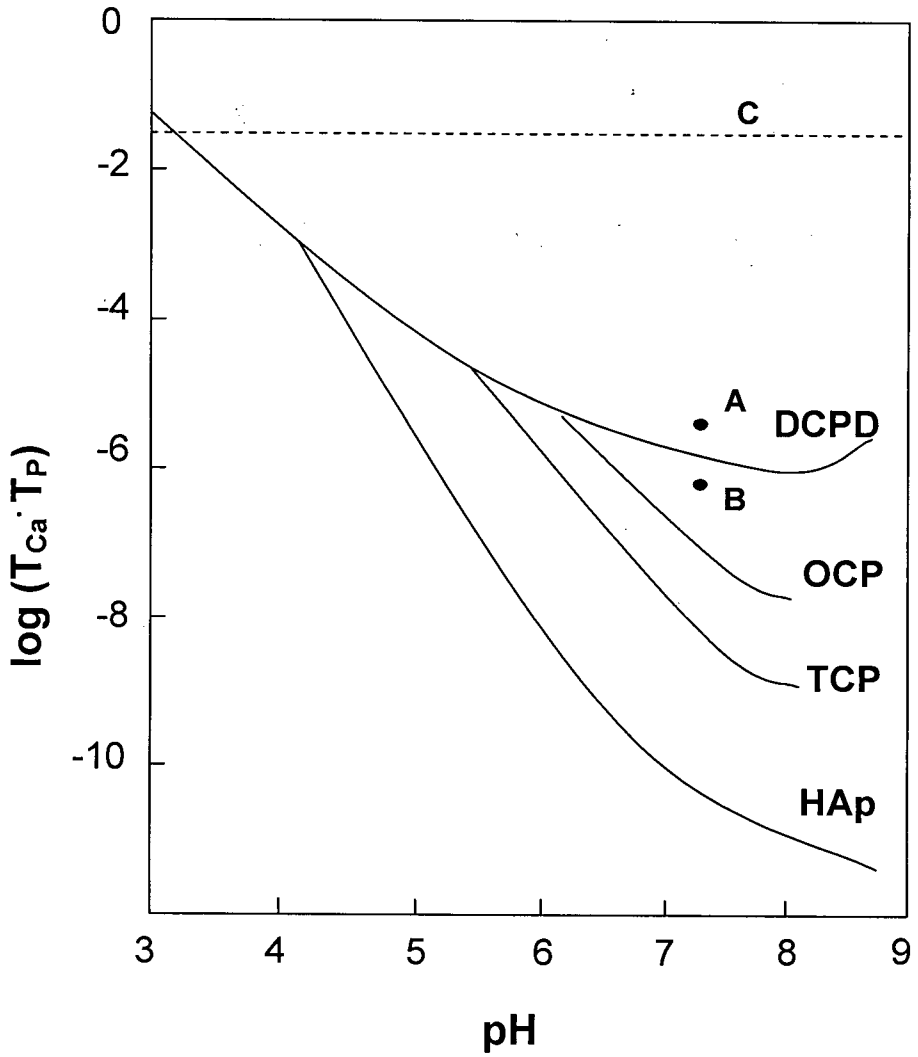

Figure 2-2 Logarithm of the product of calcium and phosphate concentrations plotted against pH in the ternary system $Ca(OH)_2$-H_3PO_4-H_2O, calculated for 37 ^{O}C, adopted from [52]. Line C represents the logarithm of the product of calcium and phosphate concentrations (-1.47) studied in this work. Reproduced with permission from *Journal of the American Chemical Society* 1980, 102, 1553-7. Copyright 2000 American Chemical Society.]

Their results indicated that OCP (octacalcium phosphate) was the first phase to precipitate which quickly (within minutes) transformed to amorphous calcium phosphate (ACP). ACP then

transformed to hydroxyapatite (HAp). They suggested the following kinetic equation for the transformation of ACP to HAp:

$$-dC_{ACP}/dt = Ae^{-E/RT} C^2_{ACP} \qquad (2\text{-}1)$$

where E is the activation energy, C_{ACP} is the concentration of the reactant ACP in the liquid at time t, R is the gas constant, and A is the pre-exponential factor. E was calculated from the experimental data to be 95 kJ/mol (22.7 kcal/mol). They inferred that the ACP to HAp transformation is a particle surface reaction controlled process.

Similar results were obtained by Lazic [74]. He too showed that the formation of HAp from medium and high supersaturated solutions in alkaline pH proceeds by the formation of amorphous calcium phosphate (ACP). He found that factors that facilitate the solubility of the ACP phase, such as lower pH, higher temperature and higher supersaturation in regards to HAp, increase the rate of the ACP to HAp transformation. However, his experimental results suggested that increasing the pH in the alkaline media increases the rate of transformation. He also observed that at pH<9.5 protonated phosphates and hydrated calcium are the dominant species which kinetically favor the formation of acidic phosphates such as OCP which transform to ACP and HAp due to thermodynamic reasons. At pH>9.5 deprotonated phosphate and dehydrated calcium are the dominant species which act as the growth unit for HAp.

2.1.2.2 Mechanisms of ACP to HAp transformation

Synthetic ACP has a tricalcium phosphate structure with occluded or adsorbed ions [75]. It has been reported that the ACP has a short range order of 9.5 Å in size and a Ca/P ratio of 3:2 which has lead to $Ca_9(PO_4)_6$ as a probable formula for the synthetic ACP. The ACP particles, mostly

hydrated calcium and acid phosphates, are closely packed to form larger particles [75]. ACP is the intermediate phase in the formation of crystalline apatite from alkaline solutions and a subsequent amorphous-crystalline transformation yields the more crystalline apatite [75-79]. Plotting the extent of ACP to HAp transformation vs. time results in an S-shaped curve (schematically represented in Fig 2-4), which includes the dissolution of the ACP phase with the subsequent nucleation and growth of the HAp [76]. The induction time includes the time necessary for the ACP particles to dissolve and the initial stable nuclei of HAp to form and is therefore affected by the parameters that influence ACP dissolution rate such as ACP particle size, lower pH and higher temperature. Presence of incorporated ions such as Mg^{2+} in ACP decreases its solubility and therefore reduces the rate of its transformation to HAp. An energy barrier should be overcome in order to form HAp nuclei, therefore increasing the temperature increases the dissolution rate of the ACP particles and also provides energy for the system to overcome the HAp nucleation barrier. The activation energy of the induction time is experimentally observed to be 138 kJ/mol (33 kcal/mol) [76]. No induction time and therefore no activation energy was observed for the systems seeded with HAp crystals therefore it was concluded that the dissolution of ACP does not require significant activation energy and that the required activation energy observed for the unseeded system is due to the nucleation of the HAp crystals [76]. Therefore the rate-limiting step in the ACP to HAp transformation is the formation of the initial HAp nuclei [76]. Formation of the HAp nuclei is followed by a proliferation period in which the already formed crystals grow in conjunction with the formation of new HAp nuclei [76]. The decrease in the conversion rate near to the completion of the conversion can be attributed to the coalescing of the nuclei already in the solution as well as the decrease in the supersaturation of the system [76].

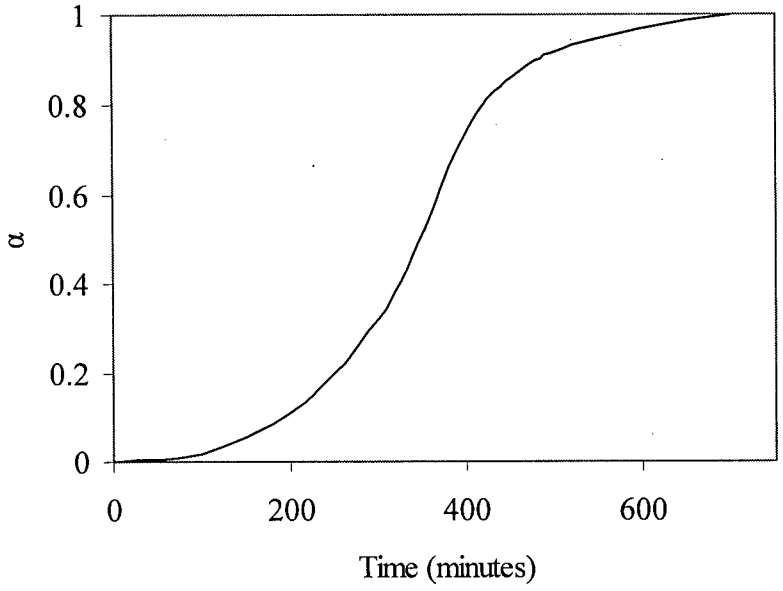

Figure 2-3 Extent of ACP to HAp conversion reaction (α) vs. time, for $CaCl_2$-$(NH_4)_2HPO_4$ system at pH=10, produced from [76].

In summary, Blumenthal et al. [77] proposed that the transformation of ACP to HAp (in a stirred system) occurs in three steps. Step 1: ACP dissolves in the solution to form dissolved and hydrated ions; step 2: dissolution products of the ACP move away from its surface, and finally; step 3: HAp nucleates and grows. They also observed a band broadening that occurs for the FTIR absorption band of OH stretching mode at around 3500 cm^{-1} due to hydrogen bonding of the surface OH groups with water molecules. They suggested that the absence of the OH band in some synthetic (those with high surface area e.g. 200 m^2/g) and the biological mineral is due to the hydrogen bonding of the surface OH groups with absorbed water on the surface. When the number of surface OH groups decreases with decrease in surface area more intense OH bands appear [75,77].

ACP is amorphous to both X-ray and electron diffraction; the IR spectra indicate the absence of crystal field splitting (the PO_4^{3-} absorptions bands are broad, unstructured, and relatively symmetrical), and they appear as homogenous spherules in SEM observations [78]. The physiochemical properties of ACP such as broad XRD maxima (showing lack of long range order) and the absence of the crystal field splitting in IR spectra can arise from a glass-like state. It is also possible that a microcrystalline structure be the cause of such physiochemical properties. The latter would mean that ACP consists of calcium phosphate crystals that are too small to produce recognizable diffraction pattern or produce characteristic crystalline IR spectra. Thus ACP could be considered an agglomeration of brushite, octacalcium phosphate, tricalcium phosphate, or apatite nanocrystals. However, if ACP is made of nano-crystals of calcium phosphates, these crystals should continually grow in size if exposed to a solution or thermal condition that favors crystal growth [78]. But the ACP particles in such solution or thermal condition never show a continuous increase in crystal size. These precipitates rather show a discontinuous transformation to crystalline state, in which the ACP precipitates are stable for a period of time and then rapidly transform to a more crystalline state. Furthermore, ACP precipitates transform to apatite in aqueous solutions while convert to nonapatitic crystalline α and β-tricalcium phosphate at temperatures at which these phases and apatite do not interconvert. The only explanation for these phenomena could be that the apatite and the tricalcium phosphate phases were produced by a third state through a phase change mechanism. Therefore, ACP can not be nano-crystalline apatite or tricalcium phosphate. As ACP is more stable in higher pH as opposed to lower stability of brushite and octacalcium phosphate at higher pH and higher thermal stability of ACP compared to these two phases, nano-crystals of brushite and octacalcium phosphate being the building blocks of ACP is also ruled out [78]. Therefore, it is concluded that ACP like many other solid materials is truly non-crystalline and is in glass-like state [78].

CO_3^{2-} ions can replace PO_4^{3-} groups in the synthetic HAp and distort its structure. HAp crystals containing CO_3^{2-} have smaller crystal size compared to those which are CO_3^{3-}-free. Biological apatite too has some of its PO_4^{3-} groups substituted by CO_3^{2-} [75]. It has also been suggested that bone mineral may contain certain amount of ACP, although the biological ACP does not react with water to form HAp whereas synthetic ACP does [75]. The ACP to HAP transformation is a relatively fast process (the extent of which depends on the exact conditions) and usually proceeds until the crystalline phase is formed. But in biological systems amorphous calcium phosphate (ACP) usually coexists with crystalline apatite (HAp) which is an indication that the biological environment regulates the transformation of the amorphous phase to a more stable crystalline entity [79].

2.1.2.3 Effect of macromolecules on HAp crystallization

Calcium phosphates are capable of removing ions from the solutions either through physical absorption or ion exchange with surface ions of the mineral [80-84]. Due to its capability to absorb ions and proteins, hydroxyapatite has been used in the chromatography columns for the separation of proteins and polynucleotides (DNA and RNA) [85-88]. Hydroxyapatite has been very successful in removing high molecular weight proteins due to their multi-attachment of the polar groups, namely carboxyl groups, to the surface.

The incorporation of some ions such as F^-, or surface absorption of others, such as pyrophosphates ($P_2O_7^{4-}$), can stabilize the amorphous calcium phosphate precursor and inhibit its transformation to HAp. Macromolecules can also absorb to the surface of ACP or HAp and hinder the HAp crystallization. For example, Blumenthal et al. [89] observed that organic phosphonates are capable of retarding HAp nucleation and growth in a supersaturated solution

(in regards to HAp) by attaching to the crystal growth sites of the HAp through Ca^{2+} bonding. They also reported that at a given pH acidic proteins bind to the calcium site of the HAp crystal surface and more basic ones bind to the surface phosphate groups [89].

The inhibitory effect of compounds on the crystallization of HAp is studied to be used in prevention of pathological calcification or for the treatment of bone and joint disorder. One example of these compounds is diphosphonate ethane-1-hydroxy-1, 1-diphosphonic acid (EHDP) which has been used for the treatment of Paget's disease in which the bone is being resorbed and formed at a higher rate than normal and therefore the crystal size of the bone mineral is smaller than those of the healthy bone [80].

In mineralized tissues, the crystal shape, morphology, and orientation of the inorganic phase is affected by the presence of the matrix proteins [90-100]. Adsorption of water-soluble macromolecules on the specific surfaces of the growing crystals changes the growth rate of these surfaces. Thermodynamic studies [80] on the absorption of compounds on the surface of apatite crystals suggest that entropic change has a significant contribution in lowering the free energy of absorption. Factors contributing to the entropic change can be identified as the disruption of the ordered hydration layer around the crystal and the conformational changes of the absorbed macromolecule. The entropy change is responsible for the absorption of a wide range of macromolecules and ions on the surface of apatites [80]. In the case of biological apatite it has been observed that the adsorption of these macromolecules on the surface of the nucleating apatite is responsible for stabilizing an amorphous calcium phosphate phase which coexists with the crystalline phase [79,98,99].

Macromolecules can influence both the initial formation of ACP and its transformation to crystalline apatite [79]. These molecules can act by partitioning or sheltering the amorphous nucleation and/or growth sites from access to free solvent. In high supersaturation conditions, in which the activation energy for the precipitation of the amorphous phase is high, the macromolecules act as binding agents between the Ca^{2+} and HPO_4^{2-}. However, in low saturation conditions the functional groups on these molecules or their salvation shell space may act as nucleation sites for the amorphous calcium phosphate and consequently sheltering it from the surrounding solution. The functional groups on these macromolecules can interact with calcium phosphate salts and are possibly responsible for matrix-mineral interactions within the connective tissue [79]. Macromolecules size and conformation are also contributing factors to their interactions with the mineral [79]. The extent of the interaction between the organic and the inorganic phase, their interfacial bonding, and the preferential orientation of the apatite crystals determine the overall mechanical behavior of bone [101].

Williams et al. [102] tried to characterize the structural features that render a macromolecule an inhibitor to HAp formation. Their research suggested that any compound with a phosphate group and an acidic group, e.g. carboxylic group, inhibits the crystallization of calcium phosphates in solution. They also found that inhibition power depends on factors such as closeness of the active groups, number of active groups, steric factors, stereochemical arrangements, and the lability of the molecule. In addition to the structural fit, the conformation of the additives on the surface of apatite plays an important role in inhibiting crystal growth. Café et al. [103] found that the performance of polyelectrolytes on inhibiting apatite crystallization is improved by the number of bonds with the surface of the crystals; therefore the molecules that stay flat on the surface of the growing crystal can hinder crystal growth even in very low concentrations.

Transformation of ACP to HAp occurs only when sufficient amount of inhibitor is removed due to hydrolysis or due to reaction with newly formed nuclei. Williams et al. [102] suggested that the inhibitors to HAp formation can be divided into two major categories. Type I are those that bind to the active sites on the HAp crystals and inhibit their growth. At high concentration these inhibitors do not allow the HAp nuclei to reach critical size and therefore the nuclei dissolve. Type II inhibitors are more efficient on ACP particles, reducing their dissolution rate and therefore affecting their transformation. The authors, however, could not explain why different macromolecules work one way or the other. They also observed that the appearance of the ACP particles before and after transformation to HAp was not altered by the presence of inhibitors. ACP particles appeared spherical while after transformation to HAp needle-like crystals were observed.

In addition to structural features, the effect of macromolecules on the nucleation, crystal growth, Oswald ripening, and phase transformation of calcium phosphates is significantly dependent on the concentration of the molecules [104]. In a given system a polyelectrolyte can act as a retardant or template depending on its concentration in the system. Although presence of a structural fit between the polyelectrolyte and the crystals in certain concentrations may render the additive a nucleating template, the absorption of the additive on the surface of the nucleating phase results in retardation of nucleation or growth processes. For example, at concentrations of about 100-200 ppm, polyglutamic acid retards the formation of calcium oxalate while at low concentration (2-5 ppm) it acts as the template for the formation of calcium oxalate. In explaining this phenomenon the authors assumed that part of the molecules act as nucleation sites while the rest of the free molecules absorb on the crystal surfaces and therefore retard crystal growth by retarding the transfer of calcium ions to the growing surfaces [104]. Therefore,

in order to design a crystal growth inhibitor Berkovitch-Yellin et al. [105] suggested that the additive should have a part that structurally matches the growing face of the crystal and is therefore incorporated into the crystal face during growth. In addition, it should possess another part that does not match the crystal surface but sterically hinders the transport of ions to the growing surface of the crystal and therefore retards the growth process.

Polymers can also affect aggregation of the particles during crystallization. The effect of the polyelectrolytes on the aggregation of particles is dependent on the polymer's concentration and molecular weight [104]. In low concentrations the polymer bridges the particles and therefore promotes aggregation. In higher concentrations the polymer encapsulates the crystals and hinders aggregation. The effect of polyelectrolytes on the aggregation of particles is also dependent on their molecular weight. For example, low molecular weight poly acrylic acid, PAA (1500 Da), does not result in hydroxyapatite aggregation while in higher molecular weigh (450000 Da) causes aggregation in low concentration (~2 ppm) and hinders aggregation in higher concentrations. This effect is attributed to the fact that low molecular weight PAA consists of short chains that can not bridge the particles at any given concentration while higher molecular weight PAA can cause aggregation in low concentrations due to the longer size of the polymer chain [106]. It has also been observed that in the presence of gelatin the aggregation of the ACP particles is hindered and the life time of ACP is significantly shortened. Brecevic et al. [107] attributed this effect to (i) higher number of nucleation sites (due to the disaggregation effect of gelatin) and (ii) templating effect of the surface absorbed gelatin for the nucleation of the OCP phase.

In case of collagen-mineral interactions, Posner suggested [80] that the polar groups of the collagen might hydrogen bond to the oxygen groups on the apatite surface. The efficiency of the collagen-mineral interactions increases with the surface area of the bone mineral. He also noted that collagen molecules bond to the surface of apatites directly rather than through the hydration layer of the HAp crystals [80]. However, Bernardi et al. [108] suggested that calcium ions on the surface of the apatite crystals, rather than the OH groups, are the bonding site for the carboxyl and phosphate groups of organic compounds. Termine et al. [109] characterized osteonectin as a bone protein that is capable to selectively bind to hydroxyapatite and collagen and is able to initiate the deposition of calcium phosphate from otherwise stable solutions. Osteonectin contains both organic phosphates and sialic acid that can bind to calcium and on the other hand can bind to the collagen surface. The authors believe that mineralization of calcium phosphates and specifically hydroxyapatite starts with the binding of calcium to osteonectin, which is attached to collagen, followed by formation of nuclei that are insoluble, stable, and can produce hydroxyapatite. They also believed osteonectin was responsible for the attachment of the HAp crystals to collagen fibrils [109].

2.1.2.4 Effect of organic solvents on HAp crystallization

Few investigators have studied the effect of the organic solvents on the precipitation of calcium phosphates. According to these studies the effect of the organic solvent is mainly due to electrostatic interactions in solvents with different dielectric constants. The solvent also affects the interionic as well as the solute-solvent interactions [58, 110].

Lerner et al. [111] observed that ethanol increases the crystallinity of calcium phosphate precipitates. On the contrary, Tung et al. [110] have found that presence of ethanol in a supersaturated calcium phosphate solution, at pH 7.4 and higher, increases the rate of

precipitation and stabilizes the ACP phase. The authors reasoned that the presence of ethanol increases the activity coefficient of the chemical species which increases the supersaturation of the solution and therefore results in faster precipitation. The presence of ethanol molecules also weakens the bonds in the hydration sphere of the ions and reduces the energy barrier for dehydration which also results in faster precipitation. ACP to HAp transformation requires the dissolution of the ACP phase and its reprecipitation as crystalline HAp. As the presence of ethanol reduces the solubility of the calcium phosphate phases in the medium, dissolution of the ACP is delayed and therefore ACP is stabilized. Larsen et al. [112] have also reported that ethanol affects the phases formed during precipitation of calcium phosphates. The authors have observed that ethanol promotes the formation of ACP.

2.1.2.5 Biocompatibility of amorphous calcium phosphate

Amorphous calcium phosphate is used as coating on implants [113] and as dental ceramic [114]. It is also being considered to be used in chewing gums [115, 116], mouth wash and sealants [117]. There have been some contradictory results regarding the bioactivity of the ACP. Some researchers have observed negative cell response to ACP [118] in in-vitro studies while other in-vivo investigations of ACP coated polymers have shown good ACP osteoconduction properties [119-121].

Ter Brugge et al. [118] reported that crystalline calcium phosphate coatings had a positive effect on expression of osteogenic markers while amorphous calcium phosphate showed no positive effect on the differentiation of the cells. According to the authors the latter is probably due to the release of the calcium phosphate particles into the surrounding environment due to the dissolution of the amorphous coating. They [118] also observed that ACP coatings inhibit

osteogenic differentiation of rat bone marrow (RBM) cells irrespective of their composition while amorphous-crystalline coatings support the differentiation of these cells.

However, results obtained by Nagano et al. [119] suggest otherwise. They argued that the surface degradation of calcium phosphate materials is directly related to their osteoconductive properties. Degradable calcium phosphate materials lead to release of Ca^{2+} and PO_4^{3-} ions and therefore enhance osteoconduction and initial implant fixation. They observed that ACP coatings (thin or thick) totally degraded and were replaced by new bone, directly in contact with the substrate. The authors conclude that if initial coating fixation and osteoinduction of porous materials (including polymers) is desired highly degradable ACP is advantageous. This is due to the fact that the resorbed ACP is replaced by new bone which is mechanically interlocked with the porous scaffold. Furthermore, due to the higher stability of ACP in saline solution compared to poorly crystalline HAp, Maxian et al. [113] suggested that when coating longevity is of importance, ACP would be more suitable as coating on medical implants. Investigation on cytotoxicity of ACP as filler in polymer-ceramic composites showed no adverse effect due to the presence of ACP [120]. The composites released calcium and phosphate ions due to the degradation of ACP which promoted new bone remineralization. In the system studied in this work, degradation of ACP into the surrounding environment of the implant should compensate for the pH drop caused by the PPF degradation and therefore slow down the degradation rate of the polymer by neutralizing the environment and reduce the inflammatory reaction in the surrounding tissue. Complexation of the carboxyl groups, formed as PPF degraded, by divalent calcium cations released from the calcium phosphate phase is also assumed to be responsible for an increasing trend of the compressive strength and compressive modulus of a PPF-β-tricalcium phosphate composite during the initial period of degradation [34].

2.1.3 Composites

In order to obtain materials that best resemble the natural bone and to overcome the limitations of bioactive ceramics, composites of polymers and bioceramics have been explored. It is observed that composites have the closest properties to the bone they are to replace [122]. Natural bone is a composite of a mineral phase (HAp) and an organic matrix (collagen). Although the composition of bone varies in different body sites, the proportions are approximately 69 wt% mineral and 22 wt% organic plus 9 wt% water [123]. Collagen is in the form of fibrils, 100-2000 nm in diameter. Calcium phosphate phase is in form of HAp crystals in the shape of needles 40-60 nm in length, 20 nm in width, and 1.5-5 nm in thickness. [122, 123].

The addition of bioceramics to polymers stiffens the otherwise compliant polymer. It also adds to the bioactivity of the composite. The surface of composites is usually machined in order to expose the bioactive phase to the surrounding tissue. The bioactive phase provides an anchorage for new bone formation [122]. HAp-polymer composites such as HAp-polyethylene [124, 125, 126], HAp-collagen [127, 128], HAp polylactide [129], and HAp-polymethylmethacrylate [130, 131] have been the subject of intense research.

2.1.3.1 Organic-inorganic composites

Fabrication of hybrid organic-inorganic materials with controlled crystallization pattern has attracted interest of researchers from various disciplines such as organic and inorganic chemistry, materials science, and biotechnology [132-141]. It is expected that research on the synthesis of such materials provides valuable information regarding the natural biomineralization

and also paves the road for the production of synthetic materials with superb functionalities and structures [98, 99, 142, 143].

Natural organic-inorganic hybrids, such as bone, are produced by the crystallization of the inorganic phase on the self-assembled organic matrix [143]. In mineralized tissues, the crystal shape, morphology and orientation of the inorganic phase is affected by the presence of the matrix proteins. Absorption of water-soluble macromolecules on the specific surfaces of growing crystals can change the growth rate of these surfaces, which then determines the crystal habit of the inorganic phase. The organic matrix provides structural information for the growth direction of the newly nucleated crystal. All these phenomena happen at the organic-inorganic interface. However, the detailed mechanism of interaction of these two phases as well as the influence of the organic matrix on the crystallization of the inorganic phase is still not clear [143]. This general idea has been adopted by researchers to produce organic-inorganic composites with controlled crystallization, for applications in microelectronics, optoelectronics, and biomedical engineering [132, 135, 138, 140, 144]. The major role of the organic phase can be defined as structural control of the morphology, size and anisotropy of the inorganic crystals and their distribution inside the organic phase [98, 99]. Directed nucleation and growth of the inorganic phase, as well as template replication would bear significant importance in the future processing of bioceramics [145]. Both synthetic and biological macromolecules have been used to produce organic-inorganic hybrids through in-situ synthesis although the application of synthetic polymers is a new trend and has recently attracted the attention of researchers.

2.1.3.1.1 Biomimetic composites with natural polymers

Biomimetic synthesis of calcium phosphate-polymer composites has been intended to investigate the effect of matrix proteins and other biopolymers such as collagen on the phase evolution of biological apatite. In one such study Walton et al. [146] investigated the influencing factors on biological calcification by developing a model system. They observed that the calcification process was facilitated by the presence of the organic matrix and that certain chemical groups within the organic matrix acted as strong binding sites for the nucleating crystals. They also found that in addition to active functional groups, the presence of physical space in the form of a cavity, channel, or capillary was also important to produce a suitable nucleation site. They suggested that C-terminal serine to be an effective nucleation site in biological calcification. They believed that the biological apatite that forms on organic matrices is of amorphous nature.

The nucleation, growth, morphology, and dissolution of biological apatite are significantly affected by the presence of matrix proteins. For example He et al. [147] observed that HAp precipitated in the presence of dentin matrix protein 1 (DMP1) with a preferred growth along the c-axis. They believed that the acidic domain in DMP1 (carboxyl terminal domain) oligomerized in the presence of calcium ion and therefore provided a nucleation and growth template for the HAp crystals. It was also observed that the dissolution and growth behavior of HAp changes in the presence of poly(sodium aspartate) [148]. The carboxylate ions were absorbed on the calcium rich surfaces of HAp and therefore inhibited their dissolution/growth by lowering their surface energy. Similarly, different functional groups (anionic aspartate and cationic lysine groups) of bovine serum albumin (BSA) were attracted to the surfaces of opposite charge (calcium rich and phosphate rich) and thus stabilized these growing surfaces [148]. Acidic phosphoproteins such as osteopontin and sialoprotein are observed to inhibit secondary

crystallization and growth of calcium phosphate crystals [149-151]. This effect has been attributed to the electrostatic interaction between the negatively charged proteins and the Ca^{2+} ions. On the other hand absorption of such proteins on the Ca^{2+} sites on the surface of the HAp particles is found responsible for the inhibition of secondary nucleation and growth of the HAp crystals [150, 152-154]. These observations are attributed to the fact that the chemisorption of calcium on these molecules provides a favorable nucleation site for the HAp crystals [155]. However, the effect of proteins on the crystallization of biominerals, in particular HAp, is complex. For example, phosphophoryn and bovine serum albumin display inhibitory effects at high concentrations and promote crystallization at low concentrations [153, 156]. Other parameters such as the spatial arrangement of functional groups on the macromolecule also play an important role in templating the formation of the crystals.

Understanding the mechanism of collagen-apatite interactions has attracted the interest of many researchers. Zhang et al. [155] investigated the nucleation sites of the apatite crystals on the collagen matrix during an in-situ precipitation. Using IR spectroscopy they observed that carbonyl groups (C=O) of the collagen matrix act as the nucleation site for the calcium phosphate crystals through formation of a chelate bond with calcium ions [155]. Kikichi et al. [157] synthesized a collagen hydroxyapatite composite through in-situ precipitation. They observed that the apatite crystals formed on the collagenous matrix had a self-assembled structure which they attributed to the interaction of the collagen matrix and the nucleating crystals. Through IR spectroscopy they found that the absorption band of the COO^- of the collagen substrate shifts to lower frequencies due to interaction with calcium. Du et al. [101] investigated the mineralization of collagen matrix through in-situ precipitation of calcium phosphate. Using XRD and IR analysis they found that a noncrystalline calcium phosphate precipitates first and its crystallinity improves over time. However, they did not elaborate on the

nature of this noncrystalline phase. They believed that the crystal size of the initial phase is so small that does not produce a diffraction pattern. They attributed the small crystal size to the effect of the collagen matrix to induce heterogeneous crystallization [101].

2.1.3.1.2 Biomimetic composites with synthetic polymers

Similar to biopolymers, biomimetic processing of synthetic polymers-calcium phosphate composites can shed light on the mechanisms of organic-inorganic interactions. At the same time synthesis of these composites can result in new materials with improved functionalities that can be employed to replace a damaged tissue.

In the study of effect of polymers on the precipitation of calcium carbonates, Naka et al. [143] showed that three polymorphs of calcium carbonate can precipitate at low temperatures (< 30°C) by triggering the polymerization of acrylic acid in a calcium carbonate supersaturated solution. They concluded that the functional group on the polymer interacts with calcium ions to locally increase its concentration and therefore to kinetically induce precipitation of thermodynamically unstable polymorphs of calcium carbonate.

It has been reported that the addition of anionic and cationic polymers suppresses HAp crystallization [144]. Kato et al. suggested that the reaction of the dissociated poly acrylic acid (PAA) with calcium ion provides a platform for the nucleation and growth of the HAp phase. In low concentration solutions the polymer absorbs some of the calcium ion, necessary to form HAp, out of the system and therefore inhibits its nucleation and growth. In saturated solutions the PAA-Ca^{2+} complex precipitates and provides a nucleation site for the HAp phase [144]. The

extent of the reaction between the polymer and the ionic components of HAp, and the concentration of the solution containing these ions (Ca^{2+} and PO_4^{3-}) play a major role in the kinetics of HAp formation. Absorption of the PAA on the surface of the growing HAp crystals is responsible for delayed crystallization of the apatite phase. It was observed that calcium phosphates formed in the presence of the polymer showed broad X-ray diffraction patterns. The authors attributed this effect to the incorporation of the polymer within the growing calcium phosphate crystals. The composite formed through the in-situ formation of hydroxyapatite showed a better tensile strength in wet state (1 MPa after 10 days of soaking in water) compared to the physically mixed composite (totally disintegrated after the 10 days of soaking). This effect was explained by the better homogeneity of the in-situ formed composite [144].

Through a similar in-situ process Shinha et al. [158] produced 5-40 nm sized hydroxyapatite in the presence of poly vinyl alcohol (PVA) and bovine serum albumin (BSA). Intermolecular interaction between the polymer chains and the sterically entrapped calcium ions in PVA system and interfacial molecular recognition of the nanosized cavities present in the structure of BSA with calcium were found responsible for the role these polymers play on the HAp formation [158]. These molecular level interactions dictated the size, morphology, and orientation of the inorganic phase.

It is possible to synthesize crystals with controlled size and aspect ratios using synthetic polymers to influence crystallization. Liou et al. [159] produced needle-like calcium deficient hydroxyapatite (cd-HAp) crystals, 5-10 nm in diameter and 20-80 nm in length, which were covered with a ~1 nm thick poly acrylic acid (PAA) shell. They found that the degree of PAA dissociation in the solution (governed by the solution pH) affects the crystal growth of the cd-

HAp phase. This process as explained by Kato et al. [144] is dependent on the concentration of the polymer. Higher degree of dissociation translates to higher degree of interaction between the polymer and the calcium ions. This in turn hinders the reaction between calcium and phosphorous ions and therefore retards the nucleation and growth of the HAp crystals. They found that the pH and concentration of the solution control the crystal size as well as the aspect ratio of the resulting HAp crystals [159].

Significant IR and XRD peak broadening was observed for a calcium phosphate phase prepared in the presence poly(ethylene glycol) (PEG) by Li et al. [160], which was attributed to the amorphous state of the calcium phosphate phase. They suggested that PEG interacts with calcium ions and provides a precipitation site for the calcium phosphate phase. The absorbed PEG on the surface of the ACP particles hinders the dissolution and reprecipitation of ACP and its subsequent transformation to crystalline HAp. They believed that ACP in composite with organic polymers is capable of reducing the degradation rate of the polymer by neutralizing the acidic environment caused by the degradation of the polymer; therefore, presence of ACP in the composite is advantageous compared to crystalline HAp or OCP. The authors suggested that the presence of PEG on the ACP particles makes these particles more compatible with other organic matrices and improves the interaction between the organic and inorganic components of a composite [160].

In order to overcome the limitation of physical mixing in preparation of composites such as agglomeration and inhomogeneous mixing of the filler particles, Li et al. [161] proposed an in-situ polymerization process. In this process needle-like HAp particles are mixed with the monomer and are then UV crosslinked to form the final composite of HAp and

poly(methacrylate pyromellitylimidoalanine). The authors pointed out that the needle shape of the HAp particles increased their surface area and thus improved their interactions with the matrix polymer. They observed that the degradation rate of the composite decreased compared to that of the polymer alone which they attributed to the neutralizing effect of the HAp degradation in the surrounding environment of the degrading composite.

In a comprehensive study Bunker et al. [162] offered a new biomimetic approach for producing ceramic coatings at low temperatures, suitable for substrates that are unable to go through heat treatment processes, such as plastics. In this process the ceramic coating nucleates and grows from an aqueous solution on a functionalized surface. The biomimetic process involves aqueous solutions of the precursor which is deposited on a substrate when solution conditions such as pH, concentration, or temperature are changed so that the precursors are no longer soluble and the solutions are supersaturated. The success of this process depends on the degree that the homogenous nucleation can be suppressed and the heterogeneous nucleation on the surface is promoted. The idea of using anionic groups (e.g. phosphate groups) to promote nucleation and growth was adopted from nature in order to produce inorganic films on organic substrates. The authors [162] used different surface modification techniques, such attachment of self-assembled monolayers (SAMs), in order to functionalize the surface of the substrate. In this approach, functionalization of the surface is achieved using SAMs. SAMs molecules consist of an anchorage head that covalently bonds to the surface of the substrate, a hydrocarbon chain that provides the force (van der Waals interactions) for self-assembly of the molecules on the surface, and an active specie that interacts with the soluble species and promote nucleation and growth [162].

2.2 Tissue engineering scaffolds

The architecture of the scaffolds contributes to the specific biological function of the new tissue e.g. controls the delivery of nutrients and provides spatial organization to the growing cells [3]. The regeneration of the tissues is dependant on the porosity and pore size of the scaffold [163]. For example, high pore volume is required to accommodate and deliver cell mass necessary for tissue growth, deliver nutrients, diffusion of waste products, and vascularization necessary for any metabolic tissue [3]. High surface area of the scaffold also promotes cell attachment. The cell diameter in suspension dictates the pore size which differs from one cell type to another, therefore the pore size of the scaffold should be carefully controlled depending on the application [3]. In addition to adequate porosity, the pore structure should be interconnected to allow for nutrient delivery. Cells more than approximately 200 μm away from blood supply are metabolically inactive or die from lack of oxygen [164]. In addition to porosity and pore size, the shape and tortuosity of the scaffold affect the ingrowth of the cells [3]. Figure 2-11 shows the SEM picture of a calcium phosphate scaffold.

The scaffold should have enough mechanical strength to perform in shape of a macroporous implant and be able to retain its shape after implantation especially in case of load bearing applications [3]. The mechanical properties of the scaffold should also be in compliance with the tissue it is supposed to replace [3].

In addition to the material of the scaffold, the porous geometry of the scaffold has significant effect on the regeneration of the new bone [165-168]. However, having pores with the right diameter is not sufficient for bone regeneration. The porosity must have enough connectivity and also possess right orientation in order to be effective [169]. Therefore, a scaffold processing

method which can produce a scaffold with suitable composition and geometry is of significant importance.

One technique for scaffold fabrication is porogen (pore generator) leaching [170]. The key feature to porogen leaching is the processing of the polymer prior to porogen removal. Solvent casting of polymer solution around porogen, high pressure and temperature molding of the polymer, and extrusion of polymer/porogen composite are conducted in order to process the polymer around porogen [170]. In this strategy, noncovalent polymer interactions such as chain entanglement or hydrophobic interactions are responsible for polymer bonding around the porogen and therefore the mechanical integrity of the scaffold. Other fabrication techniques include: fiber bonding [171], phase separation [172], solvent casting and particulate leaching [173], membrane lamination [174], melt molding [175], polymer/ceramic fiber composite foaming [3], high-pressure processing [3], and hydrocarbon templating [176].

3 Scope and objectives

New materials synthesis techniques and different combination of materials are constantly being investigated to fabricate composites for TE with improved functionalities. Ceramic-polymer composites have been the center of much attention in order to overcome this challenge. Addition of calcium phosphate materials to polymers serves to improve the mechanical properties and add bioactive properties to polymers. New composite synthesis techniques need to be introduced in order to produce composites with improved properties which can fulfill the requirements of a functional scaffold.

The general objective of this work is development of a novel biomimetic synthesis process for the preparation of PPF-HAp composites. The process was developed for polymer-HAp systems in which the synthetic polymer (PPF) is not soluble in aqueous systems. This technique offers several advantages over conventional synthesis processes. Through this technique, we hoped to obtain a molecular level interaction between polymer and the ceramic component. Such interaction between the components of the composites is difficult to achieve using other composite processing techniques such as physical mixing of the polymer with the calcium phosphate filler. Agglomeration of nano particles during composite preparation is a major challenge in making composites with nanosize reinforcing particles. Consequently, the objective was to obtain composites with a homogeneous dispersion of nanoparticles using the proposed synthesis process. This process is also capable of incorporating pharmaceutically active components which would release upon degradation of the composite. Therefore, through this process (biomimetic synthesis), functional composites with improved mechanical performance and enhanced bioactivity could be produced to serve as bone TE scaffold. Moreover, investigating the interaction between PPF and the calcium phosphate phase, which is a major focus of this work, could contribute to the science of organic-inorganic interactions which has

recently been at the centre stage for the preparation of ceramics with improved functionalities and performances. This work also aimed to contribute to understanding of similar processes that occur during natural mineralization [17, 19].

Poly (propylene fumarate) has been chosen as the matrix due to its proven biocompatibility and biodegradability as well as its ability to photocrosslink. In order to add osteoconductive capabilities to this polymer calcium phosphate was chosen as the reinforcement (filler) phase.

An in-situ crystallization process, inspired by biomineralization of living tissues, was adopted in order to produce hydroxyapatite (HAp) reinforced PPF composite. Through this process, the HAp crystals nucleate and grow in the presence of PPF. Reports on the in-situ formation of HAp in the presence of other polymer matrices have shown that a molecular level interaction between the apatite crystals and the organic matrix can be produced. Such interaction between the two components of the composite is expected to improve the mechanical properties and degradation behavior of the final biodegradable composite.

Although biomimetic processing of composites has recently gained significant attention, it has been mostly focused on composites with natural polymers, such as collagen or water soluble synthetic polymers, such as poly acrylic acid, with low concentration of the organic molecules. In this work, the objective was to expand the biomimetic process to synthetic polymers that are not soluble in water and at the same time have shown significant potential to be used as bone implants. We believe that the advancement of this work could lead to innovative processing of composites including those with pharmaceutically active components. The understanding of the influence of the polymer on the nucleation and growth behavior of HAp is of critical importance

as it will enhance the control over the composite fabrication process and is therefore one of the major objectives of this work.

The specific tasks undertaken in order to achieve the above outlined objectives of the present study can be detailed as follows:

1. Investigation of the phase evolution of the calcium phosphate phase in the presence of an organic solvent such as tetrahydrofuran (THF) in comparison to an aqueous system.
2. Process development for the biomimetic synthesis of the HAp-PPF composite using a two-solvent (water- THF) system.
3. Refinement of the synthesis process of the composite by systematic investigation of the effect of the following parameters on the phase evolution of the apatite phase in the presence of PPF:
    - Synthesis time
    - Synthesis pH
    - Molecular weight of PPF
    - Concentration of PPF
4. Development of understanding of the PPF-HAp interactions during the biomimetic synthesis in the two-solvent system.
5. Examination of the feasibility of producing a scaffold by crosslinking the PPF in the composite around the calcium phosphate phase using UV irradiation

4 Experimental methodology

4.1 PPF polymer synthesis

All materials were used as received from the manufacturers. The PPF synthesis procedure was adapted from the work of Shung et al. [177]. In order to synthesize PPF, diethyl fumarate (Aldrich, Milwaukee, WI) was reacted with propylene glycol (Aldrich, Milwaukee, WI) in a three-necked round bottom flask with a ratio of 1:3. Hydroquinone (Alfa Aesar), a crosslinking inhibitor, and zinc chloride (Aldrich), a reaction catalyst, were added to the flask with the ratio of 0.003 and 0.01 to diethyl fumarate, respectively. Due to the high moisture sensitivity of zinc chloride, its 1M solution in ether was used in this process. A Vigreux distilling column was attached to the flask and the system was kept under nitrogen while stirring with a magnetic stir bar. The flask was then submerged in an oil bath and the initial temperature was set at 100°C. The temperature was then increased to 150°C in a period of one hour. At this temperature, diethyl fumarate reacts with propylene glycol to form a diester intermediate (bis(2-hydroxypropyl) fumarate) and releases ethanol as byproduct. The ethanol was removed from the system as a distillate. Upon the removal of 90% of the theoretical ethanol from the system, the flask was cooled down to 100°C and placed under vacuum. The temperature was then slowly (10°C/15 min) increased to 150°C. At this stage the diester intermediate went through a self-transesterification[†] process and propylene glycol was collected as a distillate. The molecular weight of the polymer is dependent on the time period that the polymer is kept at the final temperature. The reaction process is summarized in Figure 4-1.

[†] Transesterification is a reaction in which alkoxy group of an ester is exchanged with that of a higher alcohol to form a new ester.

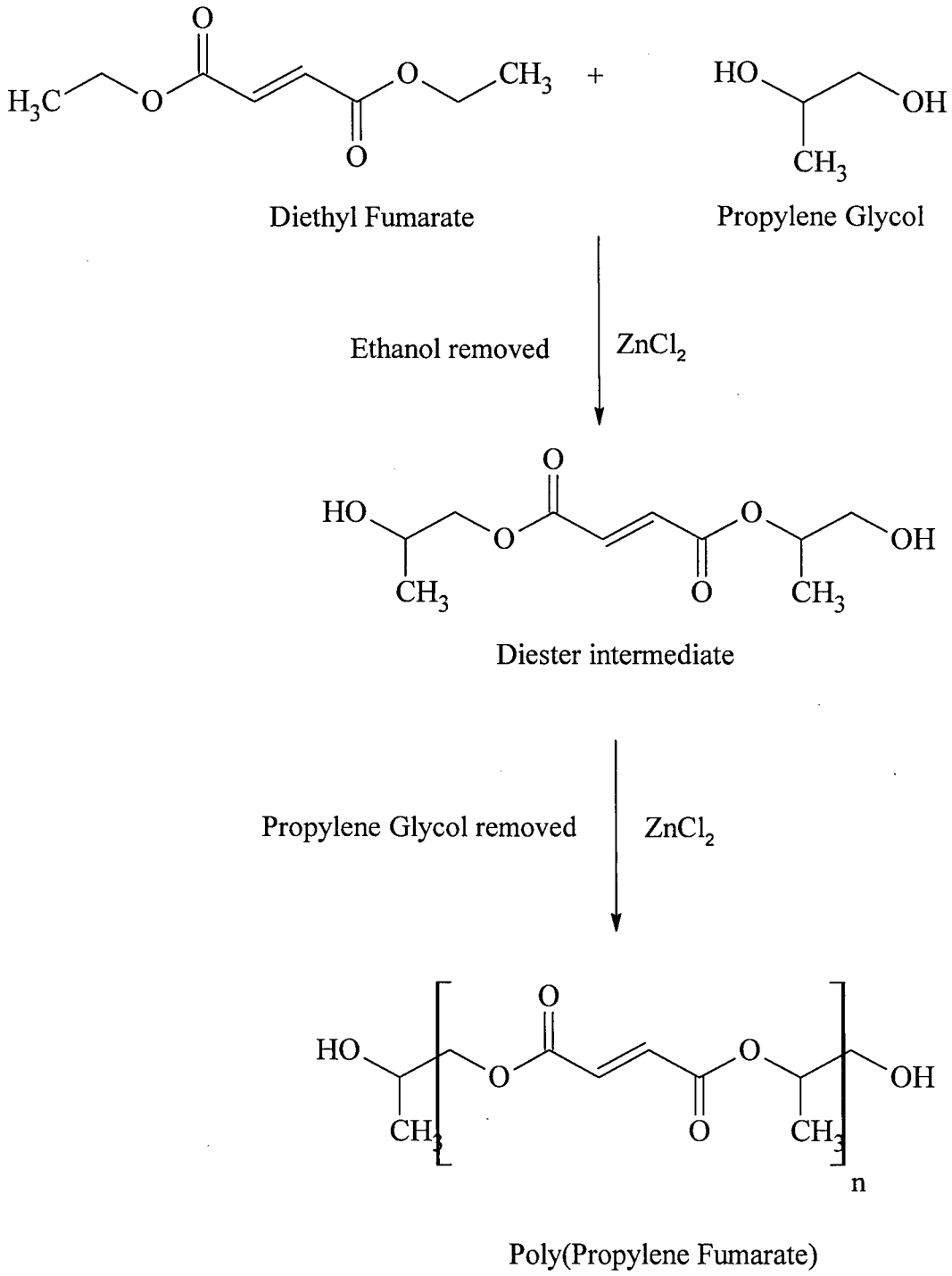

Figure 4-1 Reaction scheme for the step polymerization of PPF [179].

The polymer was then dissolved in methylene chloride (Fisher Scientific) and was subjected to a purification process. The methylene chloride solution of the polymer was washed with 1N HCl, water, and brine to remove zinc chloride and was then dried using sodium sulfate. The solution was then concentrated in a rotoevaporator. The concentrated polymer was precipitated in ethyl ether under stirring to remove hydroquinone and was then vacuum dried to remove any entrapped solvent. The resulting polymer was a yellow, clear, and viscous liquid. Gel permeation chromatography followed in order to estimate the molecular weight of the polymer.

The molecular weight of the polymer depends on the time period that the polymer is kept at the final temperature under vacuum. Three sets of polymers with different molecular weights (low, medium, and high) were prepared during the course of this research. The specifications of these polymers are listed in Table 4-1.

Table 4-1 Specifications of the polymers synthesized during the course of this research. M_n is the number average molecular weight and M_w is the weight average molecular weight of the polymers.

Polymer	Synthesis time(hrs)	M_n (g/mol)	M_w (g/mol)
LMw	3	930	1800
MMw	8	1500	3100
HMw	15	2600	4500

4.2 PPF-HAp Composite synthesis

4.2.1 Composite processing

Tetrahydrofuran (THF) (Fisher Scientific) was used as solvent to calcium nitrate (Fisher Scientific) and PPF while aqueous solution of ammonium dihydrogen phosphate (Fisher Scientific) was used as a source of phosphorous. A 0.65 M[‡] solution of calcium nitrate in THF solution was prepared (e.g. 1.7g $Ca(NO_3)_2.4H_2O$ in 11 ml THF). Aqueous solution of 0.22 M of ammonium dihydrogen phosphate (e.g. 0.5 g of $NH_4H_2PO_4$ in 19.25 ml water) was also prepared.

The theoretical weight of HAp that would be produced using the above reagents was calculated using the following equation:

$$3\ NH_4H_2PO_4 + 5\ Ca\ (NO_3)_2 + 7\ NH_4OH \rightarrow Ca_5(PO_4)_3(OH) + 10\ NH_4NO_3 + 6\ H_2O \qquad (4\text{-}1)$$

The amount of PPF for each composition was calculated using the ratio of the amount of PPF to the amount of theoretical HAp calculated from the equation 4-1. For example, 1.7 g $Ca(NO_3)_2.4H_2O$ and 0.5 g of $NH_4H_2PO_4$ produce 0.7 g of HAp, therefore for a composition with PPF:HAp=4, 2.8 g of PPF in 18 ml THF was prepared. PPF solution in THF was added to the calcium nitrate solution. The calcium nitrate-PPF solution was stirred for 15 minutes and was then made alkaline using 5 N ammonia water solution to increase the pH to the desired value (7.6, 8.8, or 10). Aqueous solution of 0.22 M of ammonium dihydrogen phosphate (e.g. 0.5 gr of $NH_4H_2PO_4$ in 19.25 ml water) was added to the above solution while stirring (this mixture will be referred to as composite mixture hereafter). The ratios of Ca:P=1.66 and THF:water=1.5 was the same for all the samples. The stirring rate of the composite mixture was similar for all the

[‡] Various calcium and phosphate concentrations with log (T_{ca} T_p) in the range of -1 to -3 were examined which returned similar results. Therefore, this particular concentration was chosen consistently throughout the experiments.

samples that were investigated in this research (1200 rpm). A Metrohm pH stat device (consisting of 614 impulsomat, 620 pH-meter, and 645 multi-dosimat, Metrohm Ltd., Switzerland) was used to keep pH constant during the experiment by the addition of ammonium-water solution. Figure 4-2 shows the picture of the pH stat device and its components that was used throughout this research project. The settings of the pH stat device were similar for all the samples.

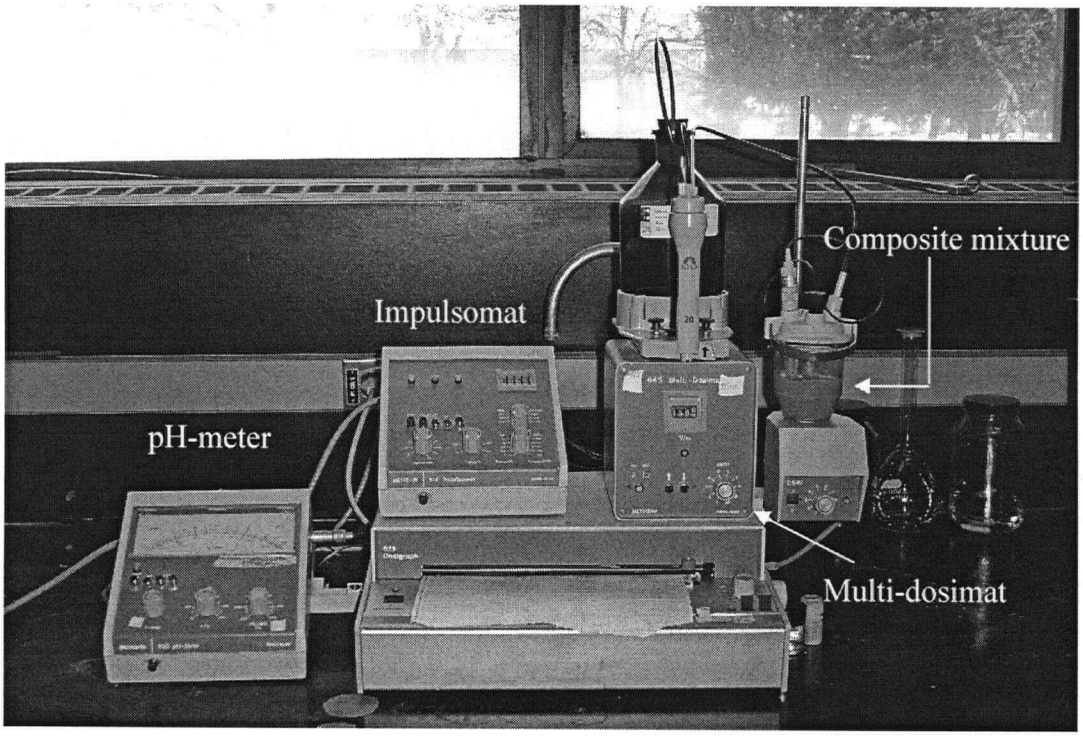

Figure 4-2 Picture of the pH-stat device that was used for composite synthesis.

Upon the completion of the synthesis time the composite mixture was vacuum filtered using Whatman #1, 9 cm filter paper, and washed with distilled water in order to wash out soluble salts such as ammonium nitrate. The filter cake was then air dried and ground in preparation for characterization procedures. The powder will be referred to as composite powder hereafter. The flow chart of the composite synthesis process is presented in Figure 4-3.

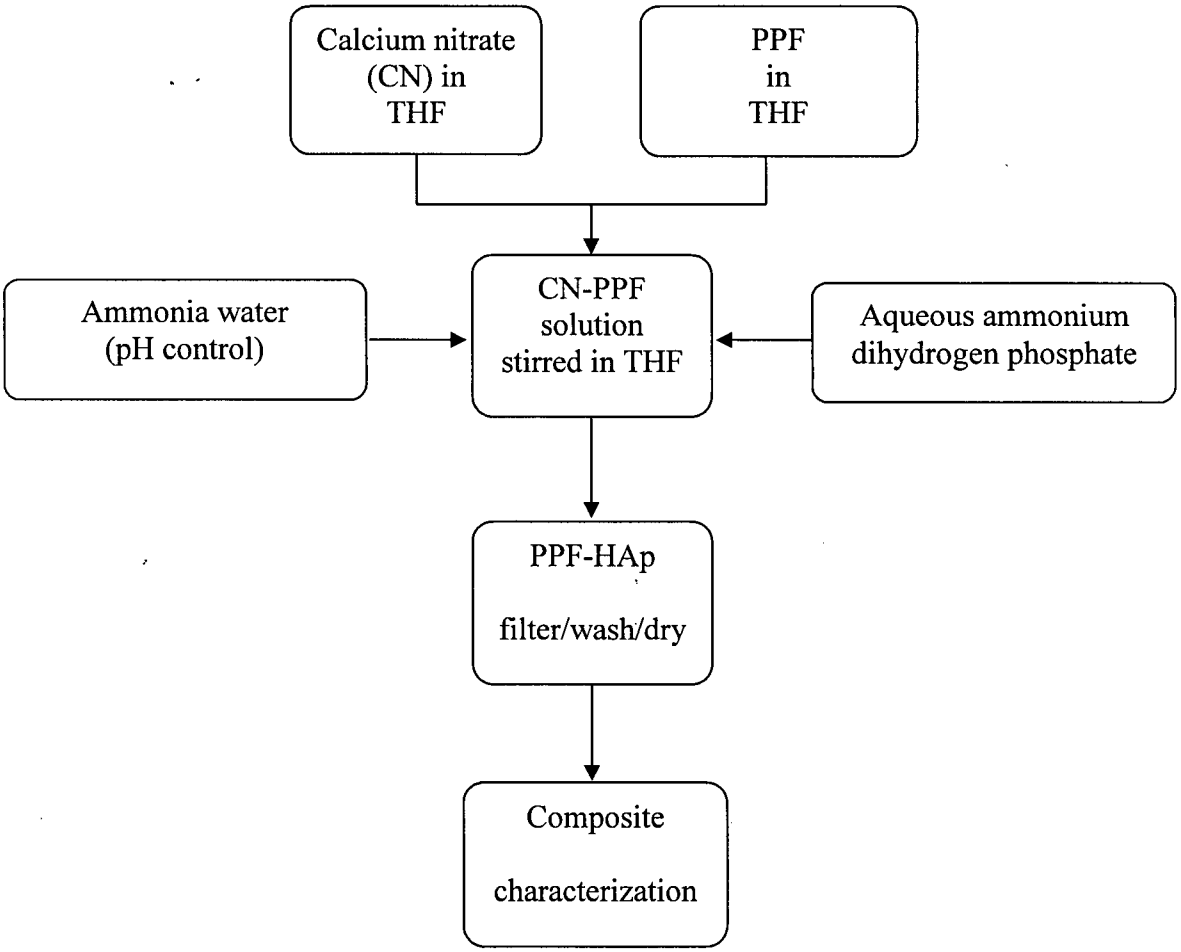

Figure 4-3 Flow chart of the composite synthesis process.

4.2.2 Effect of the solvent

In order to investigate the effect of THF on the phase formation of HAp and also to decouple the effect of the solvent from that of the PPF, a water-based and a THF-based system were compared. Water-based HAp powder was prepared in a similar procedure as the one depicted in Figure 4-3 where no polymer was added to the system and calcium nitrate was dissolved in water rather than THF. In case of the THF-based HAp powder, no polymer was added and the calcium

nitrate was dissolved in THF. The pH of the composite mixture was 10 for both systems and was kept constant throughout the experiment. Aliquots of the composite mixture were taken (in both cases) at the periods of 1min, 1hr, 3, 6, 11, and 24 hrs for characterization. The experiments were repeated three times in order to evaluate reproducibility.

4.2.3 Phase evolution of calcium phosphate in the presence of PPF

In order to monitor the phase evolution of the apatite phase in the presence of PPF, composite mixture with theoretical PPF (HMw):HAp =4 was prepared at pH=10. The mixture was stirred at room temperature for a period of 24 hours. Time zero is the time when the aqueous solution of the ammonium dihydrogen phosphate is added to the mixture of calcium nitrate and polymer in THF and pH is increased to 10. Aliquots of the composite mixture were taken from the mixture at 1min, 1, 3, 6, and 24 hrs after time zero.

4.2.4 Effect of pH

Composite powders with the theoretical PPF (HMw):HAp=4 were prepared according to the procedure depicted in Figure 4-3 under three pH values of 7.4, 8.8, and 10. Synthesis time was 1 hr for all the samples.

In order to investigate the effect of pH on the polymer alone, PPF was dissolved in THF and pH was increased to the values of 7.4, 8.8, and 10 using 5N ammonium water. The samples were stirred for 1 hr before characterization.

4.2.5 Effect of PPF molecular weight

In order to examine the effect of molecular weight of the polymer on the interaction between HAp and PPF, PPF with different molecular weights were used to prepare composite samples. Diethyl fumarate (DEF), the precursor of PPF, was also used to depict the lowest molecular weight possible. Composites were also prepared with LMw and HMw PPF as listed in Table 4-1. All composites were synthesized following the procedure described in Figure 4-3 with the PPF/DEF:HAp=4, pH=10 and after 1 and 24 hours of synthesis.

4.2.6 Effect of PPF concentration

In order to investigate the effect of the polymer concentration on the phase evolution of HAp, composites with PPF(MMw):HAp=0.05 (5 wt%), 1 (50 wt%), 4 (80 wt%), and 19 (95 wt%) were prepared. All samples were produced according to the procedure summarized in Figure 4-3 at pH=10. Samples were collected after 1 and 24 hours of stirring for the 5 and 80 wt% samples. The other samples were examined after 24 hours of stirring.

4.3 UV crosslinking

PPF and composite (PPF(MMw):HAp=4, after 24 hrs synthesis at pH=10) samples were crosslinked using photoinitiator bis(2,4,6-trimethylbenzoyl) phenylphosphine oxide (BAPO, Ciba Specialty Chemicals) and following the work of Fisher et al. [20]. BAPO with the ratio of mg BAPO/g (DEF+PPF)= 5 was first dissolved in DEF (g DEF/g PPF=0.5). The above solution was then added to the PPF/composite to produce a mixture. The mixture was then injected into a cylindrical glass vials (6.5mm x 40mm) using a 5ml syringe. The glass vials were then centrifuged for 5 minutes at 3000 rpm to remove any air bubbles trapped inside the samples. The samples were placed inside a CEX-1500 Ultralum UV crosslinker (Rose Scientific Ltd.

Edmonton, Alberta). The UV box was outfitted with four 15W UV lamps and the walls reflect the UV light. The total light emission covers a range of UV wavelengths (320–405 nm), with a peak at 365 nm and an intensity of approximately 2 mW/cm^2. For the first 5 minutes of the crosslinking the samples were placed vertically, later the samples were placed on their sides and were elevated slightly from the floor so that the UV light can penetrate the samples from all sides. After 30 minutes of crosslinking the samples were removed from the UV box and the glass vials were broken and removed. The crosslinked samples were polished to have the diameter: height ratio of 2 (6.05 mm x 12 mm) and to produce two parallel flat surfaces (Figure 4-4).

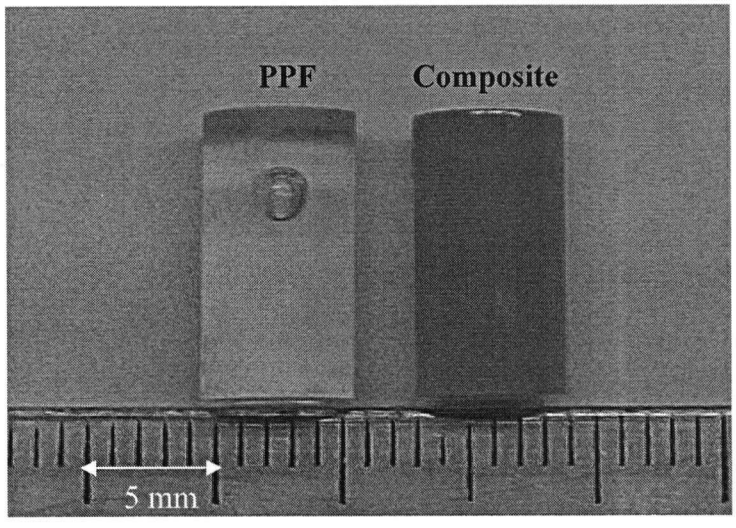

Figure 4-4 Picture of the UV crosslinked samples.

4.4 Characterization techniques and procedures

4.4.1 X-ray diffraction analysis (XRD)

X-ray diffraction analysis (XRD) was done using a Siemens D5000 powder X-ray diffractometer operated at 40 kV and 30 mA (X-ray: CuKα). All the samples were examined in the powder

form from $2\theta=20^{o}$ to $2\theta=40^{o}$ with the scan rate of 0.6 °/min. Powder samples were placed in a sample holder and were then exposed to the incident beam.

4.4.2 Fourier-transform infrared spectroscopy (FTIR)

Fourier-transform infrared spectroscopy was done on a Perkin Elmer, system 2000, FT-IR over the wavenumber range of 4000-370 cm^{-1} with the resolution of 1 cm^{-1}. 2 mg of the powder sample was carefully mixed with 400 mg of warm desiccated KBr powder (Fisher scientific, infrared grade) and was then placed in a stainless steel die and was pressed into a pellet using hydraulic press. The axial pressure was increased slowly to a maximum of 15 tons and was held at that pressure for a period of 3 minutes and was then released to atmospheric pressure. The pellet was then placed in a sample holder and was put in the spectrometer.

Liquid samples were examined using ASI ReactIR (2000) over the wavenumber of 4000-500 cm^{-1}. The liquid samples were placed in a glass tube which would fit under the IR probe. The probe was thoroughly cleaned in preparation for each sample.

4.4.3 Scanning electron microscopy (SEM)

Structural and morphological observations were performed on scanning electron microscope (SEM), Hitachi S3000N at a voltage of 20 kV. Samples were placed on a stub using a carbon sticker and were examined under the microscope after the samples were sputtered with gold in order to improve the conductivity of the samples.

4.4.4 Transmission electron microscopy (TEM)

Powder samples were examined under a Hitachi H-800 transmission electron microscope (TEM) operated at 100 kV. Samples were first suspended in methylene chloride (Fisher) and were sonicated for 15 minutes. A drop of the suspension was placed on a carbon coated copper grid and was left to air dry. The grid was then placed on the sample holder and was inserted into the microscope. Selected area diffraction (SAD) pattern of the samples were also obtained to further characterize the phases present in the samples and to investigate their crystallinity.

4.4.5 Thermal gravimetric analysis (TGA)

Thermal gravimetric analysis (TGA) was conducted using a SETARAM TGA 96 with the heating rate of 10°C/min from room temperature to 1100°C in argon environment. The THF-based HAp powder and composites prepared with DEF, LMw, and MMw PPF with the ratio of DEF/PPF:HAp=4 plus the MMw PPF were examined.

4.4.6 Electrokinetic sonic amplitude (ESA) measurements

Electrokinetic sonic amplitude (ESA) measurements were done on a zeta probe analyzer (Colloidal Dynamics, Warwick, RI). ESA occurs when an alternating electric field with known frequency and amplitude is applied to a suspension of fine, charged particles. This causes the electrically charged colloidal particles in the suspension to oscillate backwards and forwards and so generate a sound wave of the same frequency. It is this sound wave which is picked up by a transducer and analyzed to calculate the motion of the particles. As the particles oscillate in the applied electric field, the dynamic mobility/zeta potential of the particles is determined by the magnitude of the particles motion. ESA is related to dynamic electrophoretic mobility of the particles and is expressed as follows:

$$ESA(\omega)=\mu_d(\omega)c\Delta_p\Phi G_f \qquad (4\text{-}2)$$

Where $\mu_d(\omega)$ is the dynamic mobility, c is the speed of sound in the solvent, Δ_p is the difference between the density of the particles from that of the solvent, Φ is the volume fraction of particles, G_f is related to the geometry of the electrode and ω is the angular frequency of the applied field [178,179]. The dynamic mobility is related to the size of the particles and the particle charge (through zeta potential) [180]. For particle concentration for up to 5% the following relationship between the dynamic mobility and zeta potential can be drawn:

$$\mu_d=2\varepsilon\zeta/3\eta\, G(a,\omega)[1+f] \qquad (4\text{-}3)$$

where ε is the dielectric permittivity, ζ is zeta potential, and η is the viscosity of the suspension medium. Both G and f are complex functions. G depends on the particle size, a, and the measuring frequency ω.

Oscillation of small, sub micron particles follows the frequency of the field while larger particles lag behind the applied field. This effect significantly affects the dynamic mobility of the particles. As our suspension contained some coarse particles, for which the effect of inertia is significant, it was decided to report only the ESA rather than zeta potential.

ESA was measured as a function of pH on 0.02 g/lit suspension of the powder in 0.005 g/lit NaCl solution in distilled water. The suspension was sonicated for 15 minutes before measurements. The pH titration was done with 1N HCl and 1N NaOH. The pH probe and the

analyzer were thoroughly calibrated before the measurements. The effect of the background was automatically subtracted.

As ESA is directly proportional to the surface charge of the particles, measuring ESA of HAp powder produced with or without PPF provided information regarding the effect of PPF on the surface charge of the calcium phosphate particles.

5 Result and discussion[§]

5.1 Phase evolution of HAp in organic solvent

The two-solvent system protocol for biomimetic processing of organo-ceramic composites, in particular the PPF-HAp composites is reported in this work for the first time. In order to investigate the effect of the organic solvent on the HAp phase evolution and to distinguish between the effects of the solvent from that of the polymer, the phase evolution of HAp in the presence and absence of THF was investigated.

Figure 5-1 (a-f) shows the XRD spectra of the samples taken from a THF-based system after 1min, 1, 3, 6, 11, and 24 hrs of reaction, at pH=10. As can be observed from the spectra, brushite (dicalcium phosphate dihydrate, DCPD, $CaHPO_4 \cdot 2H_2O$) precipitates at the early stages of reaction. Brushite peaks observed in all the spectra are in agreement with the (JCPDS 9-77) for the synthetic brushite. In addition to the brushite peaks two broad peaks centered at $2\theta = 26^\circ$ and 32° are also present in the spectra (Fig 5-1a). These broad peaks can be attributed to a poorly crystalline apatite. As the reaction proceeds the intensity of the apatite peaks increases at the expense of the brushite peaks, suggesting a phase transformation from brushite to apatite. After 24 hrs of reaction brushite peaks are no longer observed and only broad HAp peaks (as in JCPDS 9-432) are present. It has been reported earlier that the brushite to apatite transformation occurs through the dissolution of the brushite phase and precipitation of HAp [181, 182]. Therefore, it is reasonable to believe that the reduction in the peak intensity of brushite is due to its dissolution and reprecipitation in form of apatite as evidenced by the relative increase in apatite peak intensity.

[§] Part of the results presented in this chapter are published. Hakimimehr D, Liu DM, Troczynski T. In-situ preparation of poly(propylene fumarate) - hydroxyapatite composite. Biomaterials 2005; 26 (35): 7297-7303.

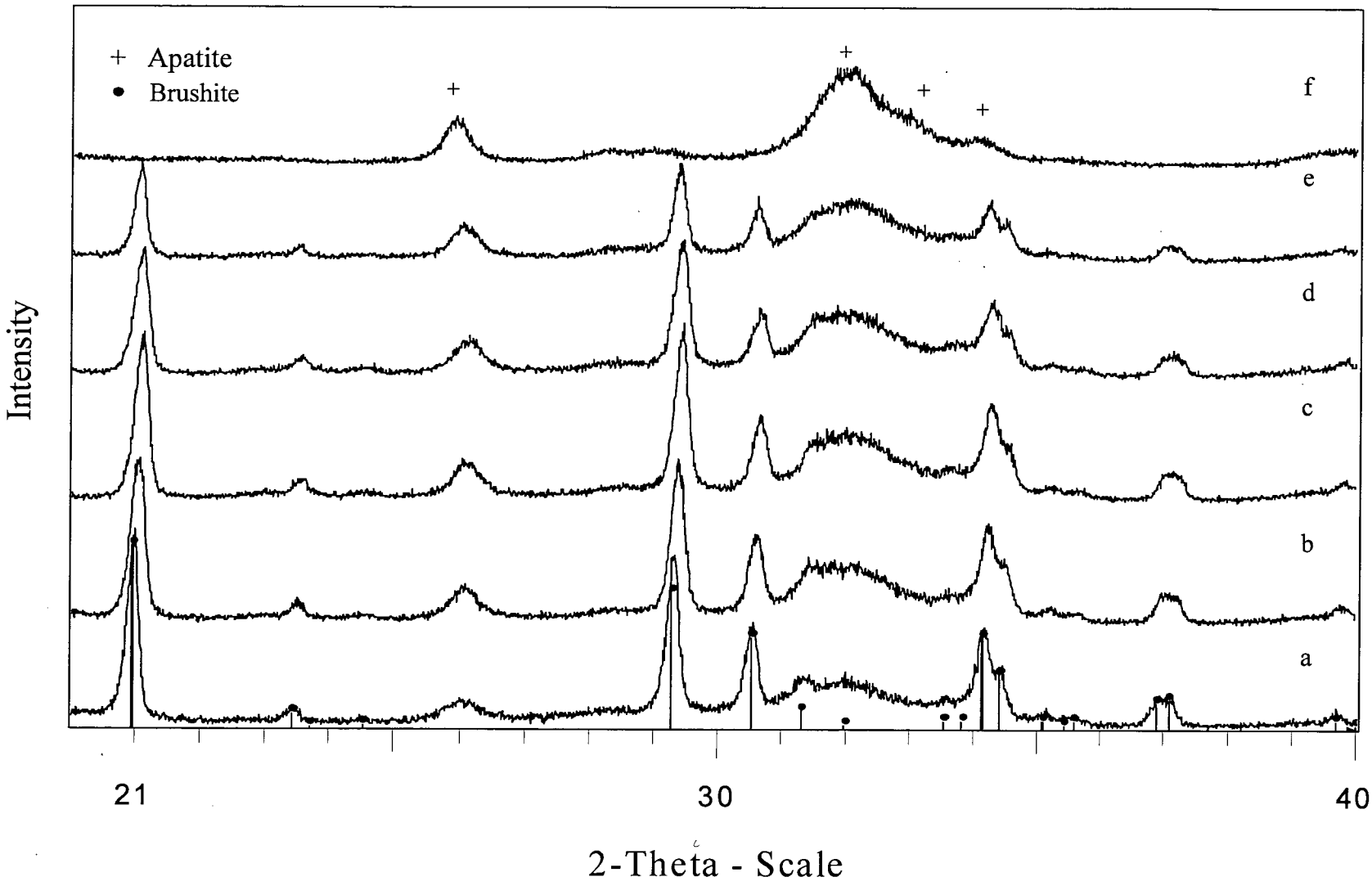

Figure 5-1 X-ray diffraction pattern of THF-based system prepared at pH=10 and after (a) 1min, (b) 1 hour, (c) 3 hours, (d) 6 hours, (e) 11 hours, and (f) 24 hours of synthesis time. The lines and dots show brushite diffraction peaks and plus signs mark apatite peaks.

The apatite peaks observed after 24 hours (Figure 5-1f) of reaction are relatively broad. It is possible that during the precipitation process appreciable amount of substitute ions (such as carbonate ions) are trapped into the crystal structure which causes the broad appearance [183]. Small (in nanometer range) crystal size also contributes to such peak broadening. This will be further confirmed through TEM studies in Chapter 5.7.

Figures 5-2 a-f show the FTIR spectra of the THF-based samples after 1min, 1, 3, 6, 11 and 24 hrs of preparation. Absorption peaks observed at around 3531 cm^{-1} 3477 cm^{-1}, 3269 cm^{-1}, and 3151 cm^{-1} of the sample prepared after 1 min of reaction (i.e. mostly brushite) are due to the intermolecular weakly bonded OH associated with the water of crystallization [183]. Peaks at around 2351 cm^{-1} and the shoulder observed around 1722-1704 cm^{-1} are due to HPO_4^{-2} [183]. Peak at 1645 cm^{-1} is due to H-O-H bending [183]. Absorption peaks at 1024 cm^{-1} and 1135 cm^{-1} are due to P=O associated stretching while the peak at 1060 cm^{-1} is because of P=O stretching. P-O-P asymmetric stretching gives rise to the peaks observed at 984 cm^{-1}, 961 cm^{-1}, 871 cm^{-1}, and 777 cm^{-1} and (H-O-)P=O causes the peak at 643 cm^{-1}[183]. Peaks at 598 cm^{-1}, 557 cm^{-1}, and 521 cm^{-1} are again due to acid phosphates [183]. Multiple peaks observed in the region of 600-500 cm^{-1} and 1100-1000 cm^{-1} confirm the good crystallinity of the brushite phase as observed earlier in the X-ray patterns. The brushite spectrum reported here is in excellent agreement with what is reported in literature [181]. The FTIR spectra of the samples prepared up to 11 hours of synthesis do not show any significant difference with the 1 min sample (Figure 5-2 b-e).

Figure 5-2f is the FTIR spectrum of the THF-based sample after 24 hours of reaction. Absorption bands at 465, 560, and 602 cm^{-1} are the ν_4 bending modes of PO_4 and the peaks at 960 and 1040 cm^{-1} are due to the ν_1 and ν_3 stretching mode of PO_4 [78]. Peaks observed in the 1500-1400 cm^{-1} region together with the sharp peak at 870 cm^{-1} arise due to the presence of

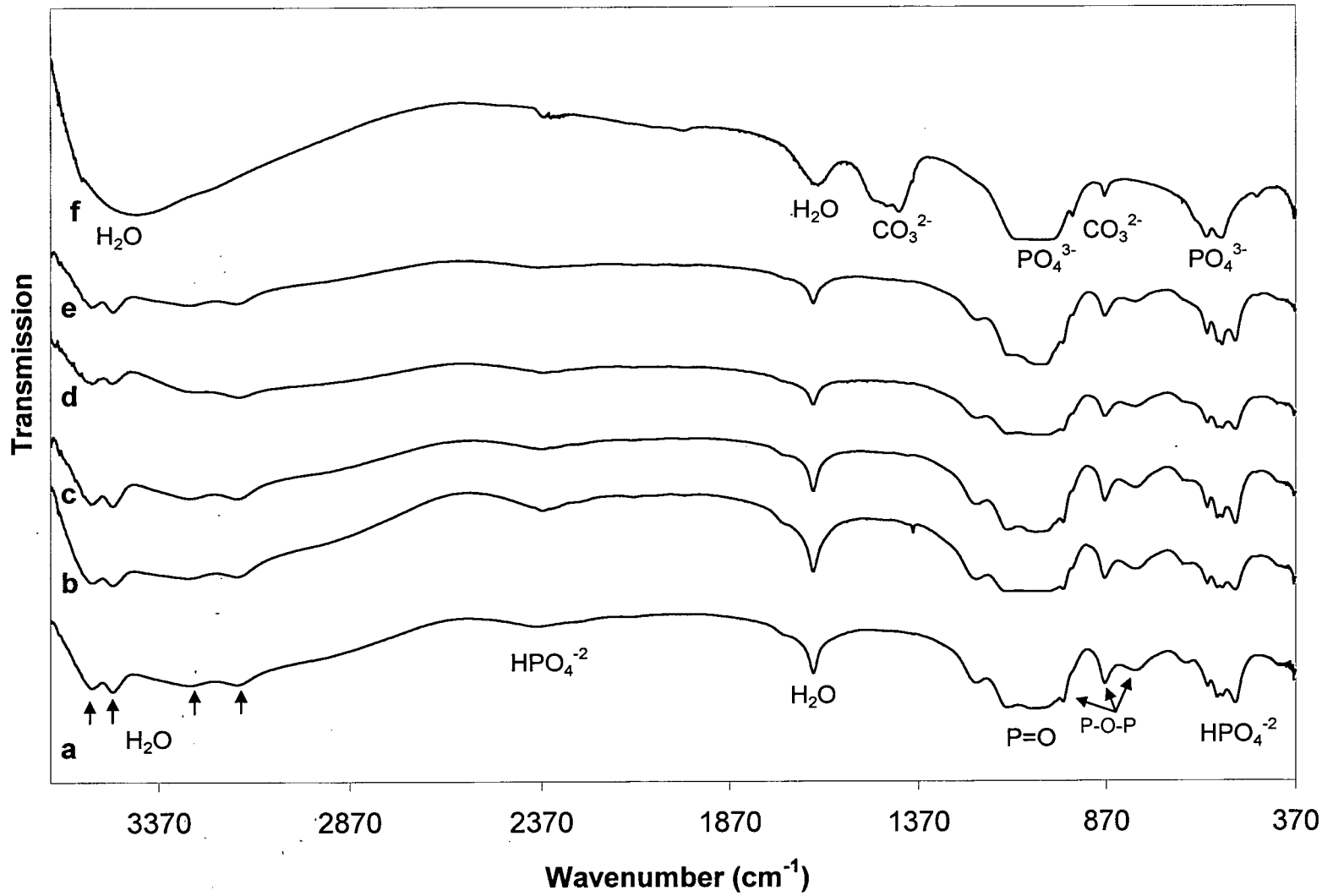

Figure 5-2 FTIR Spectra of a THF-based sample prepared at pH=10 and after (a) 1 min, (b) 1 hour, (c) 3 hrs, (d) 6 hours, (e) 11 hours, and (f) 24 hours of synthesis time.

carbonate ion (CO_3^{2-}) [78, 184]. The carbonate ion has dissolved in the system (through the dissolution of CO_2) from the surrounding air during the preparation of the samples, as also found by other investigators [78, 184]. The peak at around 3412 cm^{-1} is due to the asymmetric and symmetric stretching vibrations of H-O-H while the peaks in the 1650-1600 cm^{-1} region are due to the bending vibration of H-O-H [78, 184]. Absence of the bands at 525 and 1105 cm^{-1} distinguishes this compound from octacalcium phosphate [78] and together with the XRD result is an evidence of its apatitic nature. The HAp peak broadening observed in the XRD patterns (Fig 5-1) is partly due to the incorporation of carbonate ions (most probably for PO_4^{3-} ions) and partly due to the small HAp crystal size. It has been repeatedly reported that the carbonated apatite has a broader XRD peak compared to that of the non carbonated samples as such substitution produces smaller HAp crystals [75, 89]. Also due to substitution of CO_3^{2-} ions for PO_4^{3-} ions a significant distortion of the HAp structure would occur [75, 89]. This is due to the fact that the CO_3^{2-} ions are different in size, shape, and charge of those ions they replace which will in turn induce a structural distortion within the HAp crystals.

Figure 5-3(a-g) shows the XRD analysis of the water-based samples for 1 min to 48 hours of synthesis time. Similar to what was observed in case of THF-based samples, brushite initially precipitates and further transforms to HAp after ~24 hours of reaction. The HAp peaks observed after 24 hours of reaction (Fig 5-3f and g) are also broad in nature which can again be attributed to the presence of the carbonate ions and their small crystal size.

As explained in Chapter 2.1.4.1, during the precipitation of calcium phosphates from supersaturated solutions, due to kinetic factors, thermodynamically unstable phases may form at the early stages of precipitation. As the saturation of the solution decreases the metastable phases gradually dissolve and a more stable phase precipitates. This is despite the fact that HAp is the

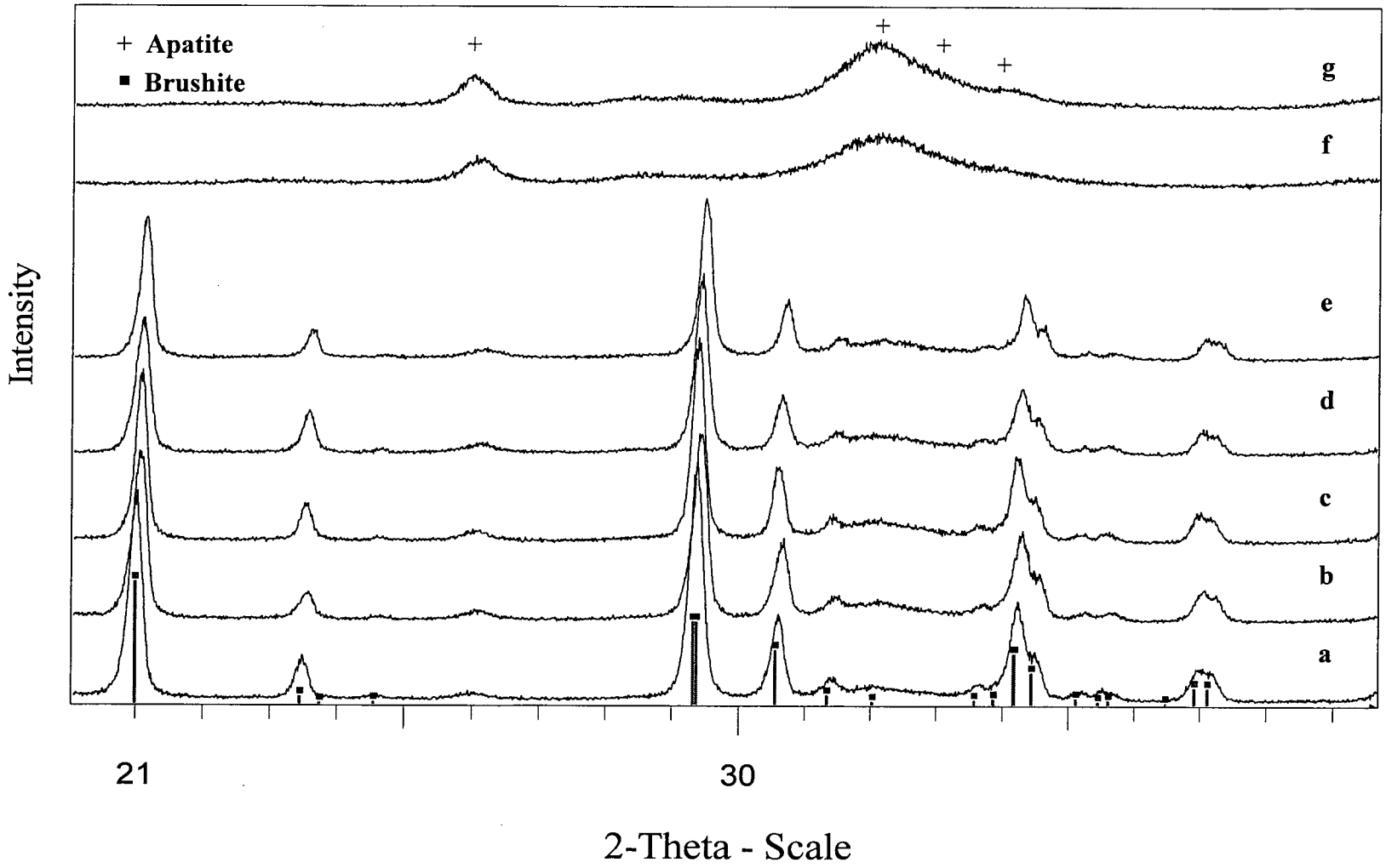

Figure 5-3 X-ray diffraction pattern of water-based system prepared at pH=10 and after (a) 1 min, (b) 1 hour, (c) 3 hours, (d) 6 hours, (e) 11 hours, (f) 24 hours, and (g) 48 hours of synthesis time. The lines show brushite diffraction peaks.

most thermodynamically stable calcium phosphate in the pH range investigated in this study. The calculated product log of the total calcium and phosphate concentrations in the system studied here (log $T_{ca}xT_p$= -1.47) is a point on line C on Fig. 2-2 (on page 14). It is observed that the precipitating solution is saturated with respect to all the calcium phosphates at pH above 7. As DCPD (brushite) has the highest solubility product constant compared to other calcium phosphate phases [52, 57], it is reasonable to observe brushite as the first phase to precipitate. As DCPD is thermodynamically unstable at the studied conditions, it further dissolves and hydroxyapatite forms after ~24 hours of aging time. The dissolution of the brushite phase and precipitation of the apatite phase is well indicated by the reduction in the intensity of the diffraction peaks of the brushite phase and respective increase of HAp peak intensity with time.

Previous studies on the effect of the organic solvents on the precipitation of calcium phosphates have shown contradictory results. Some investigators have found that organic solvents such as ethanol stabilize the amorphous calcium phosphate phase [111], while others have seen promotion of crystallinity of the HAp phase in the presence of ethanol [110]. However, X-ray diffraction and FTIR studies conducted in this work suggest that the presence of THF in the calcium phosphate solution used in this work does not significantly affect the phase evolution of the apatite phase. In both THF and water-based systems, brushite initially precipitates and further transforms to a poorly crystalline HAp, the crystallinity of which improves over a 24 hour time period.

Although no previous work on the comparison of the effect of supersaturation and that of an organic solvent is available, the combined effect of these two factors might explain the above phenomenon.

Tung et al. [110] explained that presence of ethanol in the calcium phosphate solution increases the supersaturation of the system in regards to the precipitating phases and therefore increases the rate of precipitation. At the same time as ethanol in the system reduces the solubility of the ACP phase, it retards the ACP to HAp transformation. In the case of the system studied here, the supersaturation of the system is significantly high in regards to the brushite phase, regardless of the presence of THF (refer to Fig 2-4). Therefore, the effect of THF on the brushite precipitation in this system might have been overshadowed by the high initial concentration of the precursors in the solution (demonstrated in Figure 2-4). Similarly, due to the high saturation of the system, brushite is stabilized for more that 11 hours in both aqueous and THF-based systems and therefore the effect of THF on the phase evolution of the calcium phosphate is not observed.

5.2 Phase evolution of calcium phosphate in the presence of PPF

Figure 5-4A shows the FTIR spectra of the samples taken from the composite solution (PPF(HMw):HAp=4) after 1min, 1, 3, 6, and 24 hours of synthesis time. In all the spectra presented, absorption bands at 663, 770, 834, 975, 1018, 1074, 1112, 1151, 1222, 1252, 1290, 1383, 1448, 1642, 1710, and between 3100-2800 cm^{-1} belong to PPF, as marked in the figure [177]. The 600-450 cm^{-1} region bears the v_4 bending modes of PO_4^{3-}. PO_4^{3-} absorption bands in 1100-960 cm^{-1} are overlapped by the PPF absorption bands in this region and therefore are not distinguishable.

Figure 5-4B magnifies the 600-450 cm^{-1} region of the spectra depicted in Fig. 5-4A. Sample taken after 1min shows a broad band stretching between 630 and 500 cm^{-1}. With time the broad band remains unchanged. Even after 24 hours of synthesis the broad pattern between 630 and 500 cm^{-1} persists.

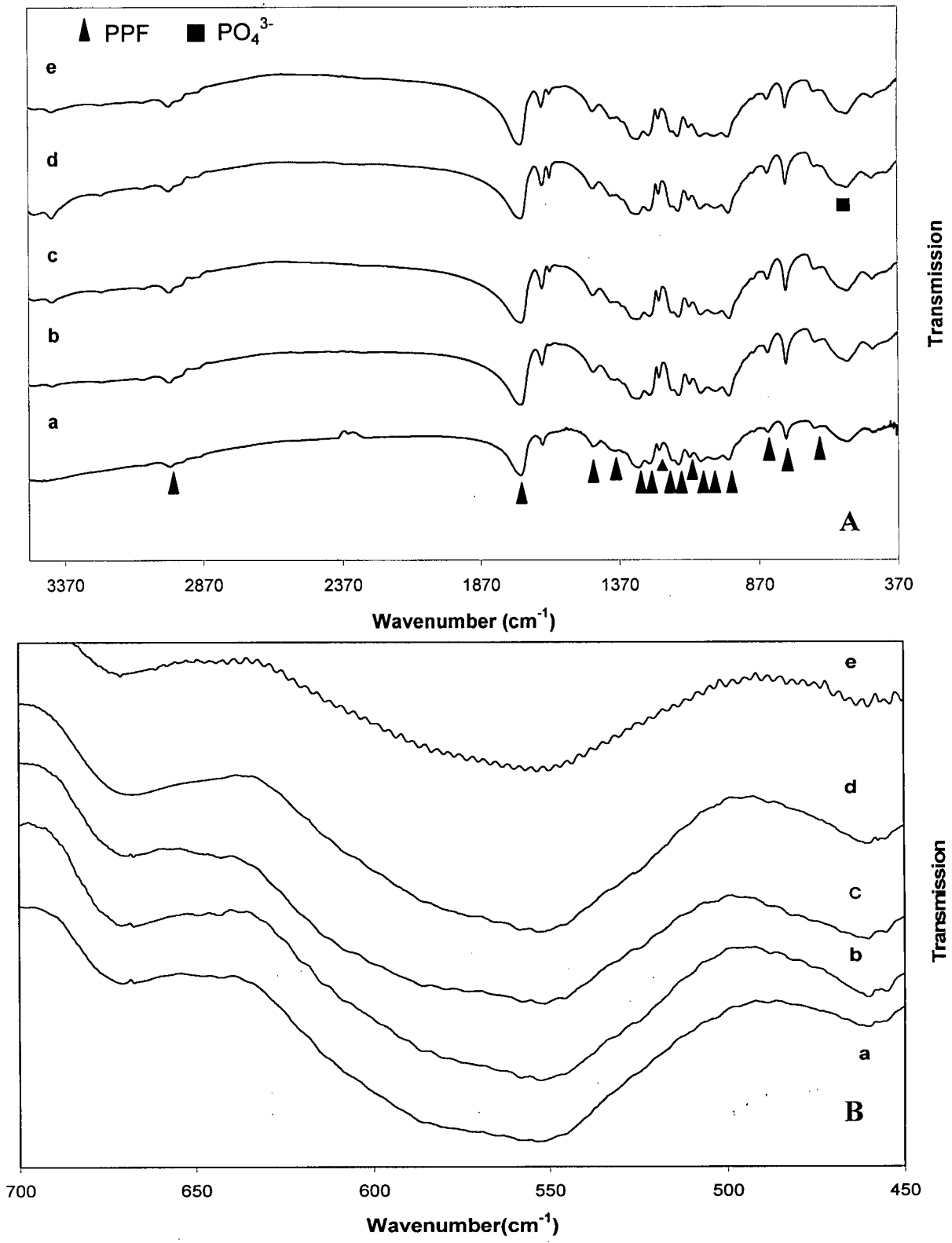

Figure 5-4 A: FTIR spectra of the composites prepared at pH=10 after (a) 1 min, (b) 1 hour, (c) 3 hours, (d) 6 hours, and (e) 24 hours of synthesis. B: FTIR spectra of the same samples as A in the 700-450 cm^{-1} region.

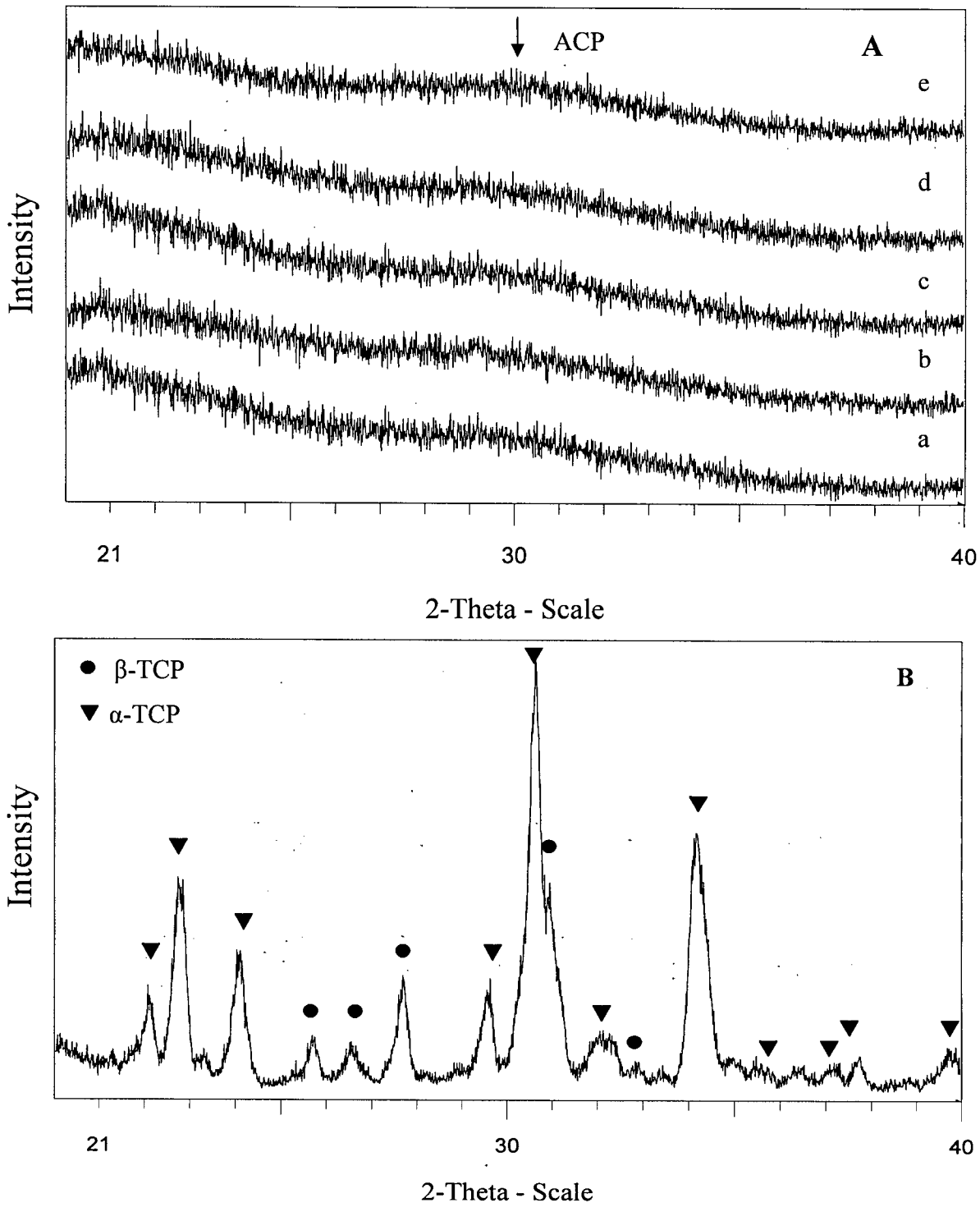

Figure 5-5 A: X-ray diffraction patterns of the composites prepared at pH=10 after (a) 1 min, (b) 1 hour, (c) 3 hours, (d) 6 hours, and (e) 24 hours of synthesis. B: XRD pattern of the sample in (e) after heat treatment at 800 °C for 1 hour.

Figure 5-5A shows the XRD patterns of the samples after 1min, 1, 3, 6, and 24 hr of synthesis time, at pH=10. All samples regardless of synthesis time show only a very broad peak stretching between 2θ=26-34° centered at about 2θ=30°, characteristic of ACP [160, 185]. Figure 5-5B shows the X-ray diffraction pattern of the sample prepared after 24 hour of synthesis time and heat treated in air at 800°C for 1 hour. As observed in this figure the composite has decomposed to α- and β-tricalcium phosphate (JCPDS 9-348 and 9-169, respectively), which is also characteristic of ACP [73, 78].

Figure 5-6 compares the FTIR spectra of the samples prepared at pH=10, after 1 hr in the presence and absence of PPF, in the 700-450 cm^{-1} region. While a well crystalline brushite phase is present in the absence of polymer (also evidenced by XRD), in the presence of the polymer only a broad band stretching between 630-500 cm^{-1} is present suggesting an amorphous phase. Figure 5-7 compares the FTIR spectra of the samples after 24 hr synthesis time in the presence and absence of polymer, in the 700-450 cm^{-1} region. While the sample prepared in the absence of polymer shows clear and resolved peaks of HAp, sample prepared in the presence of polymer shows only a broad band stretching between 630-500 cm^{-1}, suggesting the presence of ACP. This observation is also confirmed by the XRD data of the same samples (Figure 5-8). The spectrum of the apatite with no PPF clearly shows all the peaks related to hydroxyapatite (JCDPS 9-432) while the spectrum of the composite sample shows a broad peak stretching between 2θ = 25° to 35° centered at about 2θ=30° characteristic of ACP [186, 187].

The above FTIR and XRD results suggest that in the presence of polymer (PPF(HMw): HAp=4) an amorphous calcium phosphate (ACP) forms initially and remains stable throughout the experiment (up to 24 hours). Unlike the THF-based system in the absence of polymer (Figures

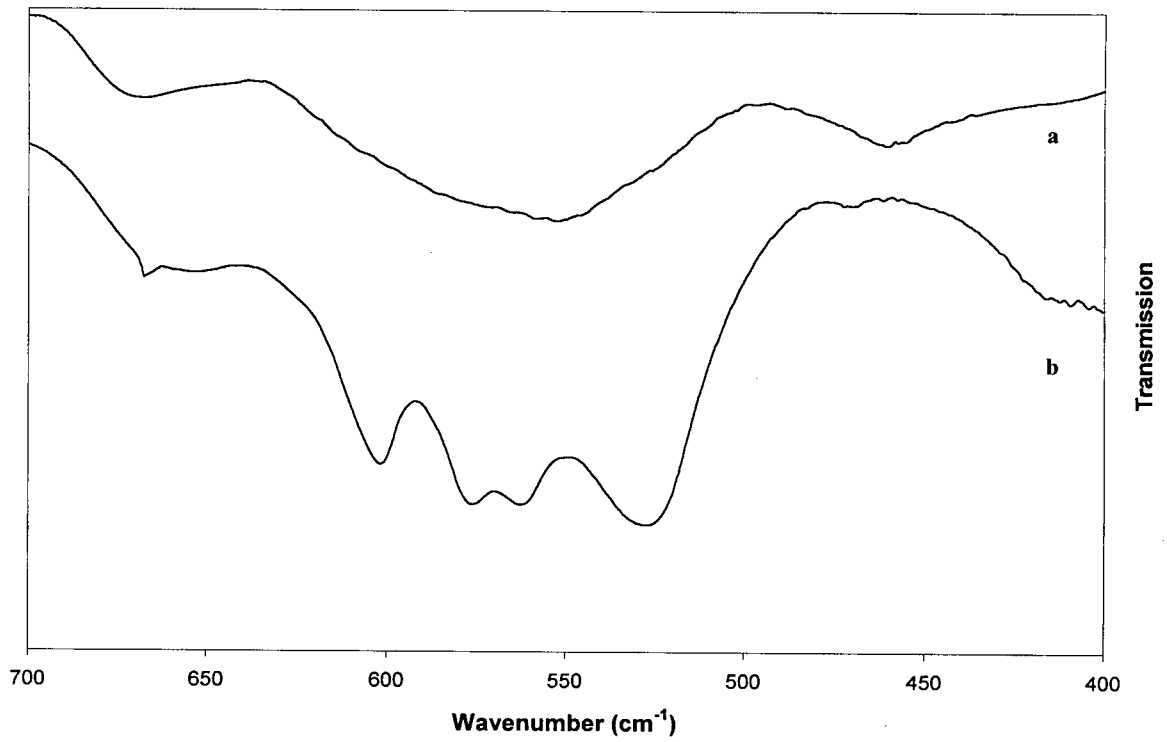

Figure 5-6 FTIR spectra of the samples prepared at pH=10 after 1 hr of synthesis (a) in the presence and (b) in the absence of PPF.

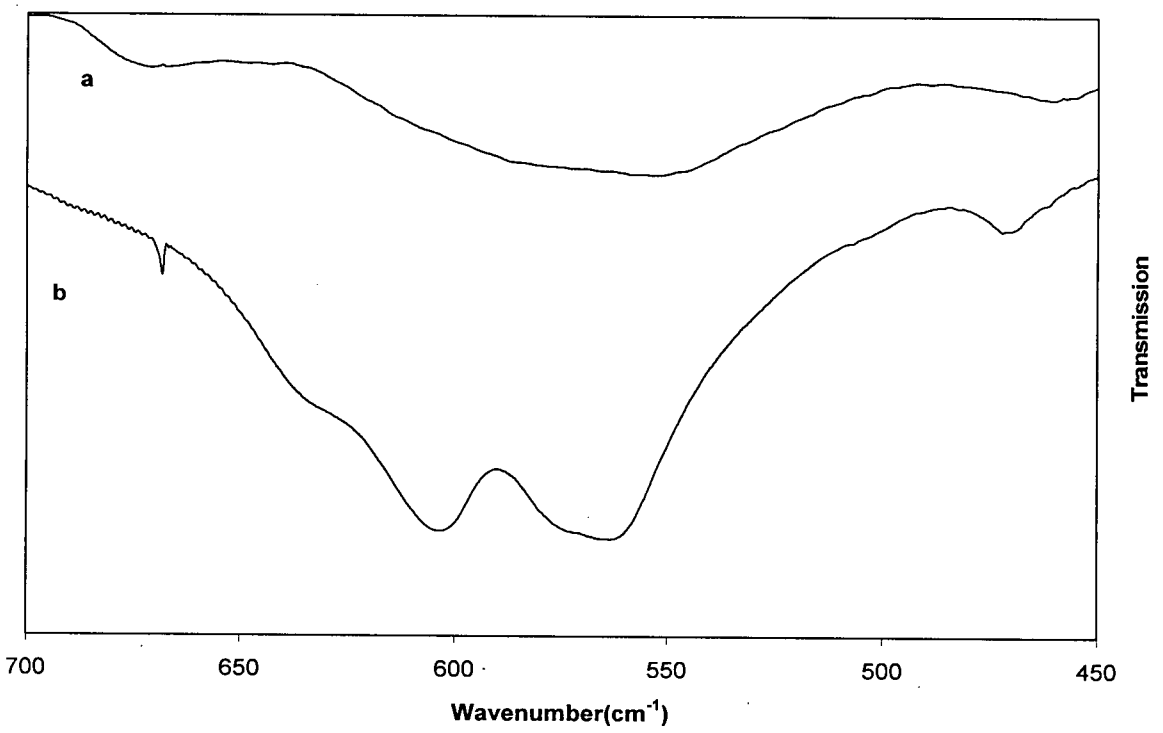

Figure 5-7 FTIR spectra of the samples prepared after 24 hr synthesis time (a) in the presence and (b) in the absence of PPF in the 700-450 cm^{-1} region.

5-1 and 5-2) no crystallization of the apatite phase (evidenced by the splitting of the PO_4^{3-} peak in the 600-450 cm^{-1} region of the FTIR results and clear and resolved diffraction peaks in the XRD data) is observed for the sample containing PPF even after 24 hrs of synthesis time.

It is therefore observed that in the presence and absence of PPF the apatite phase evolution follows different pathways. In the absence of polymer, brushite and trace amount of apatite precipitate simultaneously. The brushite phase then dissolves and the crystallinity and the crystal size of the apatite phase increases as the reaction proceeds. In the presence of PPF, at pH=10, an ACP phase forms and remains stable even after 24 hours of coexistence with the mother solution.

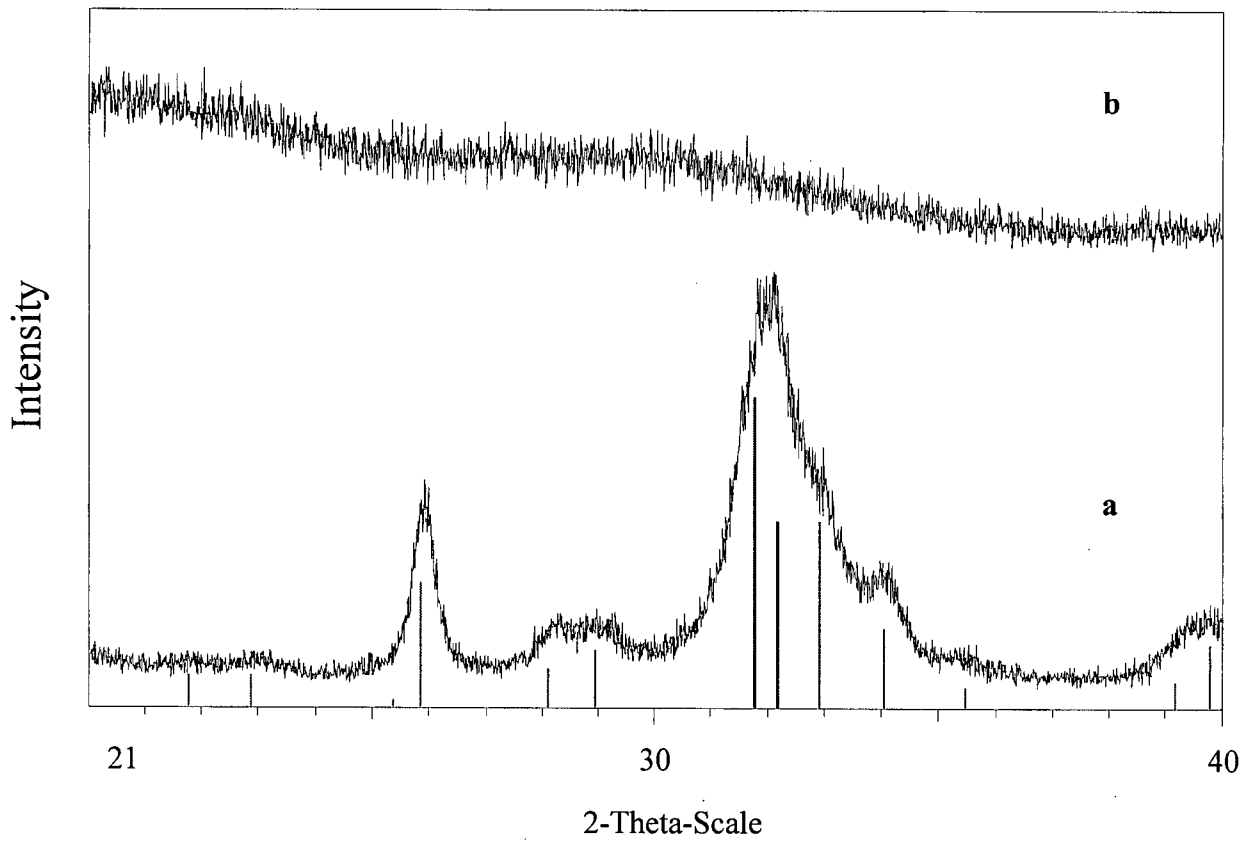

Figure 5-8 X-ray diffraction pattern of the apatite formed in (a) absence and (b) presence of PPF(HMw) at pH=10 and after 24 hours of synthesis. Lines are representative of stoichiometric hydroxyapatite (JCDPS 9-432).

In spontaneous precipitation of calcium phosphates from saturated solutions at pH values above 9, ACP is the first phase to precipitate which further converts to HAp through a dissolution-reprecipitation process [55, 57, 58, 188, 189, 190]. However, in the 7-9 pH range ACP precipitates and then transforms to octacalcium phosphate (OCP) which in turn transforms to HAp through a solid state rearrangement process [58, 188]. In the system investigated here, in the absence of PPF, due to the high initial calcium and phosphate concentrations, the solution is saturated in respect to even the least stable phase at this pH range, i.e. brushite, as explained in Chapter 5-1 and shown in Fig 2-4, page 16. It is observed that in the absence of PPF, brushite is the first phase to appear which later transforms to crystalline apatite. However, in the presence of PPF, ACP, instead of brushite, precipitates first and remains stable for over 24 hours of synthesis. It is therefore obvious that the presence of PPF influences the phase evolution of the calcium phosphate phase. In order to explain the nature of this influence we hypothesize that PPF interacts with the calcium phosphate and therefore affects its formation. We assume that this occurs through the interaction of PPF with Ca^{2+}. If true, the interaction of PPF with the Ca^{2+} from the solution (i) reduces the saturation of the solution by reducing the calcium concentration in the system and also (ii) provides a formation site for the calcium phosphate phases. Similar effect of organic molecules reducing the supersaturation of the solutions had been observed by other investigators [189, 191, 192]. Removal of the Ca^{2+} from the solution reduces the thermodynamic activity of this ion and therefore saturation of the solution. As a result no brushite is observed in the presence of PPF and instead, ACP, which is the expected precursor to crystalline HAp at pH=10, precipitates. The new complexes of PPF-Ca^{2+} could act as a substrate for the formation of ACP. The stability of the ACP at pH=10 is estimated to be around 9 hours in solution at 20°C [188]. The ACP is then expected to transform to crystalline HAp which does not occur in the investigated system in the presence of PPF. We further assume that adsorption of the PPF molecules (the chains that have not participated in the templating process) on the ACP

surface shields these surfaces from the ions in the media and therefore hinders the ACP to HAp transformation. Crystallization of the HAp phase starts on the surface of the ACP particles and further growth of the new crystals is supported by the ions released from the dissolving ACP [188]. Therefore, adsorption of the PPF molecules on the surface of the ACP particles hinders the crystallization and growth of the HAp crystals. This is in agreement with the reported observations that the adsorption of many other macromolecules and polymers on the surface of ACP particles has been found responsible for delayed/hindered ACP to HAp transformation [103, 104, 106, 107, 188, 189]. In the following sections we will continue to look into the effect of several parameters such as pH, molecular weight of the PPF, PPF concentration, and surface charge of the particles to further explore the proposed mechanism of PPF-calcium phosphate interactions.

5.3 The effect of pH

Figure 5-9A shows the FTIR spectra of the composite samples with PPF(HMw):HAp=4, prepared at pH of 7.4, 8.5, and 10, after 1 hour of synthesis. Peaks observed at 663, 770, 834, 975, 1018, 1074, 1112, 1151, 1222, 1252, 1290, 1383, 1448, 1642, 1719, and between 3100-2800 cm^{-1} belong to PPF [177]. Absorption bands in the 630-490 cm^{-1} belong to vibration modes of PO_4^{3-} [78, 184]. PO_4^{3-} absorption bands in the 1100-960 cm^{-1} region are overlapped by the PPF absorptions bands and are not distinguishable.

Figure 5-9B shows the FTIR spectra of the same samples focusing on the 650-450 cm^{-1} region. Sample prepared at pH=7.4 shows a shoulder at around 525 cm^{-1} (attributed to acid phosphates) with clear absorption bands at 557 and 599 cm^{-1} similar to those observed for a mix of brushite

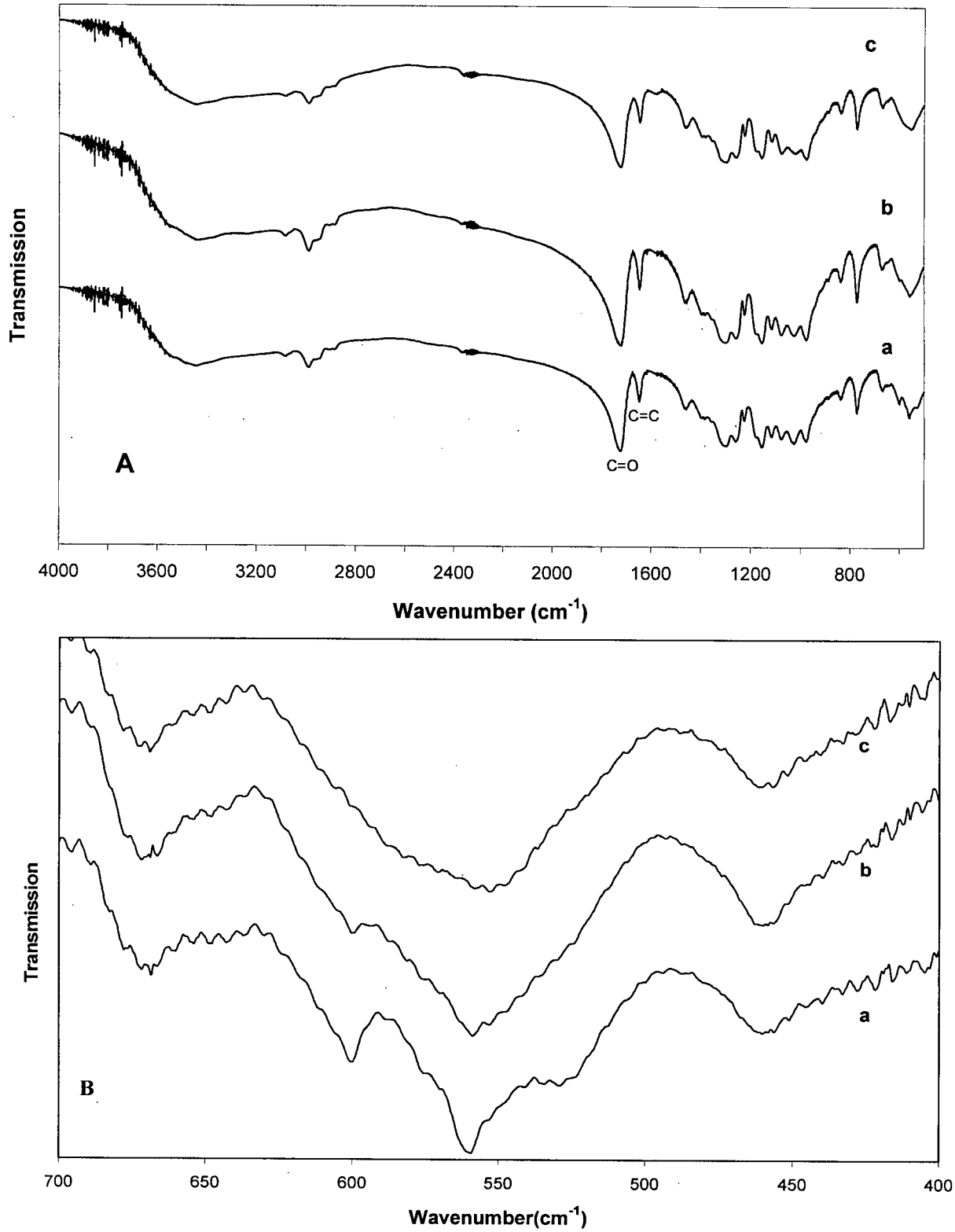

Figure 5-9 A: FTIR spectra of the composite samples with the theoretical PPF:HAp=4 prepared after 1 hour of synthesis at pH (a) 7.4, (b) 8.8, and (c) 10. B: FTIR spectra of the samples in A in the 650-450 cm^{-1} region.

and poorly crystalline apatite (Fig 5-2a). By increasing the pH to 8.5 the shoulder at 525 cm^{-1} is hardly distinguishable but the bands at 560 and 600 cm^{-1} are present consistent to those observed for the HAp sample (Fig 5-2f). Sample prepared at pH=10 shows a broad absorption band centered at around 560 cm^{-1}, characteristic of amorphous calcium phosphate (ACP) [78, 101, 160, 185].

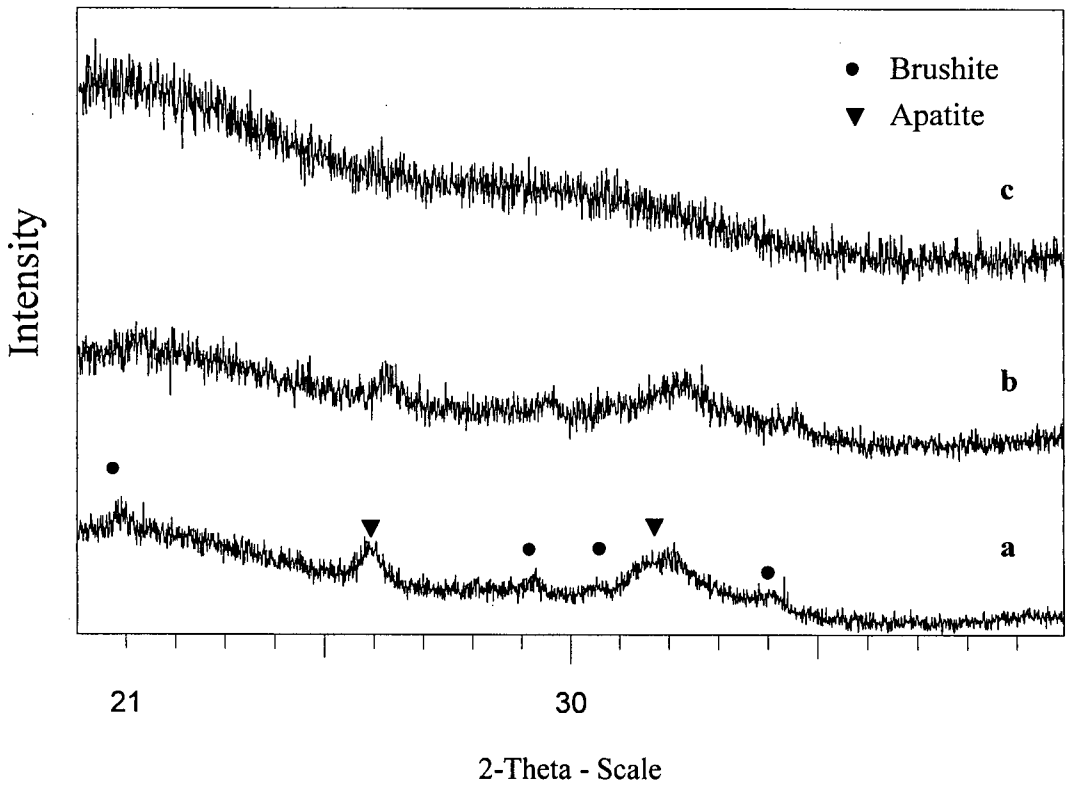

Figure 5-10 X-ray diffraction pattern of the composites prepared at (a) pH=7.6, (b) pH=8.8, and (c) pH=10.

Figure 5-10 shows the X-ray diffraction analysis of the same composite samples (i.e. prepared at pH=7.4, 8.5, and 10). The XRD pattern of the sample prepared at pH=7.4 shows a broad peak centered between 2θ= 25 to 26° and also a broad peak centered at 2θ=32°, characteristic of poorly crystalline apatite phase. Peaks observed at 2θ=21, 29.2, 30.6, and 34.2° are all

characteristic of brushite (JCPDS 9-77). The apatitic peaks broaden further for the sample prepared at pH=8.8 and the intensity of the brushite reflections decreases. For the pH=10 sample, a broad bump stretching from $2\theta=26^{\circ}$ to $2\theta=33^{\circ}$ is present rather than a well defined peak which is characteristic of ACP [160, 185].

XRD and FTIR results suggest that at lower pH conditions (pH=7.4) brushite together with a poorly crystalline apatite phase precipitates. Increasing the pH to 8.5 increases the amount of the apatite at the expense of the brushite phase. At pH=10 only ACP is present. These observations can be explained by examining the solubility map of calcium phosphates for different pH conditions (refer to page 14, Fig 2-2 [52]). The solubility of brushite (labeled DCPD in Fig. 2-3) decreases with pH up to pH of about 8 and then increases, whereas solubility of HAp continuously decreases with increase in pH. Increased solubility of brushite with pH increasing above 8 is the reason for the decrease in the amount of brushite observed in samples prepared at pH=8.5 and 10. Presence of ACP for pH=10 can be explained by the fact that transformation of ACP to HAp occurs through the dissolution of ACP and nucleation and growth of the HAp crystals [76, 78, 187]. The solubility of ACP reduces with increasing pH [76, 78, 187]. As observed earlier the presence of PPF also stabilizes the ACP in the system.

In order to investigate the effect of pH on PPF, solutions of polymer in THF were prepared at three different pH conditions (i.e. pH=7.4, 8.8 and 10 and processed similarly to the composites) and were examined by FTIR spectroscopy (Fig 5-11). The polymer had identical spectra when prepared at pH=7.4 and 8.8. In the spectrum of the polymer at pH=10 a new peak appears at 1540 cm^{-1} which might be attributed to the NH_4^+. The intensity and the broadness of the OH band around 3450 cm^{-1} increases considerably for the sample prepared at pH=10, which can be explained by the higher amount of ammonia water added to the solution in order to obtain

pH=10. However, the FTIR results show that PPF does not undergo a significant structural change by increasing the pH of its solution in THF.

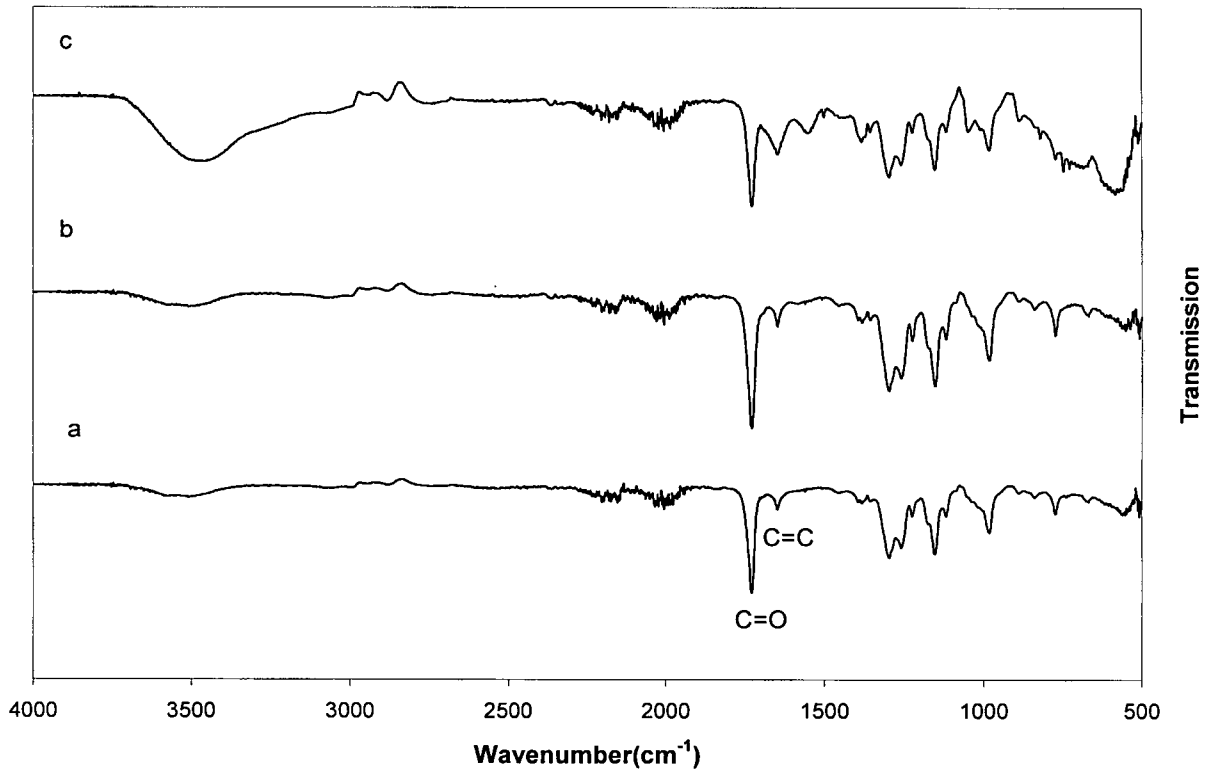

Figure 5-11 FTIR spectra of the HMw PPF in THF at pH (a) 7.4, (b) 8.8, and (c) 10.

5.4 The effect of PPF molecular weight

Figure 5-12 shows the FTIR spectra of the composite samples (pH=10, with PPF: HAp=4, after 1hr of reaction) prepared with PPF of high (HMw, Mw= 4500) and low (LMw, Mw=1800) molecular weight and also with diethyl fumarate (DEF), the precursor to PPF, to represent the smallest chain possible. The spectrum of the sample prepared with HMw (Figure 5-12a) clearly shows all the absorption bands associated with PPF (at about 663, 770, 834, 975, 1018, 1074, 1112, 1151, 1222, 1252, 1290, 1383, 1448, 1642, 1710, and between 3100-2800 cm^{-1}). The PO_4^{3-} peaks in 650-500 cm^{-1} region are broad and almost featureless and in 1100-1000 cm^{-1} region are overlapped by the polymer peaks and are not distinguishable. The spectrum of the sample

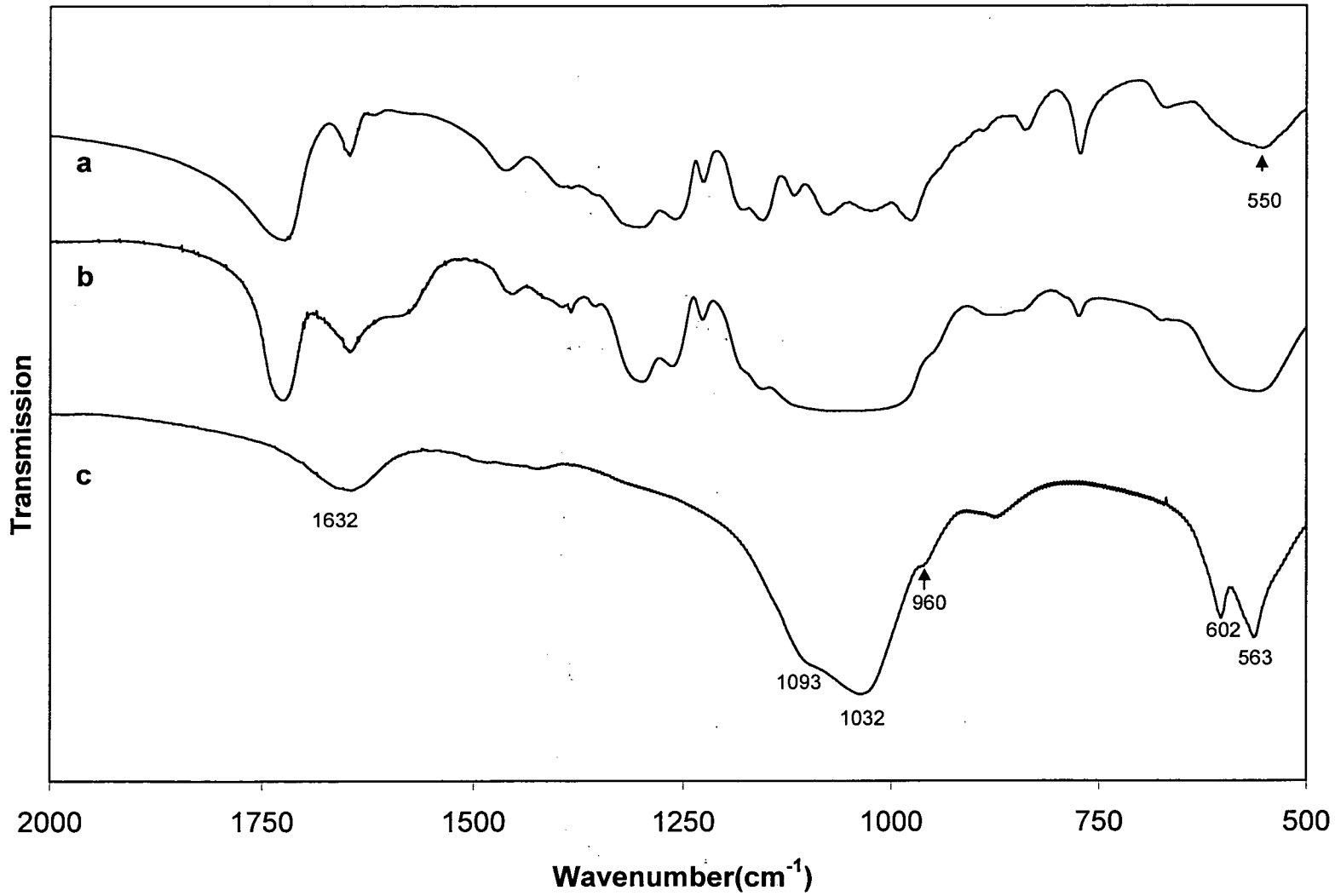

Figure 5-12 FTIR spectra of the composite samples with PPF:HAP=4, prepared at pH=10 with (a) HMw, (b) LMw, and (c) DEF, after 1 hour of synthesis time.

prepared with LMw PPF (Figure 5-12b) shows the PPF absorption bands at about 663, 770, 834, 1222, 1253, 1292, 1380, 1444, 1640, and 1710 cm^{-1}. PPF peaks at 975, 1018, 1074, 1112, 1151, and 1222 cm^{-1} are overshadowed by the PO_4^{3-} peaks in the 1200-900 cm^{-1} region.

As discussed earlier, the broad and symmetrical peak stretching between 1205-900 cm^{-1} and a broad peak stretching between 640-470 cm^{-1} are attributed to PO_4^{3-} vibrations. The broad symmetrical shape of these peaks points to the poorly crystalline nature of the calcium phosphate phase. In the spectrum of the composite sample prepared with DEF (Figure 5-12c) PO_4^{3-} absorption bands at 563, 602, 960, 1032 and 1093 cm^{-1} belong to crystalline apatite [78]. Peaks at 870 cm^{-1} and those in the 1500-1400 cm^{-1} region are due to carbonate substitution [184] while the peak at 1632 cm^{-1} is due to the bending mode of H-O-H.

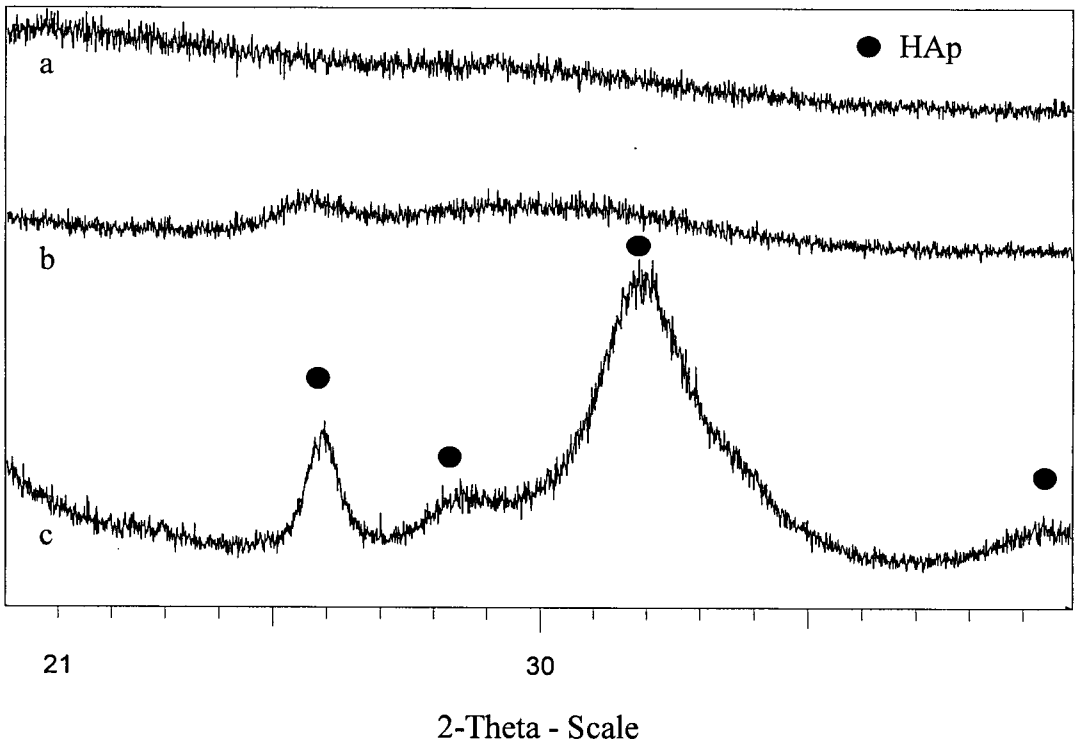

Figure 5-13 X-ray diffraction patterns of the composite samples with PPF:HAP=4, prepared at pH=10 with (a) HMw, (b) LMw, and (c) DEF after 1 hour of synthesis time.

Figure 5-13(a-c) shows the XRD pattern of the samples depicted in Figure 5-12(a-c). X-ray pattern of the sample prepared with HMw PPF (Figure 5-13a) shows only a broad bump stretching between $2\theta=26\text{-}34^{\circ}$.The sample prepared with LMw PPF (Fig 5-13b) shows a distinct peak stretching between $2\theta=25\text{-}27^{\circ}$ and another peak stretching from $2\theta=27\text{-}35^{\circ}$, characteristic of a poorly crystalline apatite phase. The composite prepared with DEF (Fig 5-13c) shows a diffraction peak at $2\theta=26^{\circ}$ and a small peak at $2\theta=28\text{-}30^{\circ}$ together with a broad but distinctive peak stretching between $2\theta=30\text{-}34^{\circ}$, all characteristic of an apatitic phase (JCDPS 9-432).

Figure 5-14(a-c) shows the FTIR spectra of the samples prepared with HMw, LMw, and DEF. All samples are characterized after 24 hrs of synthesis time. The composite sample prepared with HMw polymer (Fig 5-14a) again shows all the PPF characteristic peaks and the PO_4^{3-} peaks in 600-500 cm^{-1} region. PO_4^{3-} absorption bands in the 1100-900 cm^{-1} region are again overshadowed by the PPF peaks. The composite prepared with the LMw polymer (Fig. 5-14b) shows a broad and symmetrical peak stretching between 1205-900 cm^{-1} and a broad peak stretching between 640-470 cm^{-1} which are attributed to PO_4^{3-} vibrations. Absorption bands at around 1470, 1410, and 870 cm^{-1} belong to carbonate ions. A broad absorption band with centre at about 1632 cm^{-1} is also present which can be attributed to H-O-H bending modes. It is interesting to observe that PPF peaks are no longer present in this spectrum (although they are clearly observed in the spectrum of the same sample prepared after 1 hr of synthesis, Fig 5-12b). The composite sample prepared with DEF after 24 hour of synthesis time did not show significant difference compared to the sample prepared after 1 hour of preparation time.

Figure 5-15 (a-c) shows the XRD pattern of the composite samples prepared with HMw, LMw, and DEF, after 24 hours of synthesis, respectively. The X-ray pattern of the HMw composite

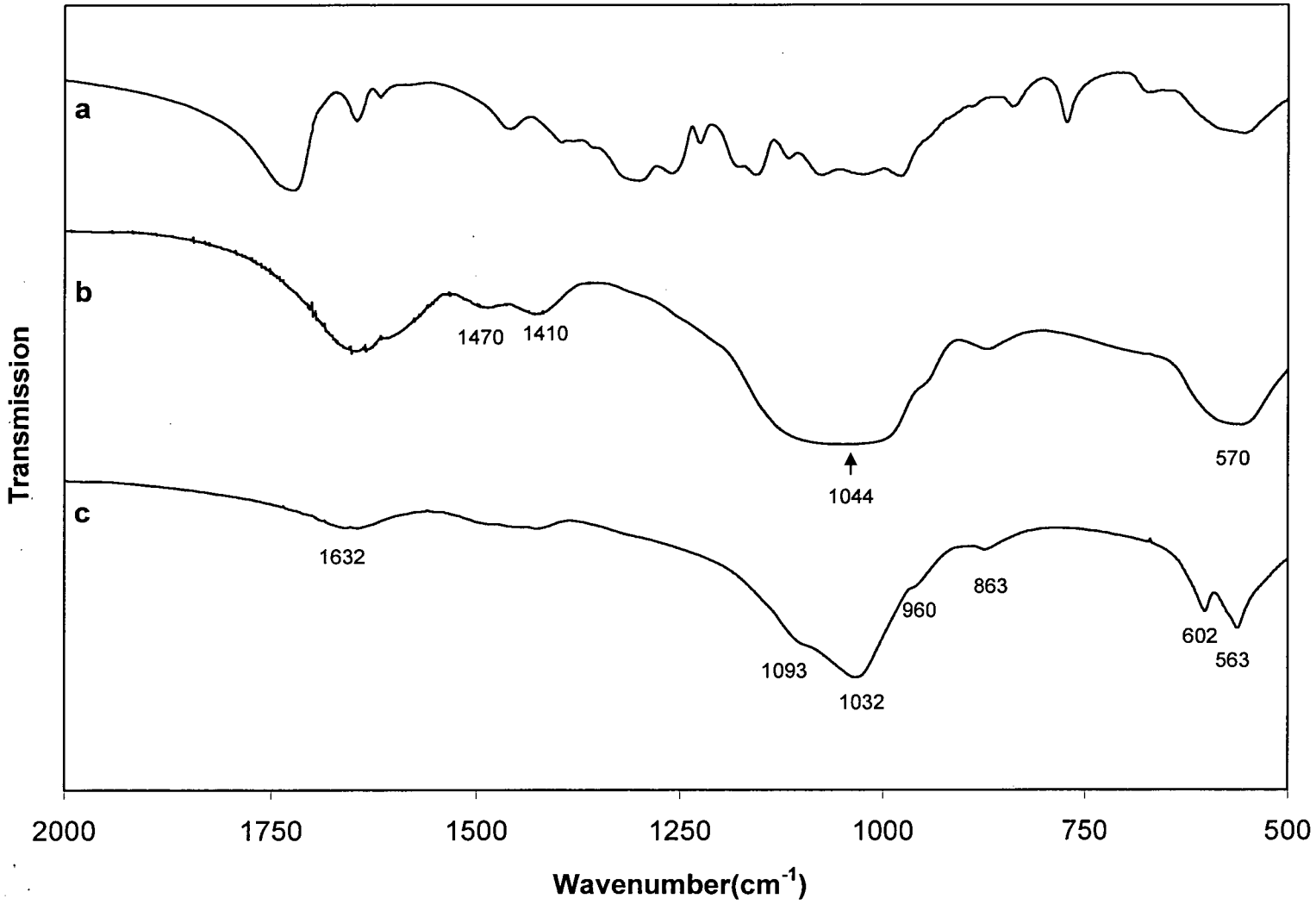

Figure 5-14 FTIR spectra of the composite samples with PPF:HAP=4, prepared at pH=10 with (a) HMw, (b) LMw, and (c) DEF, after 24 hours of synthesis time.

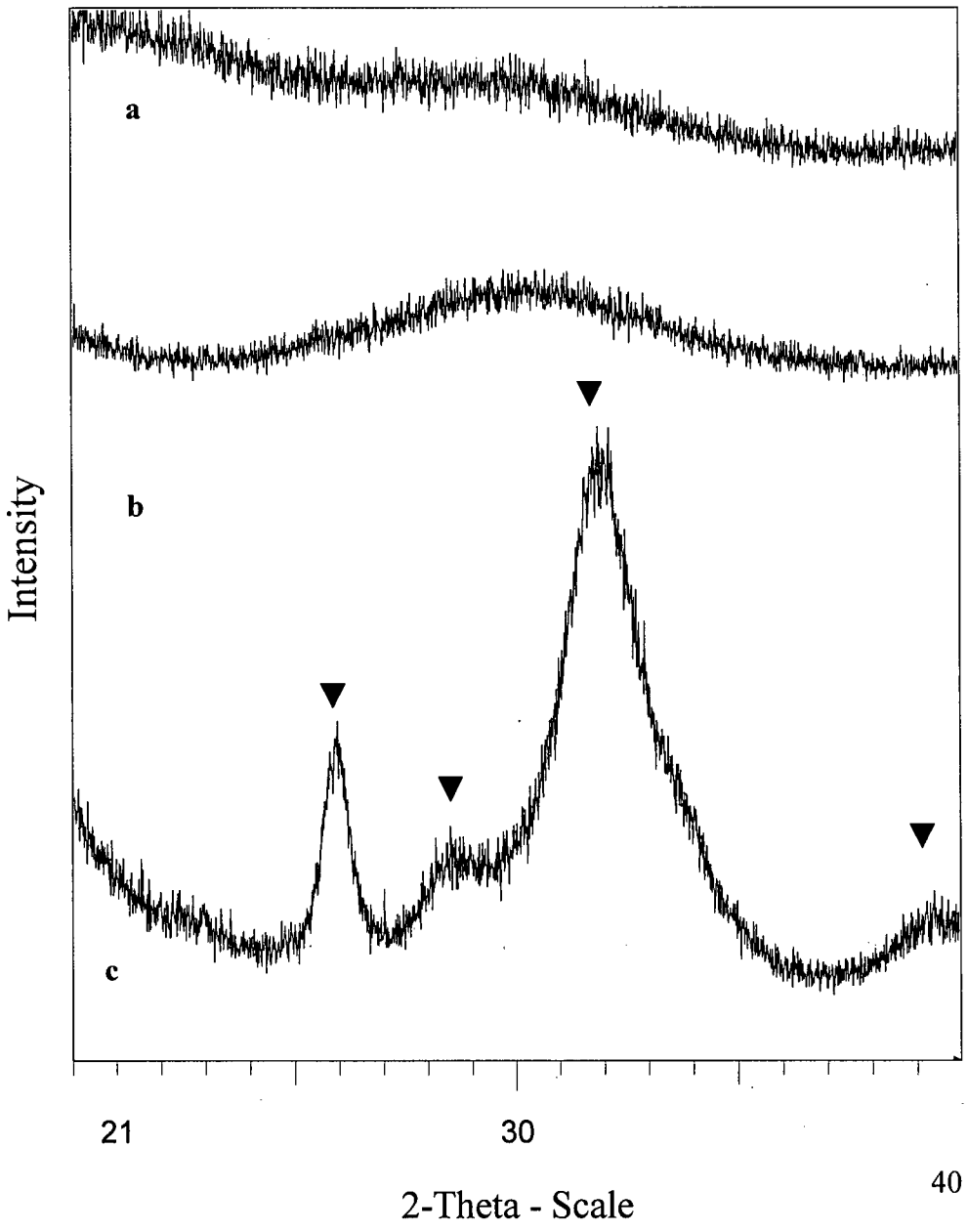

Figure 5-15 X-ray diffraction patterns of the composite samples with PPF:HAP=4, prepared at pH=10 with (a) HMw, (b) LMw, and (c) DEF, after 24 hours of synthesis time (triangles mark the HAp peaks).

(Fig 5- 15a) shows a broad bump stretching between 2θ=26-34°. The LMw composite (5-15b) also shows a diffuse peak stretching between 2θ=25-35°. The diffraction peak observed at 2θ= 26° for the same sample prepared after 1 hr of synthesis time (5-13b) is no longer observed. The X-ray pattern of the DEF composite shows a diffraction peak at 2θ=26° and a small peak at 2θ=28-30° together with a broad but distinctive peak stretching between 2θ=30-34°, characteristic of an apatitic phase (JCDPS 9-432).

Comparing the XRD and FTIR results for the HMw sample after 1 hr (5-12a and 5-13a) and 24 hrs (5-14a and 5-15 a) synthesis time, no apparent difference could be observed. It was proposed earlier that the presence of the HMw PPF has facilitated the formation of the ACP. The PPF peaks are clearly present in the FTIR spectra of samples both after 1 hr and 24 hrs of synthesis but no crystallization of HAp has occurred. Based on these results we hypothesized that adsorption of the PPF chains on the surface of the ACP particles hinders the ACP to HAp transformation.

The FTIR and the XRD results also show that higher molecular weight polymers are more efficient in stabilizing the amorphous phase (ACP) and hindering the crystallization of the apatite phase (HAp) while all polymers regardless of their molecular weight have facilitated ACP formation. Increased inhibiting effect of polymers with molecular weight has also been observed by other investigators [144, 193]. It is also interesting to observe that DEF, which is almost equivalent to one repeat unit of PPF, has significantly affected the apatite phase evolution. When no organic molecule interference is present, after 1 hr of synthesis time, a mixture of dominantly brushite is present. The brushite phase further dissolves and reprecipitates as an apatite phase after 24 hrs of synthesis time. In the presence of DEF this process occurs in a significantly shorter time frame, i.e. after only one hour of reaction both FTIR and XRD show

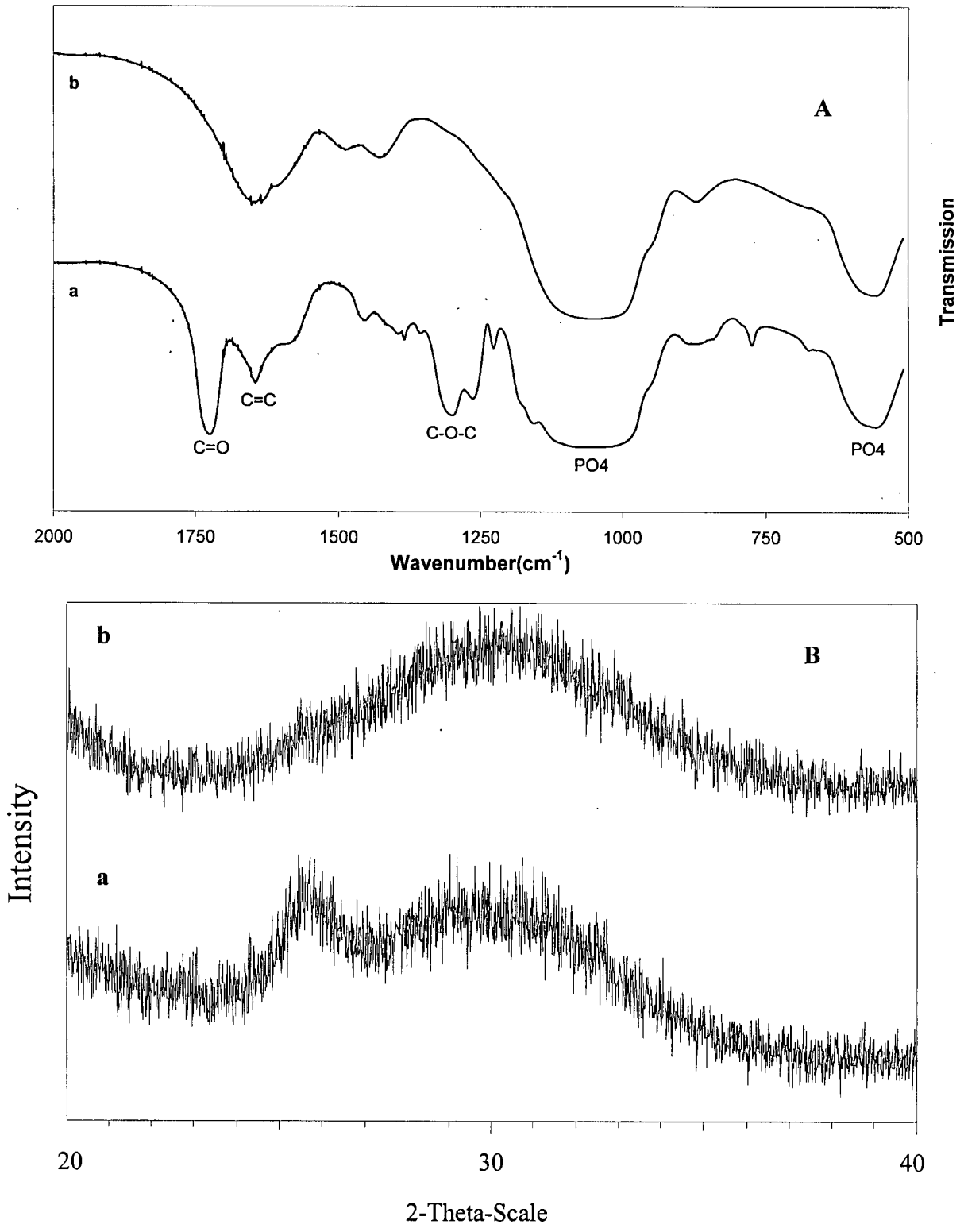

Figure 5-16 A: FTIR spectra of the composite prepared (PPF:HAp =4) at pH=10 using the LMw polymer after (a) 1 hour and (b) 24 hours of synthesis. B: X-ray diffraction spectra of the composite prepared at pH=10 using the LMw polymer after (a) 1 hour and (b) 24 hours of synthesis.

the presence of an apatite phase. Although DEF has been efficient in facilitating ACP formation it has not been an efficient inhibitor of HAp crystallization but on the contrary has facilitated the crystallization of the apatite phase.

The sample prepared with the LMw PPF bears the most interesting results therefore the FTIR and the XRD spectra are presented again in Figures 5-16A and 5-16B for more clarity. The FTIR spectra of the sample prepared after 1 hr (referred to LMw-1hr hereafter) clearly bears the PPF peaks except for the 1100-900 cm^{-1} region in which the apatite peaks are dominantly present. However, after 24 hrs of synthesis the PPF peaks are no longer observed. The XRD data for the LMw-1hr sample shows a clear and distinct peak at $2\theta = 26^{\circ}$ which is no longer present in the spectra of the LMw-24hr (composite sample prepared with LMw PPF and after 24 hr of synthesis) and is rather replaced by a broader peak stretching over $2\theta = 25\text{-}35^{\circ}$. Loss of peak resolution in the XRD spectra and the presence of diffuse peaks is an indication of the lack of crystallinity of the LMw-24hr sample. Reduced crystallinity of the LMw-24hr sample in comparison to the LMw-1hr sample could be explained by assuming that the LMw PPF has been incorporated into the growing crystals. The absence of the PPF peaks from the FTIR spectra of the LMw-24hr also supports the incorporation of the LMw PPF chains into the HAp deposits.

The fact that no DEF absorption bands was observed in the spectra of the HAp-DEF composite (Fig. 5-12c) although considerable amount of DEF was present (DEF:HAp=4) and also considering the diffuse XRD pattern (Fig. 5-13c) observed for the composite (where the amount of carbonate ions was not significant (Fig. 5-12c) it is possible that the DEF molecules are incorporated within the growing apatite particles. Other workers have also observed a similar phenomenon [144]. It is also possible that due to the small size of the DEF molecules (~ 1.5 nm) and their higher solubility in the mixed solvent compared to higher molecular weight PPF, they

might be washed out during the filtering process. These hypotheses are further explored by investigating the thermal behavior of the composite samples.

5.4.1 Thermo-gravimetric analysis (TGA)

Figure 5-17 (a-e) shows the TGA patterns for the THF-based samples with no polymer, DEF, LMw, MMw composites, and the PPF, respectively. All the composite samples have the PPF: HAp=4 and were prepared at pH=10 and after 24 hours of synthesis time. The THF-based sample (Fig 5-17a) shows a weight loss up to 200°C which slows down at temperatures above 200°C. The THF-based sample lost about 11% of its weight during heating to 1100°C mostly due to the loss of water. The DEF composite (Fig 5-17b) follows a similar pattern to that of the THF-based sample with the exception that its total weight loss amounts to around 15% by 1100°C. The TGA pattern of the LMw composite (Fig 5-17c) shows a weight loss of about 30%. The MMw composite (Fig 5-17d) shows a pattern similar to that of PPF (Fig 5-17e) with a weight loss of about 60% while PPF shows a weight loss of about 96%.

We observe that the retention of the polymer within the composite increases with the molecular weight of the polymer. This is due to the higher solubility of the lower molecular weight polymer in the solvents compared to higher molecular weight polymers. Higher solubility together with the small size of the molecules facilitates the polymer wash-out during the filtering and washing step. Although the FTIR spectra of the LMw weight polymer after 24 hours of synthesis time did not show the PPF absorptions bands, the TGA results show an extra 19% weight loss compared to the sample prepared with no polymer (Fig. 5-17a). The extra weight loss can be explained by the presence of the PPF within the calcium phosphate particles. TGA data therefore support the hypothesis that the polymer incorporates within the growing calcium

phosphate particles. It has also been previously postulated by other investigators that the organic molecules can be incorporated within the growing particles causing the FTIR peaks not to be observed [144]. We believe TGA data provide more direct evidence regarding the incorporation of PPF within the calcium phosphate particles. It also provides a mean to experimentally measure the amount of polymer in the composite.

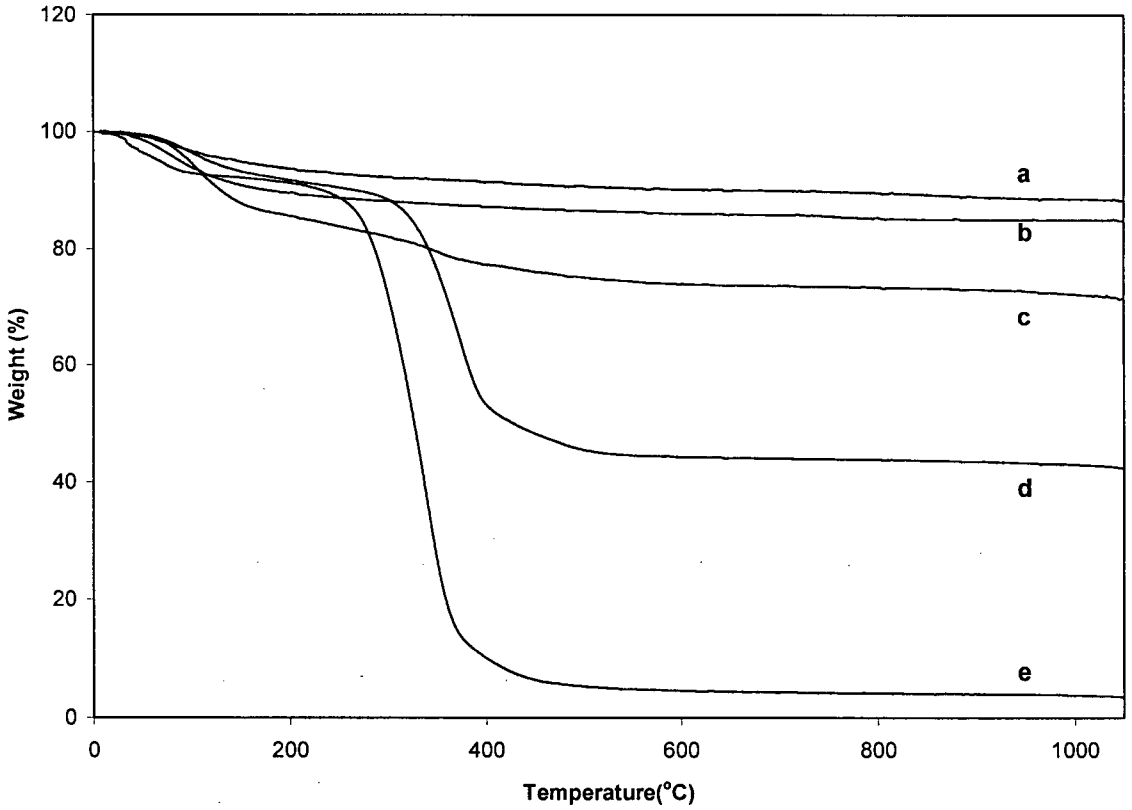

Figure 5-17 TGA analysis of the (a) THF-based, (b) DEF-HAp, (c) LMw-HAp, (d) MMw-HAp, and (e) PPF samples. The THF-based and the composite samples were prepared at pH=10 and were collected after 24 hours of synthesis.

The TGA results also suggest that the amount of the theoretically calculated PPF in the final composite deviates from the experimental results and is dependent on the molecular weight of the polymer. Although the theoretical calculations were based on 80% PPF in all the samples that were examined in the TGA analysis, the actual amount of PPF within the composite varied

between 4-60% depending on the molecular weight of the polymer. Therefore, when exact amount of PPF in the final composite is desired the amount of PPF lost during the synthesis process, according to its molecular weight, should be taken into account.

5.5 Mechanisms of PPF-calcium phosphate interactions

In order to explain the formation of different phases of calcium phosphate in the presence and absence of PPF, we hypothesized that PPF interacts with Ca^{2+} in the solution to form PPF-Ca^{2+} complexes, schematically shown in Fig 5-18. Such complexes further act as formation sites for the ACP particles. In the case of the higher molecular weight polymers the fraction of the PPF that does not participate in the PPF-Ca^{2+} complexation adsorbs on the surface of the ACP particles shielding it from the surrounding media and therefore hindering the ACP to HAp transformation. Presence of higher molecular weight PPF on the surface also produces a stearic hindrance for the migration of precipitating ions to the surface of the ACP particles [189, 194]. Low molecular weight PPF and especially DEF also participate in forming PPF/DEF-Ca^{2+} complexes and therefore provide a substrate for the precipitation of ACP. However, due to their small sizes (roughly calculated to be ~ 10 and 1.5 nm, respectively) these molecules are more soluble in the solution compared to the HMw PPF and therefore can move back and forth from the surface to the solution exposing the ACP surface to the mother solution. Moreover, the small molecules attached to the surface (especially in case of DEF) can also act as "active centers" [193] attracting oppositely charged precipitating ions and therefore promoting the ACP to HAp crystallization. Such molecular weight dependence of the effect of polymers on the precipitation of inorganic phases has been observed by other workers [103, 104, 107, 144 193, 194]. It has been reported previously that synthetic polymers or macromolecules that are able to bind with calcium have also facilitated the nucleation and growth of the apatite phase [144, 155, 195].

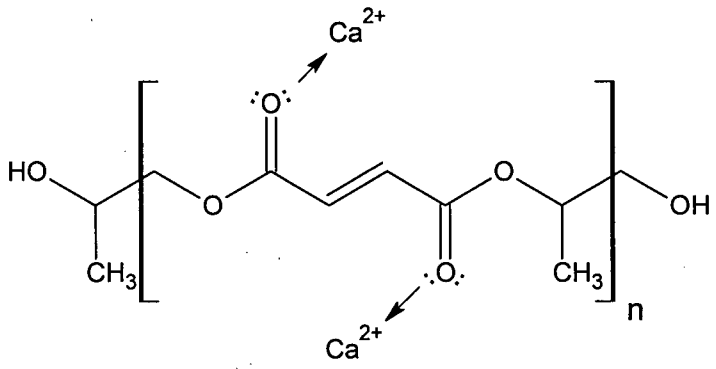

Figure 5-18 Schematic presentation of the PPF-Ca^{2+} interaction. Calcium ions might form a complex with the unpaired electrons of the oxygen in the carbonyl group.

In order to examine our hypothesis regarding the formation of the PPF-Ca^{2+} complex, various amounts of calcium nitrate were added to PPF. Figure 5-19 shows the FTIR spectra of the polymer after different amount of calcium nitrate is added to its solution in THF (PPF:$Ca(NO_3)_2$ from 0.1 to 1.64). It can be clearly seen that the addition of calcium nitrate to PPF causes the absorption band of the PPF at around 1714 cm^{-1} (which is attributed to the C=O bond) to shift to lower frequencies (1700 cm^{-1}). The observed shift suggests that the C=O bond is weakened due to the formation of a new bond with Ca^{2+} ions. Ca^{2+} is able to form a coordination bond with the two unpaired electrons of oxygen atom in the carbonyl bond of the PPF. Formation of such a complex weakened the carbonyl bond and caused its shift to lower frequencies. Similar phenomenon has been observed by Zhang et al. during the in-vitro mineralization of collagen [155]. They observed that the C=O FTIR absorption band of amide I of pure collagen shifts to lower frequencies upon the addition of Ca^{2+} which they attributed to the formation of a chelate bond between Ca^{2+} and the carbonyl group (C=O).They therefore suggested that the C=O is a possible nucleation site for calcium phosphates during collagen mineralization.

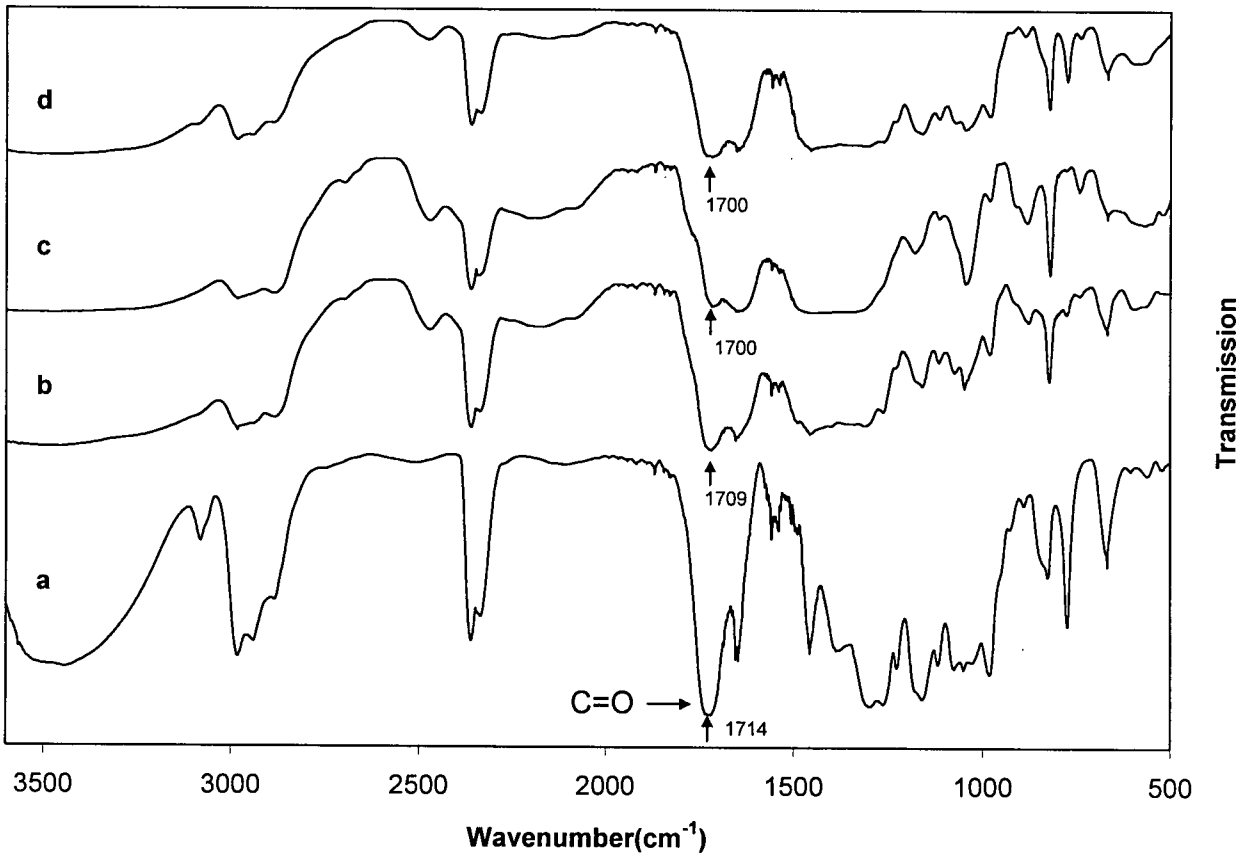

Figure 5-19 FTIR spectra of PPF-$Ca(NO_3)_2$ solutions with various amounts of calcium nitrate (a) PPF, (b) PPF:$Ca(NO_3)_2$=0.1, (c) PPF:$Ca(NO_3)_2$=0.4, and (d) PPF:$Ca(NO_3)_2$=1.64, added to the PPF solution in THF. The absorption band of the carbonyl group shifts to lower frequencies due to PPF-Ca^{2+} complexation.

This observation provides evidence that PPF added to the precipitating calcium phosphate solution interacts (in form of a coordination bond) with Ca^{2+}. PPF interaction with Ca^{2+} reduces the saturation of the solution by removing Ca^{2+} ions and therefore reducing their concentration in the solution. Furthermore, PPF-Ca^{2+} complexes could act as substrates for the precipitation of the ACP phase. The remaining PPF molecules that do not participate in the templating process are adsorbed on the surface of ACP and depending on their molecular size induce or inhibit ACP to HAp transformation. Higher molecular weight PPF likely covers the surface, shielding it from

the surrounding media, and therefore hinders ACP to HAp transformation. On the other hand low molecular weight PPF, and especially DEF, show less inhibitory effect due to their higher solubility in the solution. DEF can also act as an "active center" to induce HAp crystallization. It was observed that in the presence of DEF, crystalline HAp can form within 1 hour of the synthesis process.

5.6 The effect of PPF concentration on calcium phosphate precipitation

Figure 5-20 (a-c) shows the X-ray diffraction patterns of the THF-based sample after 1 hour of synthesis time (Fig 5-20a) and the composite samples prepared with 5%-MMw (Fig 5-20b) and 80% MMw (Fig 5-20c), after 1 hour of synthesis time.

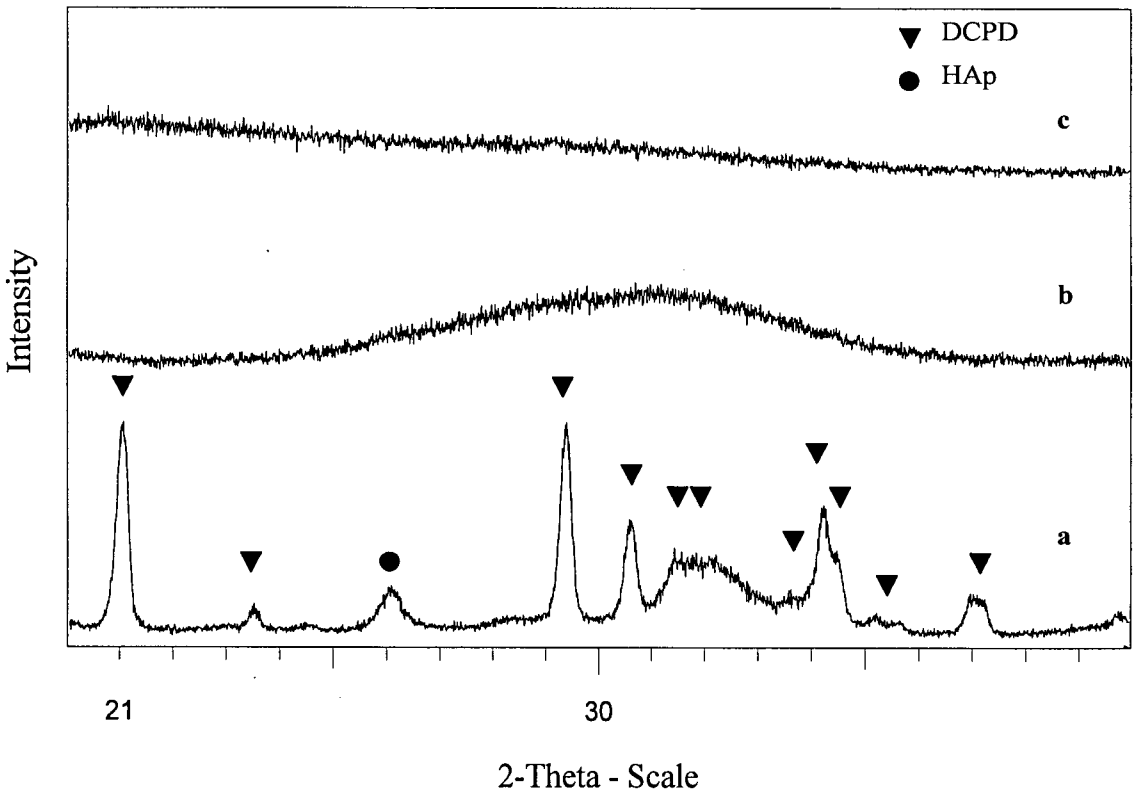

Figure 5-20 X-ray diffraction pattern for the (a) THF-based sample, (b) 5%-PPF composite, and (c) 80%-PPF composite. All samples were prepared at pH=10 and after 1 hour of synthesis.

As discussed earlier, the THF-based sample consists of well crystalline brushite together with poorly crystalline apatite. The 5% composite contains only poorly crystalline apatite. The composite with 80% PPF contains amorphous calcium phosphate. It is interesting that addition of only 5% of MMw PPF has significantly facilitated the formation of the apatite phase.

Figure 5-21 (a-f) shows the FTIR spectra of the composite samples prepared with 0, 5, 50, 80, 95, and 100% of PPF, respectively, after 24 hrs of synthesis time and with MMw PPF(Mn=1500). Composite sample containing 5% PPF (Fig 5-21b) shows a doublet at 560 and 600 cm^{-1} which together with the absorption bands at 960, 1023 and the shoulder at 1093 belong to the PO_4^{3-} vibrations, as discussed previously. The peak at about 1632 cm^{-1} is attributed to the H_2O bending vibration. No PPF peak is observed in this sample. The spectrum of the sample containing 5% PPF is similar to the spectrum of the sample prepared in the absence of the polymer with smaller amount of carbonate ions (peaks in the 1500-1400 cm^{-1} are not noticeable in comparison to the sample that contains no polymer). By increasing the PPF content to 50% (Fig 5-21c) the PO_4^{3-} in the 600-400 cm^{-1} region lose their resolution and a featureless symmetrical band stretching between 630-470 cm^{-1} replaces the split bands at 557 and 600 cm^{-1} observed for the 5% sample. The PPF absorption bands are also observed except for the peaks in 1100-900 cm^{-1} region where they overlap with the PO_4^{3-} absorption bands. FTIR spectra of the composite sample with 80% (Fig 5-20d) polymer also shows a broad featureless band stretching between 630-480 $cm^{-1}$with a broad band stretching over 1100-900 cm^{-1} (PPF peaks are reflected on this broad band) which are attributed to PO_4^{3-} absorption peaks. All the PPF peaks are clearly observed. PPF peaks are also dominantly present for the sample with 95% PPF (Fig 5-20e). A small peak at 558 cm^{-1} is the only indication of the presence of phosphate ions.

Figure 5-22 (a-e) shows the X-ray diffraction patterns for the composite samples containing 0, 5, 50, 80, and 95% MMw PPF, after 24 hours of synthesis, respectively. The sample with 5% PPF (5-22b) returns a diffraction pattern similar to that of the sample with no PPF (5-22a), with peaks at 2θ= 26, 28, 29° and a broad peak over 2θ=30-33° which belong to poorly crystalline apatite. The spectrum of the sample with 50% PPF (5-22c) shows a diffuse peak stretching over 2θ=25-27° centered at 2θ=26° and a broad bump stretching over 2θ=29-34°. By increasing the PPF content to 80% (5-22d) only a broad peak over the 2θ=25-34° region is observed. Sample with 95% (Fig 5-22e) shows three distinct diffraction peaks at 2θ=22, 36.5, and 39° which have close resemblance to those of calcium ammonium hydrogen phosphate (JCDPS 20-0204).

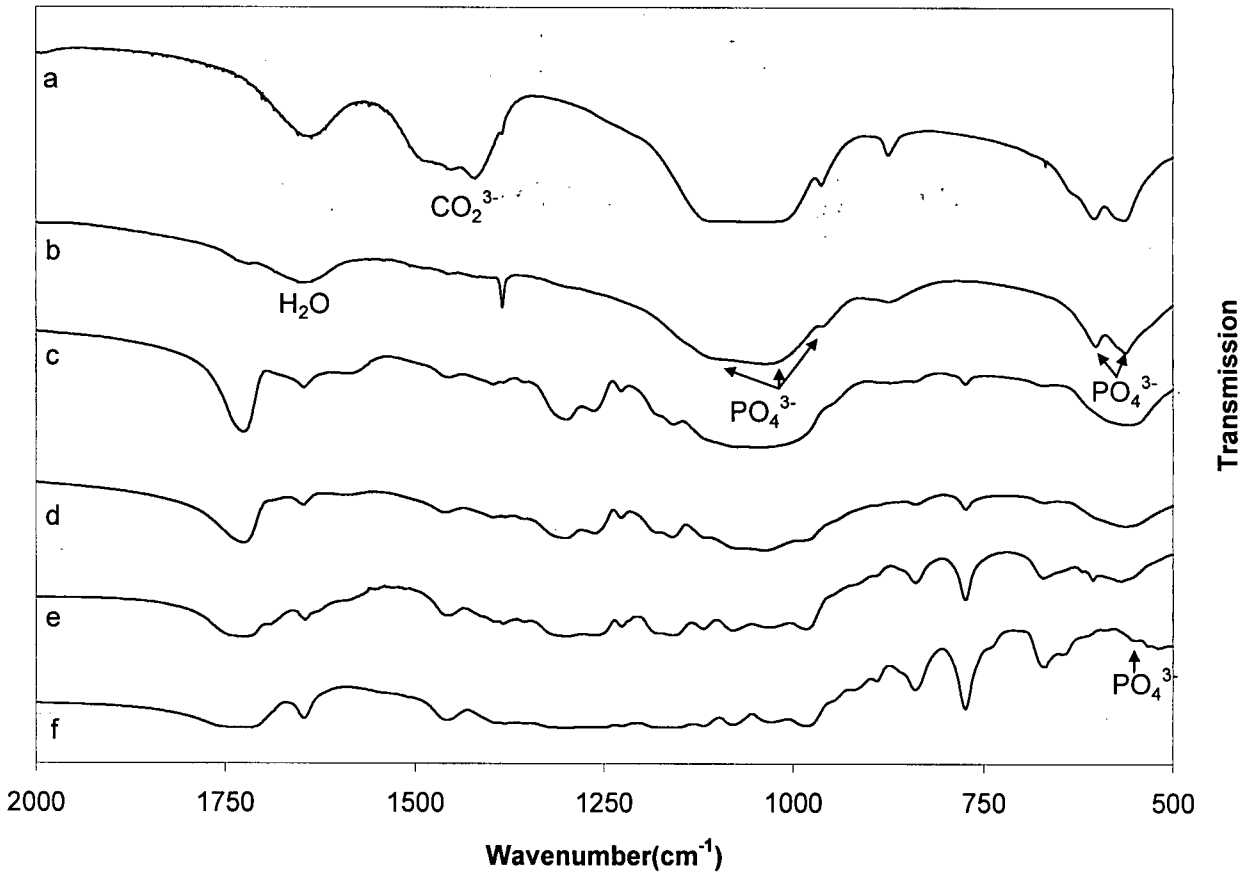

Figure 5-21 FTIR spectra of composite samples prepared with (a) 0% , (b) 5%, (c) 50%, (d) 80%, (e) 95%, and (f) 100%, MMw PPF, prepared at pH=10 and after 24 hours of synthesis.

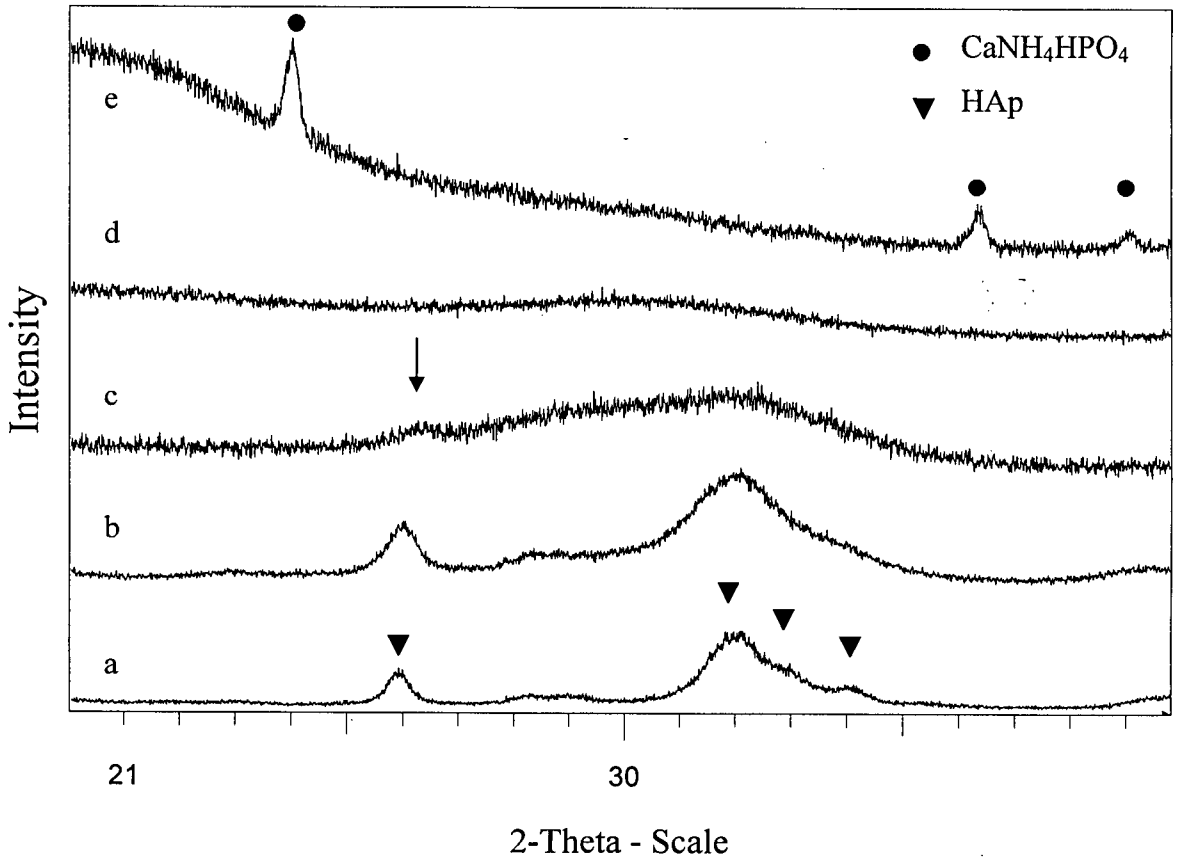

Figure 5-22 X-ray diffraction patterns of (a) THF-based HAp and composites with (b) 5%, (c) 50%, (d) 80%, and (e) 95% MMw PPF after 24 hour of synthesis time at pH=10.

The presence of calcium ammonium hydrogen phosphate in the 95% composite suggests that the calcium ions were not readily available to the phosphate precursors to form calcium phosphate compounds. Two factors might have contributed to the formation of calcium ammonium hydrogen phosphate rather than calcium phosphates such as ACP; first due to the high concentration of the PPF and the availability of C=O bonds, numerous PPF-Ca^{2+} clusters could have formed and therefore the thermodynamic activity of the Ca^{2+} and the supersaturation of the solution could have been reduced with respect to calcium phosphates [189, 191]. As a result, calcium ammonium hydrogen phosphate would precipitate. Secondly, the steric hindrance of the PPF chains might have blocked the calcium precursor from interacting with the phosphorus

precursor. If the latter is true crystalline calcium nitrate should have also been observed in the X-ray diffraction spectrum. No calcium nitrate was present neither in the XRD nor in the FTIR results. Therefore, formation of calcium ammonium hydrogen phosphate in higher concentrations of PPF provides another evidence that PPF interacts with the Ca^{2+} in the solution and therefore affects the calcium phosphate precipitation.

The concentration dependence of the effect of polyelectrolytes on the crystallization and growth of inorganic salts has been established by several investigators [103, 104, 106, 107, 189, 192, 193, 196, 197]. It has been observed that macromolecules or polyelectrolytes can act as nucleation template or crystallization inhibitors depending on their concentration. This is due to the fact that the mechanism by which the polyelectrolytes affect the nucleation and growth processes is mainly governed by the absorption of the additive on the surface of the nucleating phase [103, 104, 106, 107, 189, 192, 193, 196, 197]. In the system studied here, PPF binds with the Ca^{2+} in the solution to form PPF-Ca^{2+} complexes as evidenced in Chapter 5.5. Such complexes further act as templates for the formation of ACP particles which subsequently transform to crystalline HAp. For low concentrations of PPF, PPF-Ca^{2+} complexes form, providing a suitable substrate for the formation of ACP. At the same time, PPF binding to Ca^{2+} in the solution reduces the saturation of the solution and therefore promotes the formation of ACP rather than DCPD. Our experimental results also confirm this explanation. While brushite is the dominant phase in the absence of PPF after 1 hr of synthesis time, only ACP is present in the sample with 5wt% PPF confirming that the solution is no more saturated in respect to brushite upon the addition of PPF. For higher concentrations of polymer, the formation of PPF-Ca^{2+} complexes promotes the formation of ACP but at the same time the PPF chains that do not participate in the templating effect absorb on the surface of the ACP particles shielding their surface from the surrounding medium. As the nucleation of the HAp crystals takes place on the

surface of ACP particles [188], presence of the organic molecules on the surface that hinders ion diffusion to the surface, slows ACP to HAp transformation. Other investigators have also found the absorption of the polyelectrolytes or macromolecules on the surface of growing crystals to be the main reason for the inhibition of nucleation and growth of crystals [104, 107, 189, 193, 196].

The above X-ray diffraction data together with the FTIR results lead to two major conclusions: (i) the presence of PPF, regardless of its concentration in the composite, facilitates the formation of the ACP particles due to the formation of PPF-Ca^{2+} complexes which act as the preferred formation site and also reduce the saturation of the solution, and (ii) the inhibiting effect of PPF on the ACP to HAp transformation increases with increase in the concentration of PPF in the solution. The latter is due to the possibility that the PPF molecules that do not participate in templating effect are absorbed on the surface of ACP particles hindering nucleation of the HAp phase.

Figure 5-23 shows the electrokinetic sonic amplitude (ESA) measurements for the THF-based sample and the composite with PPF(MMw):HAp=4, which were collected after 24 hours of synthesis time. The THF-based sample (Fig 5-23a) shows a natural pH of 7.5 and an isoelectric point at pH=8.2. The THF-based particles show negative surface charge in the pH range above 8.2. The composite sample (Fig 5-23b) has a starting pH of about 8.5 and shows positive surface charge throughout the experiment. Titrating the samples to lower pH (less than 6) shows a steep curve in the positive region which might be attributed to the dissolution of the calcium phosphate phase in that pH range.

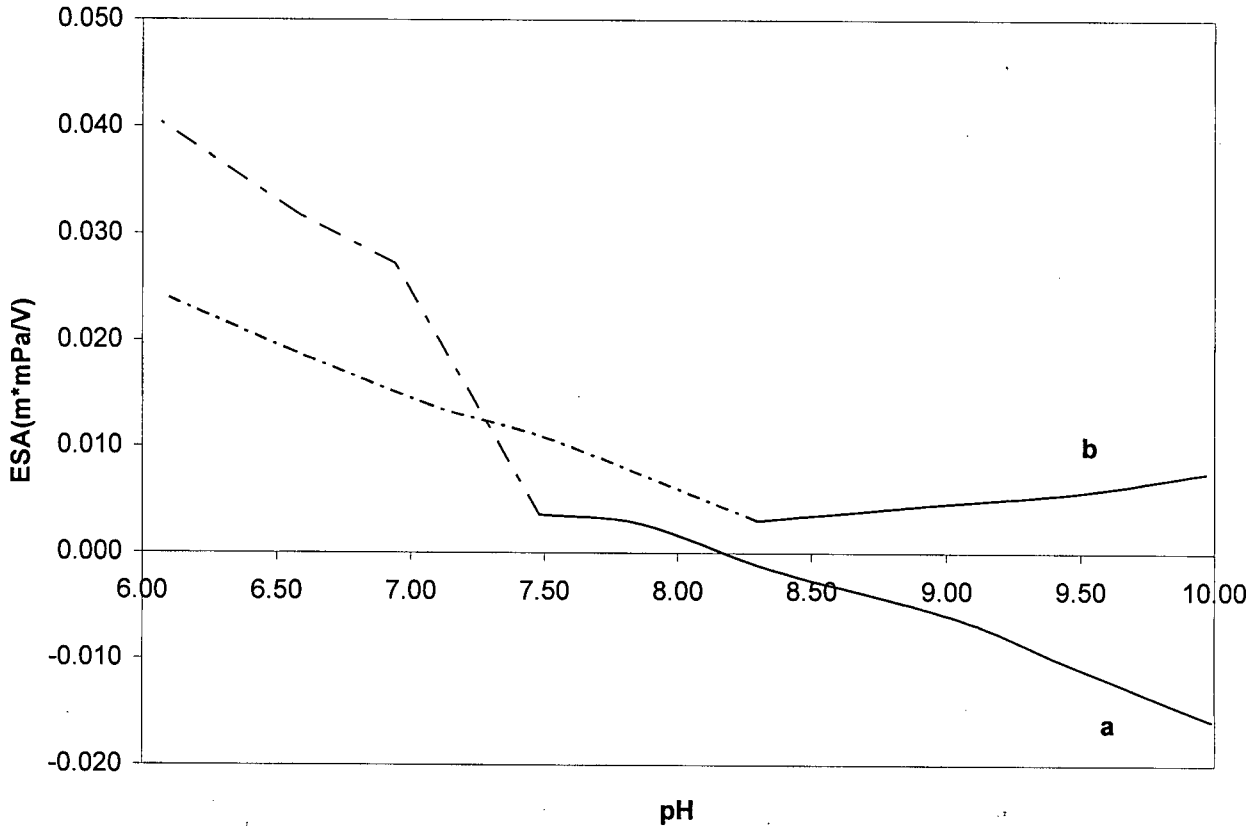

Figure 5-23 ESA measurements of (a) THF-based sample and (b) composite with PPF (MMw): HAp=4. Both samples were prepared after 24 hour of synthesis and at pH=10. Dotted lines represent reverse titration of the samples to lower pH.

It can be clearly seen that the addition of PPF to calcium phosphate particles significantly changes (i.e. reverses) the surface charge of the calcium phosphate particles for pH>8.2. This observation supports the above hypothesis that the PPF molecules are present on the surface of calcium phosphate particles. For low concentrations or small molecule size of PPF this phenomenon facilitates the ACP to HAp transformation while for higher concentrations or higher molecule size of PPF, PPF molecules mask the surface and prevent ion transportation on the ACP surface. Larger PPF molecules or higher concentration of PPF might also produce

significant steric hindrance for the movement of ions within the medium as in high PPF concentration (PPF: HAp=19) no ACP is formed.

5.7 The effect of PPF on calcium phosphate morphology

Figure 5-24(a-f) shows the SEM micrographs of the THF-based powder together with composites prepared with 5%, 50% and 80% of PPF (MMw). The THF based sample (5-24a) shows a poorly defined morphology consisting of very fine grains (<1 μm) which are not clearly distinguishable under SEM. Higher magnification micrograph of the same sample (5-25e) reveals smaller agglomerates within the size range of 0.3-1 μm. It can be observed that by the addition of PPF to the system, the powder appears "smoother" in SEM micrographs. For the PPF content of 80% (5-24d) only a featureless solid is observed. Higher magnification of the same sample (5-24f) does not reveal any further details about the constituent grains.

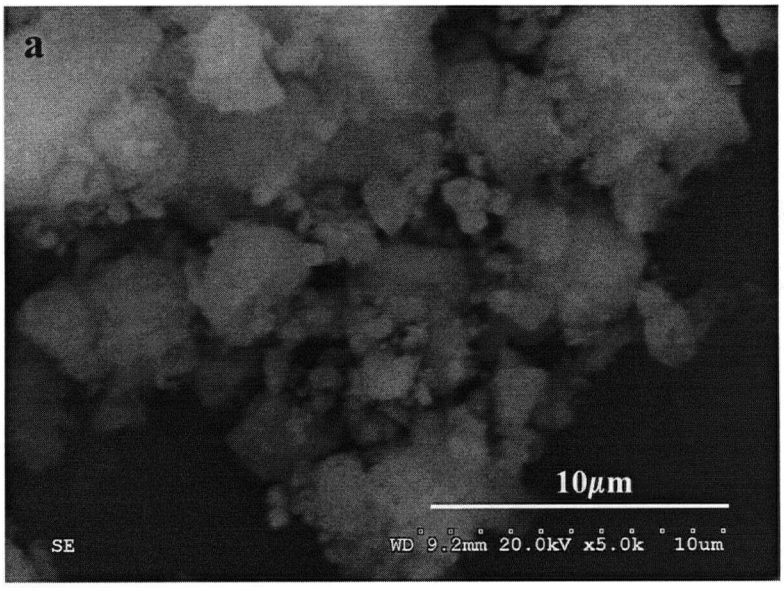

Figure 5-1 SEM micrographs of the (a) THF-based sample and composites with (b) with 5% (c) 50%, and (d) 80% PPF. (e) and (f) are micrographs of the THF-based and 80%-PPF samples in higher (X12K) magnifications, respectively.

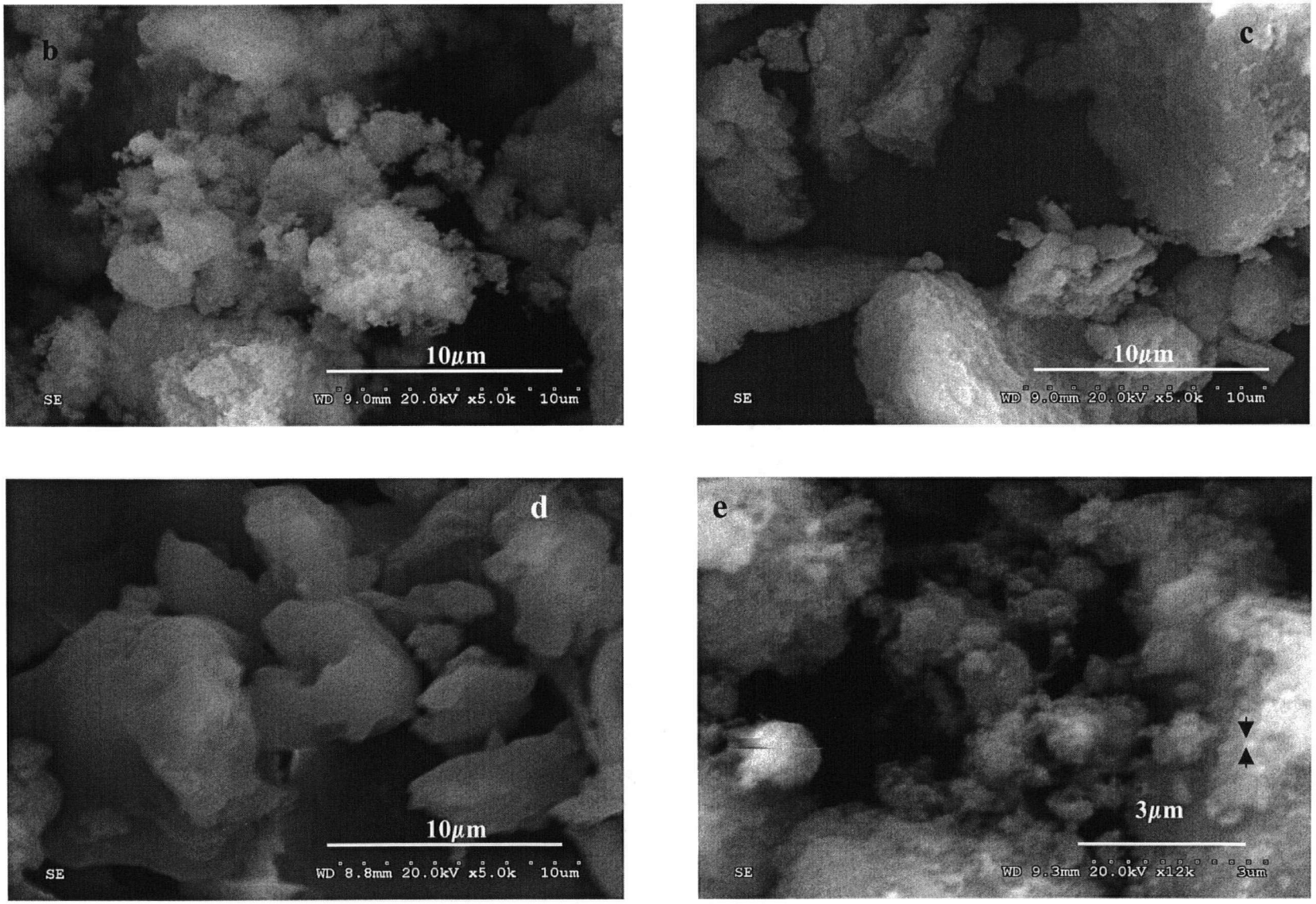

Figure 5-24 Continued.

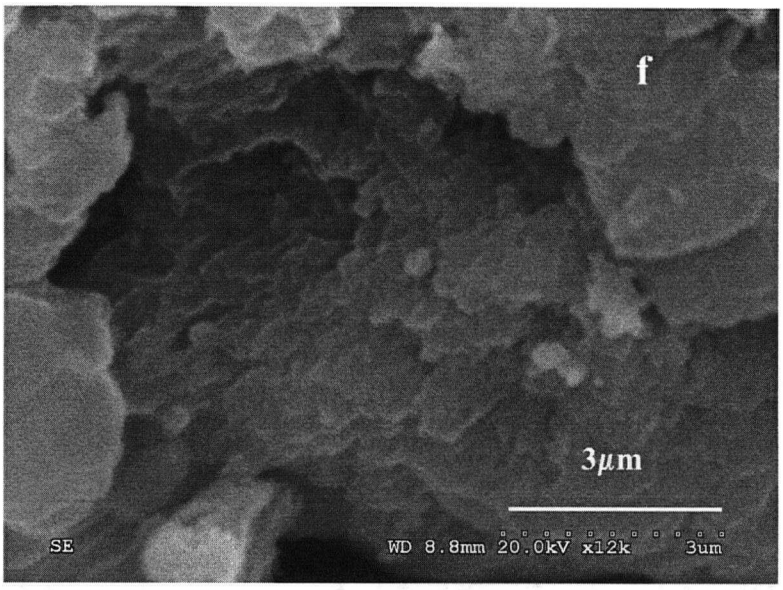

Figure 5-24 Continued.

By addition of PPF to the composite the calcium phosphate particles might be "wrapped" by layers of the polymer and therefore the particles appear smoother under SEM observations. By increasing the PPF content to 80% in the composites, the ACP particles are scattered within the polymer matrix and therefore the grain-like morphology observed for the samples with low or no polymer content is no longer observed.

Figures 5-25 a and b show the TEM micrographs and selected area diffraction (SAD) patterns of the THF-based sample and the sample with (PPF(MMw):HAp=4) after 24 hours of synthesis, respectively. The sample prepared in the absence of PPF (Fig 5-25a) shows agglomeration of "flake-like" crystals, characteristic of crystalline apatite [188], ranging between 50-150 nm in length. The SAD pattern of the same sample shows the diffraction rings of the crystalline apatite.

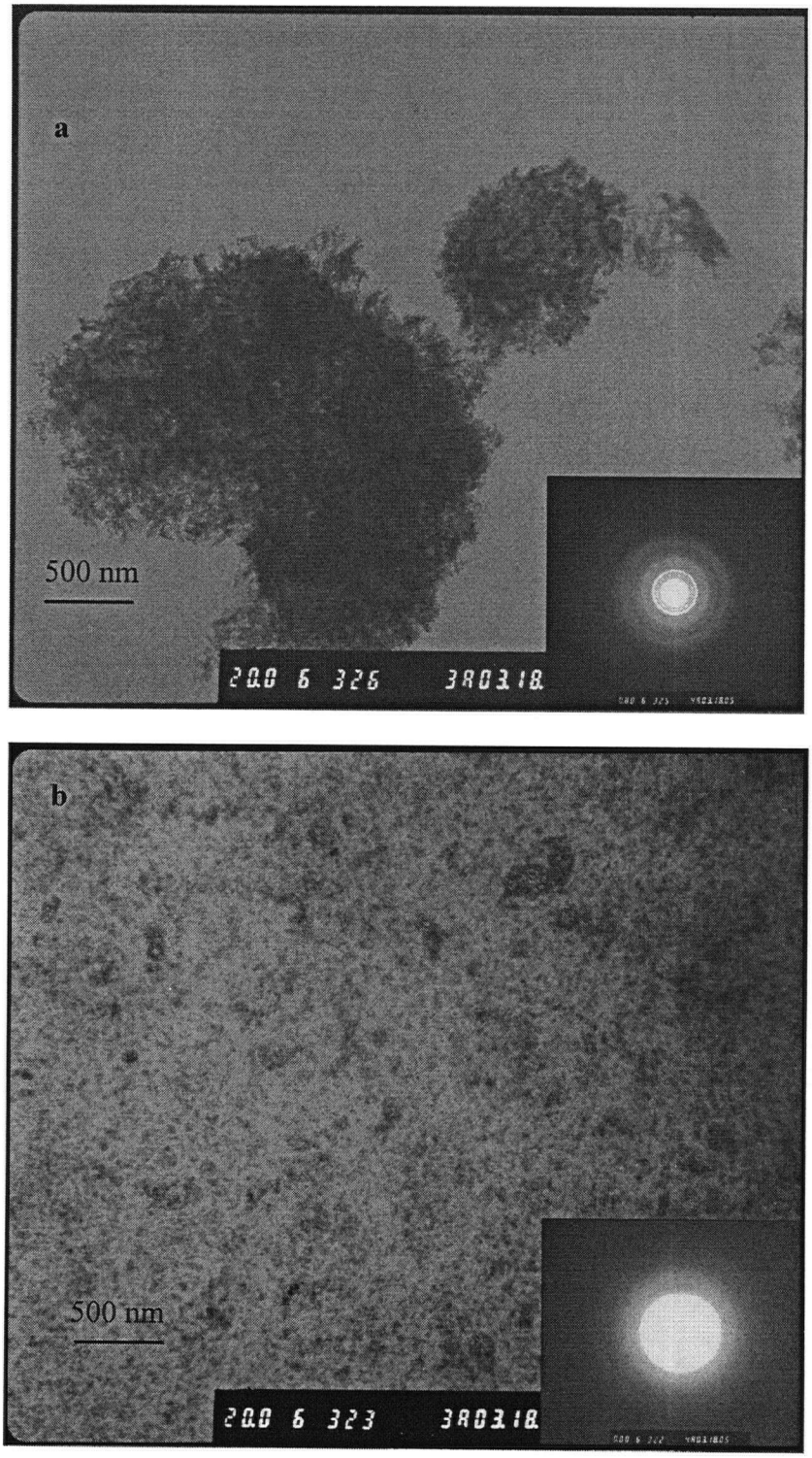

Figure 5-25 TEM micrographs and SAD patterns of the samples prepared after 24 hrs of synthesis at pH=10 (a) in the absence and (b) in the presence of PPF.

The TEM micrograph of the composite sample shows a distinct difference. The calcium phosphate phase present in the composite as confirmed by EDX, Appendix I, has disk shape morphology, characteristic of ACP [188]. The ACP particles are about 50-100 nm in diameter and are homogenously distributed within the PPF matrix. No significant agglomeration of the ACP particles is observed in the composite. SAD pattern of the composite sample does not show the characteristic diffraction rings of the crystalline apatite and further confirms the amorphous nature of the calcium phosphate phase.

Organic molecules and other macromolecules have been observed to cause deagglomeration of inorganic particles through surface absorption [104, 106, 107, 189]. Similar to other macromolecules, we conclude that the PPF molecules cover the surface of ACP particles and prevent them from agglomeration due to steric and electrostatic repulsive forces. As discussed earlier, surface coverage of ACP particles with PPF molecules appears to be the main reason for the stabilization of ACP in the composite. Similar effect of macromolecules on deagglomeration of mineral particles is perceived to be an inhibitor of pathological conditions such as kidney stone and dental calculus [104]. The homogenous dispersion of nanosized ACP particles within the PPF matrix also explains the fact that no calcium phosphate particles were observed in the SEM micrographs of the composite samples.

5.8 UV crosslinking of the PPF-calcium phosphate composites

Both the PPF and the composite (PPF(MMw):HAp=4) samples were crosslinked in a cylindrical mold by the addition of a photoinitiator (BAPO) and by UV irradiation. Figure 5-26 a-d show the fracture surface of the crosslinked PPF and composite samples. Figure 5-26a shows the low magnification of the fracture surface of the PPF sample. The 1-2 mm bubble-like defects present in the PPF samples (also observed in Fig 4-4) are not present in the PPF before crosslinking and

start to appear after few minutes of UV irradiation. We believe that these defects are produced due to the release of solvent (most probably ether, introduced during the purification process of the PPF) entrapped within the polymer during the synthesis of PPF. As the polymer starts to crosslink from outside inward, the solvent is vaporized (due to the heat of crosslinking, ~ 150 J/g with the maximum temperature of crosslinking of about 40-45 ^{o}C [20]) and is pushed out of the crosslinked structure and appears as a bubble inside the sample. In order to remove these bubbles, solvent extraction from the PPF after synthesis of the polymer should be carried out more efficiently. However, the composite samples were either defect free or had minimal bubble like defects. This can be explained by the fact that the PPF was dissolved in THF and precipitated again by the addition of water and therefore it is possible that the entrapped solvents were removed during the composite synthesis process. Figure 5-26b shows higher magnification of the fracture surface of the PPF sample, appearing smooth and featureless, characteristic of amorphous brittle fracture. Figure 5-26c and d show the fracture surface of the composite sample. It can be clearly seen that compared to the PPF sample the composite's fracture surface shows ~1μm large ridge-like patterns on the surface. These patterns are believed to be produced due to the interaction of the propagating crack with the embedded calcium phosphate particles.

Although, due to the presence of defects within the PPF samples, no conclusions on the final compressive strength of PPF and composite samples can be drawn, it is possible to speculate that the addition of the calcium phosphate particles to PPF will affect the mechanical behavior of the polymer. The effect of the calcium phosphate particles on the fracture of the polymer allows speculating that the fracture toughness of the composite will also be improved as compared to that of the PPF alone.

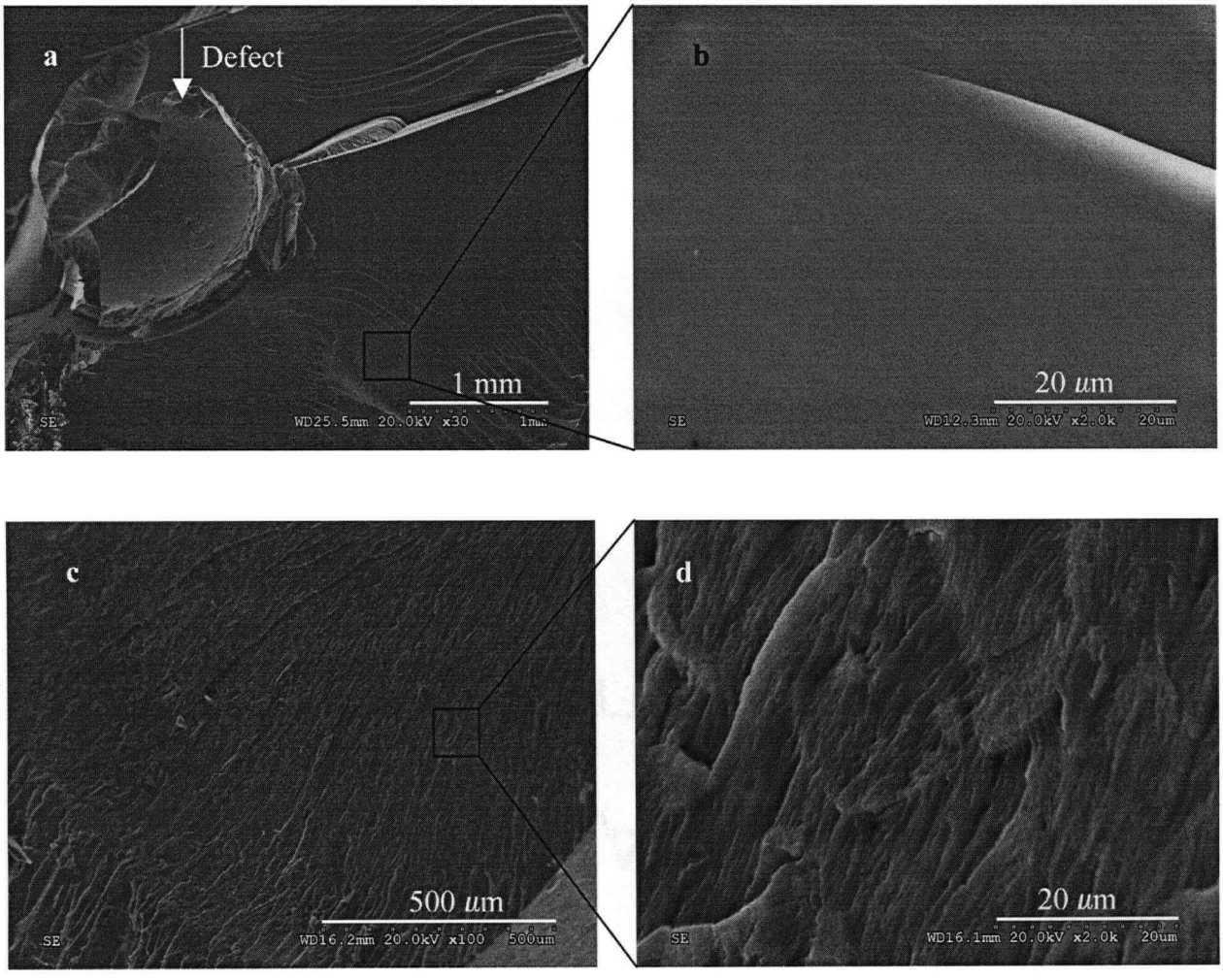

Figure 5-1 SEM micrographs of the fracture surface of (a) and (b) PPF and (c) and (d) of the composite (80% MMw PPF) samples fractured in compression.

It is known that the addition of calcium phosphates to polymers in the synthesis of composites for bone substitute materials has two advantages: first, it enhances the osteoconductivity of the polymer, and second, it improves the mechanical properties of the composites [198, 199]. The important issue in these composites is the interfacial bonding between the ceramic and the polymer. Poor interfacial bonding between the components detrimentally affects the mechanical properties of the composites [198, 199]. Many attempts have been made to improve the interfacial boding between the components of the composites. For example, Liu et al. have used diisocyanate coupling agent to

modify the surface of HAp to improve its bonding with polyethylene glycol/poly(butylene terephthalate) [200]. In another example, Ignjatovic et al. explored different processing techniques such as hot pressing the polymer and the HAp filler to improve the interfacial bonding [198]. In the case studied here there is an interaction between the calcium phosphate particles and the PPF through the formation of a complex between the carbonyl group of the PPF and the calcium ions. While the presence of PPF on the surface of calcium phosphate particles hinders the crystallization of HAp, at the same time it could ensure a good interfacial bonding between the PPF and the calcium phosphate particles. Moreover, adsorption of PPF on calcium phosphate particles leads to the formation of a well-mixed composite with nanometer sized (<100 nm) ACP particles homogeneously distributed within the polymer matrix (Fig 5-25b). Homogeneous distribution of nanoparticles within a viscous polymer is difficult to achieve [20]. Therefore, strong interfacial bonding and homogeneous distribution of nanosize particles, gained through the in-situ synthesis of the composite developed in this work, will likely play a crucial role in improving the mechanical properties of the PPF-calcium phosphate composites.

5.9 Summary

Biomimetically fabricated polymer-calcium phosphate composites are promising materials for hard tissue implants. However, mimicking the hierarchical structure of tissues like bone still remains a distant, far-reaching goal. This work investigated a novel, two-solvent, biomimetic process for the preparation of PPF-calcium phosphate composites.

The hypothesis of this work was that an interaction between PPF molecules and calcium ion (and further the surface of the calcium phosphate particles) exists that affects the phase evolution of the calcium phosphate phase. This hypothesis stemed from the fact that the calcium phosphate phase

formed in the absence and presence of PPF are significantly different, suggesting that PPF exerts an influence on the phase evolution of the calcium phosphate phase. Such observation, however, comes as no surprise. In the studies of the mechanisms of biomineralization, it has been repeatedly observed that the deposition, morphology, and orientation of the inorganic phase on the organic matrix are controlled by the matrix proteins. Although the exact mechanism of protein-mineral interactions is not yet fully known, significant body of research points to the electrostatic nature of such interactions.

In order to gain a better understanding of the effects of PPF on the crystallization of the inorganic phase, the principal process parameters such as the solvent type, pH, synthesis time, PPF molecular weight, and PPF concentration were systematically studied. In investigating the phase evolution of the calcium phosphate in presence and absence of THF (in the absence of PPF), we observed that due to the high initial calcium and phosphate concentrations in the solution, brushite (the least stable calcium phosphate phase at pH=10) precipitates first, regardless of the solvent. Therefore, replacing some of the water content of the solution with THF did not significantly affect the calcium phosphate phase evolution in this system. In both cases (i.e. water-based and THF-based systems) brushite was the first phase to appear, which further dissolved to form crystalline apatite after ~24 hours of synthesis time.

The additions of PPF to the precipitating calcium phosphate solution lead to the formation of PPF-Ca^{2+} complexes in the solution through a coordination bond between the Ca^{2+} and the carbonyl group of the polymer. The FTIR absorption band of the carbonyl group of PPF shifted to lower frequencies upon the addition of calcium ions to the system, supporting the above conclusion. This effect was found to be reproducible and consistent for various concentrations of Ca^{2+} in the system. Formation of such complexes preferentially removed Ca^{2+} from the solution, thus reducing the

concentration of Ca^{2+} ions and therefore affecting the phase formation of the calcium phosphate. Other calcium binding polymers were also observed to effectively promote the formation of HAp crystals. Similar to these bio-molecules, the effect of PPF on the phase evolution of the calcium phosphate was found in this work to be concentration dependent.

Molecular weight of the PPF also played an important role in hindering or promoting the crystallization of HAp. Figure 5-27 schematically summarizes our observations regarding the combined effects of concentration and molecular weight of PPF on the type of the calcium phosphate phases that form after 24 hours of synthesis at pH=10. Figure 5-27 is only a qualitative representation of the trends observed in the system studied, and the "phase boundaries" are schematic and approximate. The black circles represent the actual results of experiments.

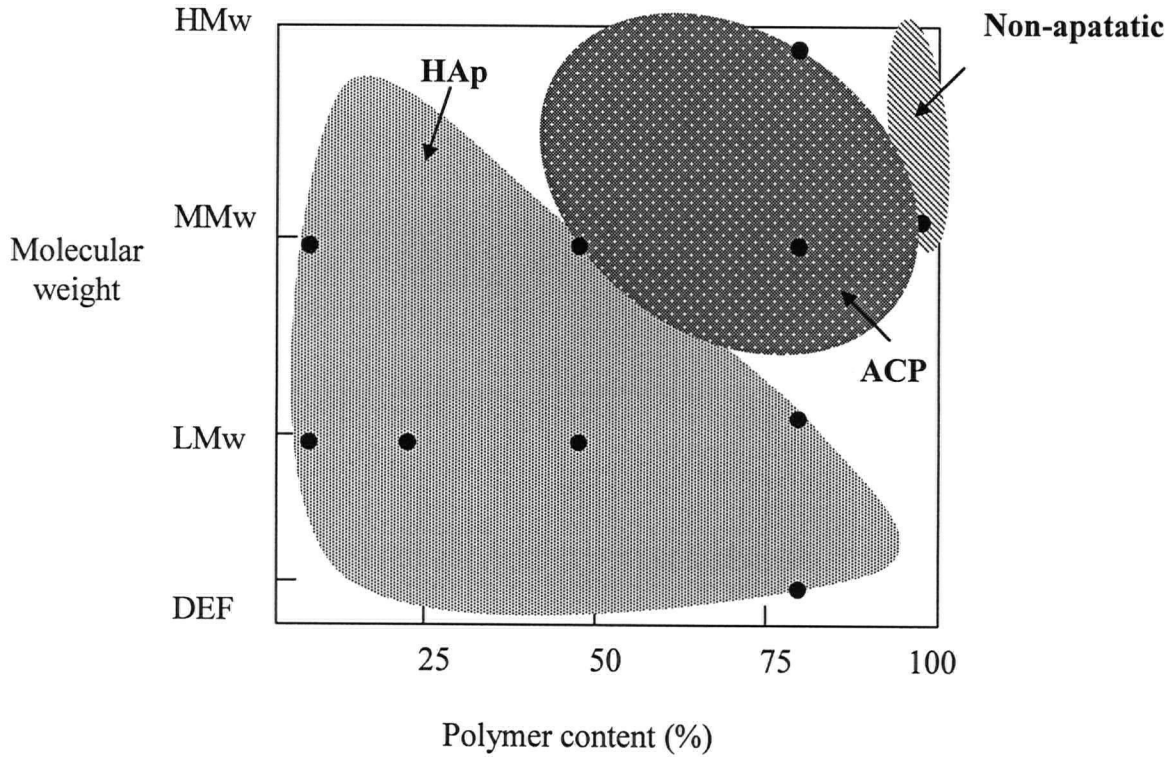

Figure 5-27 Schematic representation of the effect of PPF content and molecular weight on the calcium phosphate phase formed at pH=10 after 24 hours of synthesis.

When low molecular weight PPF was used (and also DEF) the formation of PPF-Ca^{2+} complexes promoted the precipitation of the ACP phase. ACP precipitates as a precursor to crystalline HAp at pH=10 [58, 188], which was also observed in this work. We hypothesized that the excess PPF molecules that did not participate in this templating effect were absorbed to the surface of calcium phosphate particles. This hypothesis was further supported by ESA measurements on calcium phosphate particles prepared in the absence and presence of PPF. In the presence of PPF, the surface charge of the particles was significantly affected (reversed), indicating the presence of PPF molecules on the surface of calcium phosphate particles. LMw/ DEF molecules could absorb/desorb easier from the surface of the inorganic phase, exposing the surface of these particles to the surrounding media and therefore allowing the ACP to HAp transformation. On the other hand, small PPF/DEF molecules that absorb on the surface could also act as active centers [193] and therefore facilitate the precipitation of the HAp crystals to the surface of the ACP particles by accumulating high surface charge at the ACP/solution interface and attracting oppositely charged ions. It has been observed by various investigators that this amorphous-crystalline transformation is significantly affected by the presence of organic molecules [189, 192, 193]. In the presence of the LMw PPF/DEF crystalline HAp can form after only 1 hr of synthesis compared to the 24 hrs time period needed for the induction of HAp in the absence of these molecules.

We believe that in case of LMw PPF a small amount of PPF (<20%) was incorporated within the ACP particles as suggested by TGA analysis. If LMw PPF acts as active center, it is reasonable to believe that by attracting the oppositely charged ions these molecules can be incorporated within the growing particles. This could explain the loss of diffraction peak in the XRD data after 24 hours of synthesis time (Fig. 5-16B). This may also explain the disappearance of the PPF peaks from the FTIR spectrum of the composite after 24 hrs of synthesis time (5-16A).

In the presence of HMw PPF, the molecules that did not participate in producing PPF-Ca^{2+} complexes were expected to be absorbed to the surface of the ACP particles, shielding them from the surrounding solution. Therefore, the adsorption/desorption process could not readily occur due to the larger size of the PPF chains and their low solubility in the solution. The surface of the ACP particles was shielded from the surrounding media by PPF. At the same time these molecules produced a steric hindrance for the precipitating ions to reach the ACP surfaces. As a result of these interactions ACP was stabilized in the solution for more that 24 hours, Fig. 5-27. The final washing process of the composite did not affect the stability of the ACP phase as the particles were encapsulated by the PPF molecules. Encapsulation of the ACP particles with PPF was also found responsible for the dispersion of the ACP particles observed in TEM micrographs (Fig 5-25).

The effect of PPF on the ACP to HAp transformation was found to also be concentration dependent. For low concentrations of PPF (5%), PPF molecules participated in templating the formation of ACP. The ACP particles further transformed to crystalline HAp. By increasing the PPF concentration (5%-80%) the PPF molecules that did not participate in the templating effect covered the surface of the ACP particles and therefore hindered/delayed the ACP to HAp transformation. At 95% PPF concentration, PPF molecules preferentially removed significant amount of Ca^{2+} ions from the solution and therefore ACP and consequently HAp were not formed and only non-apatitic calcium phosphate phases, such as calcium ammonium hydrogen phosphate were present. These observations are schematically illustrated in Fig 5-27.

Both PPF and composite samples were crosslinked using UV irradiation into cylindrical samples. Addition of calcium phosphate to the PPF polymer served to affect the interaction between the propagating crack and the matrix as suggested by the SEM observation of fractured surfaces of PPF and composite samples (Fig 5-26).

6 Conclusions

The major conclusion drawn from this work can be summarized as follows:

1- This work, for the first time, investigated the precipitation of calcium phosphate in a THF-water system. THF is a commonly used organic solvent which dissolves a wide rage of organic molecules and polymers. Therefore, a THF-water system opens the door for the application of other non-water soluble polymers (including drugs) in the co-precipitation process. It was observed that the phase evolution of calcium phosphate was not affected by the presence of the organic solvent.

2- Regardless of the presence of the organic solvent, brushite was the first phase to appear in the system studied here. The brushite phase further recrystallized to hydroxyapatite. Although at pH=10 amorphous calcium phosphate (ACP) was expected to be the first precipitated phase, due to the high initial concentration of calcium and phosphate ($\log (T_{ca} x\ T_P) = -1.47$) in the system brushite appeared first.

3- This work, for the first time, studied the precipitation of calcium phosphate in the presence of poly(propylene fumarate). A two-solvent system for the synthesis of PPF-HAp was developed and the effect of process parameters and the PPF characteristics were systematically studied. The results obtained suggested that:

   a. A coordination bond could form between the carbonyl group of PPF and the Ca^{2+} upon the addition of calcium ion to the PPF solution. It was postulated that formation of such PPF-Ca^{2+} complexes significantly affected the observed phase evolution of the calcium phosphate phase in the presence of PPF. We believe

that PPF-Ca^{2+} complex provides a site for the formation of the calcium phosphate phase.

b. The effect of pH on calcium phosphate precipitation was not influenced by the presence of PPF. At lower pH (pH ~7) brushite precipitated while by increasing pH to ~10 amorphous calcium phosphate (ACP) was the first phase to precipitate.

c. In the presence of PPF and at pH=10, ACP was the first phase to appear while in the absence of PPF brushite was the first phase to precipitate. This phenomenon was explained by the fact that the formation of PPF-Ca^{2+} complexes removed calcium ions from the solution and therefore reduced the saturation of the system in respect to calcium phosphates.

d. Despite the 24 hour coexistence with the mother solution, ACP remained stable in the system with 80% PPF, at pH=10. We believe that the PPF molecules that did not participate in forming PPF-Ca^{2+} complexes, were absorbed on the surface of the ACP particles, shielding them from the surrounding solution. Therefore, the precipitating ions (Ca^{2+} and PO_4^{3-}) would not reach the ACP surface to initiate HAp crystallization. This hypothesis was further confirmed by ESA measurement showing that the surface charge of the particles was positive in the presence of PPF while in the absence of PPF particles were negatively charged (for pH> 8.2). The change in the surface charge of the particles, due to the adsorption of PPF on the surface, also prevented the

similarly charged ions from moving toward the surface and therefore further hindered the ACP to HAp transformation.

e. The ability of PPF to stabilize ACP was significantly affected by the molecular weight and concentration of PPF.

f. In the presence of DEF (a precursor to PPF), crystalline HAp formed within 1hr of synthesis, further supporting the idea that the PPF-Ca^{2+} complexes provide a formation site for the formation of calcium phosphate.

g. Low molecular weight PPF (M_w=1800) was less efficient in stabilizing ACP compared to the higher molecular weight PPF (M_w= 4500). This was explained by the fact that LMw PPF is more soluble and therefore can readily adsorb/desorb on/from the surface, exposing the ACP particles to the surrounding solution. At the same time, small molecules of PPF on the surface of ACP particles attract oppositely charged ions (Ca^{2+} or PO_4^{3-}, depending on the charge of the polymer) and therefore promote the ACP to HAp transformation, acting as an "active center".

h. LMw PPF might be incorporated within the growing ACP particles. This could explain loss of crystallinity in the XRD patterns and the loss of PPF absorption bands in the FTIR spectra. TGA data also showed an extra 20% weight loss compared to the sample prepared in the absence of PPF.

i. PPF was more efficient in stabilizing ACP at higher concentrations (above 50 wt%). By increasing the PPF concentration within the system, more PPF was available to absorb on the ACP particles and therefore encapsulated these particles, shielding them from the ions in the solution. It is possible that the absorbed PPF also produced steric hindrance for the precipitating ions (Ca^{2+} and PO_4^{3-}) to reach the ACP surface.

j. At PPF concentration of 95%, $CaNH_4HPO_4$ precipitated. This observation further suggested that PPF interacts with Ca^{2+} ions within the solution. As a result, more calcium ions were removed from the solution and calcium ammonium hydrogen phosphate rather than ACP was formed.

k. TEM observations of the composite samples showed that while flake-like hydroxyapatite crystals formed in the absence of PPF, spherical ACP particles formed when PPF was present. The ACP particles in the composite were 50-100 nm in diameter and did not show agglomeration.

4- The composite was crosslinked using BAPO as the photoinitiator and by UV irradiation.

5- The fracture surface of the crosslinked PPF was smooth and featureless while a rough ridge-like surface was observed for the PPF-ACP composite suggesting different fracture mechanism for the PPF-ACP composite compared to that of the PPF alone.

7 Future work

Additional studies concerning the synthesis of PPF-HAp scaffolds for bone TE application, using the findings presented in this thesis, are suggested as follows:

7.1 Fabrication of porous scaffold

A suitable porogen material should be identified to produce a porous scaffold using PPF-HAp composite. The porogen can be added to the composite before the crosslinking step. It will be later washed out to produce appropriate porosity.

We have recently started and demonstrated the process of identification and fabrication of a sugar-based porogen. The viscous, sugar-based material can be easily shaped into different morphologies. A sugar-based material resolves some of the issues related to the currently used salt-based porogens. The remainder of the salt in the scaffold causes inflammation within the surrounding tissue [21, 33]. It also reduces the pH of the environment adjacent to the scaffold and therefore increases the degradation rate of the polymer [33]. The sugar-based material can be easily shaped into microspheres or fibers to produce different scaffold morphologies. Our early investigation using the sugar-based material with epoxy resin has shown that interconnected porosity can be produced using this porogen (Figure 7-1).

The effect of the porogen material on the crosslinking efficiency of the composite should also be investigated. This can be assessed by calculating the curing efficiency of the composite before and after the addition of the porogen. The crosslinking efficiency is calculated by measuring the swelling degree of the crosslinked composite.

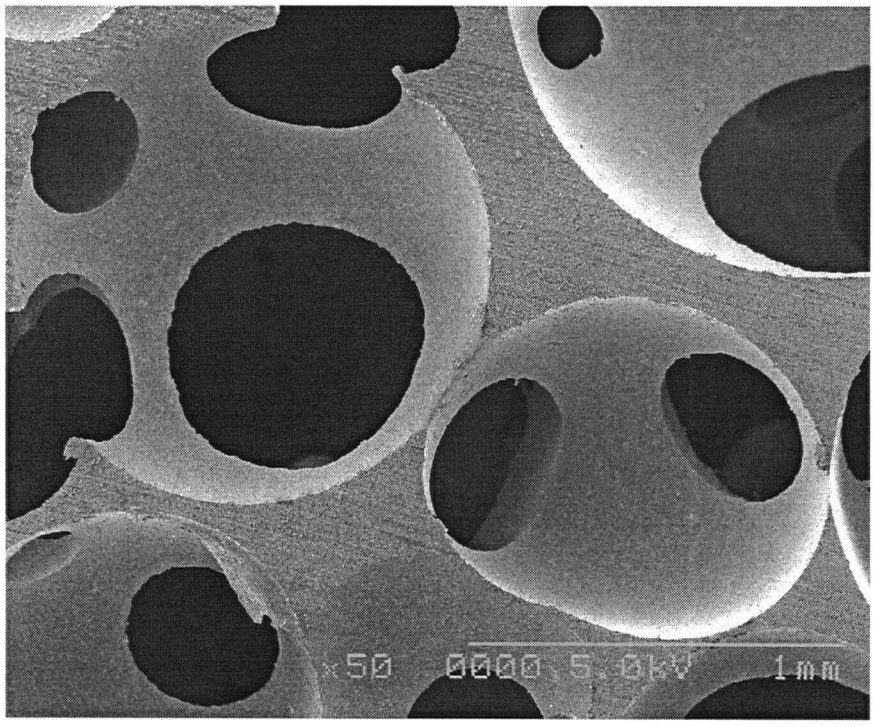

Figure 7-1 Cross-section of a scaffold made of epoxy. The porosity is produced using sugar-based porogen.

7.2 Mechanical behavior of the composite scaffolds

The mechanical properties of the porous scaffolds should be evaluated. Our initial tests show that the addition of nano-sized calcium phosphate particles significantly improves the elastic modulus of the polymer. Further investigation of the strength and fracture of the scaffold with appropriate porosity should be conducted.

7.3 Degradation behavior of the composite scaffold

Degradation rate of the composite is an indication of the time period that the scaffold is mechanically viable after implantation. Recent reports show that inclusion of calcium phosphates

in polymers reduces their degradation rate [201, 202]. This is due to the fact that dissolution of calcium phosphates increases the pH of the surrounding environment and therefore reduces the hydrolytic degradation of the polymer [201, 202]. It has been shown in case of mechanically mixed PPF-HAp composites that the mechanical strength of the polymer increases after few hours of degradation due to the formation of PPF-Ca^{2+} complexes which reduces the degradation rate of the polymer [203]. We believe that the in-situ process, developed and studied in this work, produces a strong bond between PPF and the calcium phosphate phase and therefore should act more efficiently in reducing the degradation rate of the composite and also maintaining the mechanical strength of the scaffold for longer periods of time.

We have also shown that the crystallinity and the nature of the calcium phosphate phase can be altered by the molecular weight and concentration of PPF. As the degradation rate of the calcium phosphates is dependent on their crystallinity we believe by controlling the process parameters of the synthesis process we can produce composite materials with various degradation rates for different applications.

7.4 Incorporation of pharmaceutical agents within the scaffold

Tissue engineering scaffolds are expected to release biological or pharmaceutical agents into their local environment upon degradation. These agents illicit a positive cell response within the surrounding tissue and therefore facilitate the healing process.

We believe that the in-situ synthesis process proposed in this research work provides flexibility for the incorporation of pharmaceutical agents within the composite. Degradation of the composite modulates the release of the drugs. As the degradation of the composite can be

adjusted using the process parameters, we believe that the release of the pharmaceutical agents can also be modified in order to fabricate a scaffold that can release the required drugs in a timely manner at the specific site.

7.5 In-vivo behavior of the composite scaffold

In-vivo animal test is the ultimate measure of compatibility and suitability of biomaterials. The optimum scaffold should be tested in-vivo to confirm its biocompatibility and also to evaluate its performance.

References

1. Hench L, Polk JM. Third generation biomedical materials. Science 2002; 295: 1014-1017.

2. Langer R, Vacanti JP. Tissue engineering. Science 1993; 260(5110): 920-6.

3. Yang Sh, Leong KF, Du Z, Chua CK. Design of scaffolds for use in tissue engineering. Part 1: Traditional factors. Tissue engineering 2001;17: 679-689.

4. Murphy WL, Mooney DJ. Molecular-scale biomimicry. Nature Biotechnology 2002; 20(1): 30-31.

5. Hubbell JA. Biomaterials in tissue engineering. Bio/technology 1995; 13(6): 565-76.

6. Wickware P. Exploring the territory in tissue engineering. Nature 2000; 403(6768): 464-465.

7. Crane GM, Ishaug SL, Mikos AG. Bone tissue engineering. Nature Medicine 1995; 1(12):1322-4.

8. Saltzman WM, Olbricht WL. Building drug delivery into tissue engineering. Nature Reviews Drug Discovery 2002; 1(3): 177-186.

9. Reddi AH. Role of morphogenetic proteins in skeletal tissue engineering and regeneration. Nature Biotechnology 1998; 16(3): 247-252.

10. Nakashima M, Reddi AH. The application of bone morphogenetic proteins to dental tissue engineering. Nature Biotechnology 2003; 21(9): 1025-1032.

11. Shea LD, Smiley EBJ, Mooney DJ. DNA delivery from polymer matrices for tissue engineering. Nature Biotechnology 1999; 17(6): 551-4.

12. Miller WM, Peshwa MV. Tissue engineering, bioartificial organs, and cell therapies: 1. Biotechnology and Bioengineering 1996; 50: 463-463.

13. Lysaght MJ, Reys J. The growth of tissue engineering. Tissue Engineering 2001; 7: 485-493.

14. Griffith LG, Naughton G. Tissue engineering - current challenges and expanding opportunities. Science 2002; 295 (8): 1009-1014.

15. U.S. department of health and human services. 2020: a new vision- a future for regenerative medicine. U.S. department of health and human services website (www.hhs.gov/reference/newfuture) Jan. 2005.

16. Ishaug SL, Crane GM, Miller J, et al. Bone formation by three dimensional stromal osteoblast cultures in biodegradable polymer scaffolds. J Biomedical Materials Research 1997; 36: 17-25.

17. Sanchez C, Arribart H, and Guile MMG. Biomimetism and bioinspiration as tools for the design of innovative materials and systems. Nature 2005; 4: 277-288.

18. Arias JL and Femandez MS. Biomimetic processes through the study of mineralized shells. Materials Characterization 2003; 50: 189-195.

19. Douglas T. A bright bio-inspired future. Science 2003; 299 (5610): 1192-1194.

20. Fisher JP, Holland TA, Dean D, et al. Synthesis and properties of photocrosslinked poly(propylene fumarate) scaffolds. J Biomaterials Science Polymer Edition 2001; 12: 673-687.

21. Fisher JP, Vehof JWM, Dean D, et al. Soft and hard tissue response to photocrosslinked poly(propylene fumarate) scaffolds in a rabbit model. Journal of Biomedical Materials Research 2002; 59(3): 547-556.

22. Fisher JP, Dean D, Mikos AG. Photocrosslinking characteristics and mechanical properties of diethyl fumarate/poly(propylene fumarate) biomaterials. Biomaterials 2002; 23: 4333-4343.

23. Horch RA, Shahid N, Mistry AS, Timmer MD, Mikos AG, Barron AR. Nanoreinforcement of poly(propylene fumarate)-based networks with surface modified aluminoxane nanoparticles for bone tissue engineering. Biomacromolecules 2004; 5(5): 1990-1998.

24. Hench LL. Bioceramics. J American Ceramic Society 1998; 81(7): 1705-28.

25. Chang YL, Lew D, Park JB, Keller JC. Biomechanical and morphometric analysis of hydroxyapatite-coated implants with varying crystallinity. Journal of oral and maxillofacial surgery 1999; 57 (9): 1096-1108.

26. Cohen S, Bano MC, Cima IG, et al. Design of synthetic polymeric structures for cell transplantation and tissue engineering. Clinical Materials 1993; 13: 3-11.

27. Whang K, Healy KE, Elenz DR, et al. Engineering bone regeneration with bioadsorbable scaffolds with novel microstructure. Tissue Engineering 1999; 5: 35-51.

28. Brunski JB. Metals. In: Ranter BD, Hoffman AS, Schoen FJ, et al., ads. Biomaterials science: An introduction to materials in medicine. New York: Academic press, 1996. p. 37-50.

29. Mano JF, Vaz CM, Mendes SC, et al. Dynamic mechanical properties of hydroxyapatite-reinforced and porous starch-based degradable biomaterials. J Material Science: Materials in Medicine 1999; 10: 857-862.

30. Freed LE, Vunjak-Novakovic G, Biron RJ, Eagles DB, Lesnoy DC, Barlow SK, Langer R. Biodegradable polymer scaffolds for tissue engineering. Bio/Technology 1994; 12(7): 689-93.

31. James K, Kohn J. New biomaterials for tissue engineering. Materials Research Bulletin 1996; 21(11): 22-26.

32. Cooke, MN, Fisher JP, Dean D, Rimnac C, Mikos AG. Use of stereolithography to manufacture critical-sized 3D biodegradable scaffolds for bone ingrowth. J Biomedical Materials Research 2003; 64B (2): 65-69.

33. Peter SJ, Kim P, Yasko AW, et al. Crosslinking characteristics of an injectable poly(propylene fumarate)/β-calcium phosphate paste and mechanical properties of the crosslinked composite for use as a biodegradable bone cement. J Biomedical Materials Research 1999; 44: 314-321.

34. Yaszemski MJ, Payne RG, Hayes WC, et al. In vitro degradation of a poly(propylene-fumarate)-based composite material. Biomaterials 1996; 17: 2127-2130.

35. Shikinami Y, and Okuno M. Bioresorbable devices made of forged composites of hydroxyapatite particles and poly-L-lactide (PLLA): Part 1. Basic characteristics. Biomaterials 1999; 20: 859-877.

36. Cornell C N, Lane JM. Newest factors in fracture healing. Clinical Orthopedics and Related Research 1992; 277: 297.

37. Yang ZJ, Yuan HP, Tong WD, et al. Osteogenesis in extraskeletally implanted porous calcium phosphate ceramics: variability among different kinds of animals. Biomaterials 1996; 17: 2131-2137.

38. Jarcho M. Calcium phosphate ceramics as hard tissue prosthetics. Clinical Orthopedics and Related Research 1981; 157: 259-278.

39. Wilson J, Clark AE, Douek, Krieger J, Smith WK, and Zamet SJ. Clinical applications of bioglass® implants. In: Anderson DH, Happonen RP, and Urpo A-Y, editors. Bioceramics. Butterworth-Heinemann, Oxford, UK, 1994.

40. Amjad Zahid Z, John F, Thomas-Wohlever JA. Inhibition of calcium phosphate precipitation by polymers in the presence of iron (III): The influence of chelating agents. Book of Abstracts 1999; 218th ACS National Meeting, New Orleans, Aug. 22-26.

41. Kato N, Niikura Y, Tokuoka Y, Kawashima N. Removal of phosphorus from water using bio-cement composed of fragments of china plate, bone ash, and alumina cement. Material Technology (Tokyo, Japan) 2004; 22(2): 43-49.

42. Yi WG, Lo KV. Phosphate recovery from greenhouse wastewater. Journal of Environmental Science and Health. Part. B, Pesticides, Food contaminants, and Agricultural Wastes 2003; 38(4): 501-9.

43. Eanes ED, Meyer JL. The maturation of crystalline calcium phosphates in aqueous suspensions at physiologic pH. Calcified Tissue Research 1977; 23(3): 259-69.

44. Nancollas GH. Enamel apatite nucleation and crystal growth. Journal of Dental Research 1979; 58(Spec Issue B): 861-70.

45. Heughebaert JC. Nancollas GH. Mineralization kinetics: the role of octacalcium phosphate in the precipitation of calcium phosphates. Colloids and Surfaces 1984; 9(1): 89-93.

46. Nancollas GH, Zawacki SJ. Calcium phosphate mineralization. Connective Tissue Research 1989; 21(1-4): 239-44.

47. Ishikawa K, Eanes ED, Tung MS. The effect of supersaturation on apatite crystal formation in aqueous solutions at physiologic pH and temperature. Journal of Dental Research 1994; 73(8): 1462-9.

48. Eanes ED, Posner AS. Intermediate phases in the basic solution preparation of alkaline earth phosphates. Calcified Tissue Research 1968; 2(1): 38-48.

49. Eanes ED, Gillessen IH, Posner AS. Intermediate states in the precipitation of hydroxyapatite. Nature 1965: 208(8): 365-7.

50. Despotovic R, Filipovic-Vincekovic N, Furedi-Milhofer H. Precipitation of calcium phosphates from electrolyte solutions. III. Radiometric studies of the kinetics of precipitation and aging of calcium phosphates. Calcified Tissue Research 1975; 18(1): 13-26.

51. De Rooij JF, Heughebaert JC, Nancollas GH. A pH study of calcium phosphate seeded precipitation. Journal of Colloid and Interface Science 1984; 100(2): 350-8.

52. Koutsoukos P, Amjad, Z, Tomson, MB, Nancollas GH. Crystallization of calcium phosphates. A constant composition study. Journal of the American Chemical Society 1980; 102(5):1553-7.

53. Amjad Z, Koutsoukos P, Tomson, MB, Nancollas GH. The growth of hydroxyapatite from solution: A new constant composition method. Journal of Dental Research 1978; 57(9-10): 909.

54. Tomson MB, Nancollas GH. Mineralization kinetics: a constant composition approach. Science 1978; 200(4345):1059-60.

55. Nancollas G H, Tomazic B. Growth of calcium phosphate on hydroxyapatite crystals. Effect of supersaturation and ionic medium. Journal of Physical Chemistry 1974; 78(22): 2218-25.

56. Meyer JL, Nancollas GH. Effect of pH and temperature on the crystal growth of hydroxylapatite. Archives of Oral Biology 1972; 17(11):1623-7.

57. Nancollas G H, Amjad Z, Koutsoukos P. Calcium phosphates - speciation, solubility, and kinetic considerations. ACS Symposium Series 1979, 93: 475-97.

58. Tung MS. Calcium phosphates: structure, composition, solubility, and stability. Calcium Phosphates in Biological and Industrial Systems 1998, 1-19.

59. Eanes ED, Hailer AW. Calcium phosphate precipitation in aqueous suspensions of phosphatidylserine-containing anionic liposomes. Calcified Tissue International 1987; 40(1):43-8.

60. Eanes ED, Rattner SL. The effect of magnesium on apatite formation in seeded supersaturated solutions at pH 7.4. Journal of Dental Research 1981; 60(9):1719-23.

61. Eanes ED, Meyer JL. The influence of fluoride on apatite formation from unstable supersaturated solutions at pH 7.4. Journal of Dental Research 1978; 57(4): 617-24.

62. Meyer JL, Eanes ED. A thermodynamic analysis of the amorphous to crystalline calcium phosphate transformation. Calcified Tissue Research 1978; 25(1):59-68.

63. Wuthier RE, Rice GS, Wallace JE Jr, Weaver RL, LeGeros RZ, Eanes ED. In vitro precipitation of calcium phosphate under intracellular conditions: formation of brushite from an amorphous precursor in the absence of ATP. Calcified Tissue International 1985; 37(4): 401-10.

64. Barone JP, Nancollas GH. The seeded growth of calcium phosphates. The kinetics of growth of dicalcium phosphate dihydrate on enamel, dentin, and calculus. Journal of Dental Research 1978; 57(1):153-61.

65. Zieba A, Sethuraman G, Perez, F, Nancollas GH, Cameron D. Influence of Organic Phosphonates on Hydroxyapatite Crystal Growth Kinetics. Langmuir 1996; 12(11): 2853-2858.

66. Johnsson M, Perich JW, Reynolds EC, Nancollas GH. The hydroxyapatite binding domains of statherin: influence of size and charge. Journal of Colloid and Interface Science 1993; 160(1):179-82.

67. Johnsson M, Raj PA, Levine MJ, Nancollas GH. The influence of molecular structure on apatite adsorption. Materials Research Society Symposium Proceedings 1992; 252(Tissue-Inducing Biomaterials): 55-60.

68. Sharma VK, Johnsson M, Sallis JD, Nancollas GH. Influence of citrate and phosphocitrate on the crystallization of octacalcium phosphate. Langmuir 1992; 8(2): 676-9.

69. Liu ST, Hurwitz A, Nancollas GH. The influence of polyphosphate ions on the precipitation of calcium oxalate. Journal of Urology 1982; 127(2):351-5.

70. Wu W, Zhuang H, Nancollas GH. Heterogeneous nucleation of calcium phosphates on solid surfaces in aqueous solution. Journal of biomedical materials research 1997; 35(1): 93-9.

71. Wikiel K, Burke EM, Perich JW, Reynolds EC, Nancollas GH. Hydroxyapatite mineralization and demineralization in the presence of synthetic phosphorylated pentapeptides. Archives of Oral Biology 1994; 39(8):715-21.

72. Richardson CF, Johnsson M, Raj PA, Levine MJ, Nancollas GH. The influence of histatin-5 fragments on the mineralization of hydroxyapatite. Archives of Oral Biology 1993; 38(11): 997-1002.

73. Liu C, Huang Y, Shen W, Cui J. Kinetics of hydroxyapatite precipitation at pH 10 to 11. Biomaterials 2001; 22: 301-306.

74. Lazic S. Microcrystalline hydroxyapatite formation from alkaline solutions. Journal of Crystal Growth 1995; 147: 147-154.

75. Posner AS, Blumenthal NC, Boskey AL, and Betts F. Synthetic analogue of bone mineral formation. Journal of Dental Research 1975; B(54): B88-B93.

76. Boskey AL, and. Posner AS. Conversion of amorphous calcium phosphate to microcrystalline hydroxyapatite: A PH-dependent, solution-mediated, solid-solid conversion. Journal of physical Chemistry 1973; 77(19): 2313-2317.

77. Blumenthal NC, and Posner A. S. Hydroxyapatite: mechanism and properties. Calcified Tissue Research 1973; 13: 235-243.

78. Termine JD, and Eanes ED. Comparative chemistry of amorphous and apatitic calcium phosphate preparations. Calcified Tissue Research 1972; 10: 171-197.

79. Termine JD, Peckauskas RA, and Posner AS. Calcium phosphate formation in vitro. II effects of environment on amorphous-crystalline transformation. Archives of Biochemistry and Biophysics 1970; 140: 318-325.

80. Posner AS. The structure of bone apatite surfaces. Journal of Biomedical Materials Research 1985; 19 (3): 241-250.

81. Nakagawa S, Kaji F, Yamagami T, Sakurai M, Watanabe M. Pb^{2+} ion removal ability of hydroxyapatite. Phosphorus Research Bulletin 2002; 14:119-122.

82. Lusvardi G, Malavasi G, Menabue L, Saladini M. Removal of cadmium ion by means of synthetic hydroxyapatite. Waste Management 2002; 22(8): 853-857.

83. Reichert J, Binner JGP. An evaluation of hydroxyapatite-based filters for removal of heavy metal ions from aqueous solutions. Journal of Materials Science 1996; 31(5): 1231-41.

84. Mehta SR, Conrad D, Sandler R, Morgan J, Montagna R, Maizel AL. Purification of human B cell growth factor. Journal of Immunology 1985; 135(5): 3298-302.

85. Schroder E, Jonsson T, Poole L. Hydroxyapatite chromatography: altering the phosphate-dependent elution profile of protein as a function of pH. Analytical Biochemistry 2003; 313(1): 176-178.

86. Deppert WR, Lukacin, R. Hydroxyapatite chromatography. Journal of Chromatography Library 2000; 61(Protein Liquid Chromatography): 271-299.

87. Okazaki J, Embery G, Hall RC, Wassell DTH, Waddington RJ, Kamada A. Adsorption of glycosaminoglycans onto hydroxyapatite using chromatography. Biomaterials 1999; 20(4): 309-314.

88. Shibusawa Y, Mugiyama M, Matsumoto U, Ito Y. Complementary use of counter-current chromatography and hydroxyapatite chromatography for the separation of three main classes of lipoproteins from human serum. Journal of Chromatography, B: Biomedical Applications 1995; 664(2): 295-301.

89. Blumenthal NC, Betts F, and Posner AS. Effect of carbonate and biological macromolecules on formation and properties of hydroxyapatite. Calcified Tissue Research 1975;18: 81-90.

90. Boskey AL. Noncollagenous matrix proteins and their role in mineralization. Bone and Mineral 1989; 6(2): 111-23.

91. Addadi L, Weiner S. Interactions between acidic proteins and crystals: Stereochemical requirements in biomineralization. Proceedings of the National Academy of Sciences of the United States of America 1985; 82(12): 4110-14.

92. Binderman, I.; Greene, R. M.; Pennypacker, J. P. Calcification of differentiating skeletal mesenchyme in vitro. Science 1979; 206(4415):222-5.

93. Boskey AL, Wians FH, Hauschka PV. The effect of osteocalcin on in vitro lipid-induced hydroxyapatite formation and seeded hydroxyapatite growth. Calcified Tissue International 1985; 37(1): 57-62.

94. Boskey AL. Hydroxyapatite formation in a dynamic collagen gel system: effects of type I collagen, lipids, and proteoglycans. Journal of Physical Chemistry 1989; 93(4): 1628-33.

95. Chandrasekhar S, Laurie GW, Cannon FB, Martin GR, Kleinman HK. In vitro regulation of cartilage matrix assembly by a Mr 54,000 collagen-binding protein. Proceedings of the National Academy of Sciences of the United States of America 1986; 83(14): 5126-30.

96. Chen CC, Boskey AL. Mechanisms of proteoglycan inhibition of hydroxyapatite growth. Calcified Tissue Research 1985; 37(4): 395-400.

97. Cuervo LA, Pita JC, Howell DS. Inhibition of calcium phosphate mineral growth by proteoglycan aggregate fractions in a synthetic lymph. Calcified Tissue Research 1973; 13(1):1-10.

98. James J, Dove PM. Materials science: Shaping crystals with biomolecules. Science 2004; 306(5700):1301-1302.

99. Beniash E, Addadi L,Weiner S. Cellular control over spicule formation in sea urchin embryos: A structural approach. Journal of Structural Biology 1999; 125(1): 50-62.

100. Raggio CL, Boyan BD, Boskey AL. In vivo hydroxyapatite formation induced by lipids. Journal of Bone and Mineral Research 1986; 1(5):409-15.

101. Du C, Cui FZ, Ahang W, Feng QL, Zhu X D, De groot K. Formation of calcium phosphate/collagen composites through mineralization of collagen matrix. Journal of Biomedical Materials Research 2000; 50 (4): 518-527.

102. Williams G, Sallis D. Structural factors influencing the ability of compounds to inhibit hydroxyapatite formation. Calcifed Tissue International 1982; 34: 169-177.

103. Cafe MC, Rob JD. The absorption of polyelectrolytes on barium sulphate crystals. Journal of Colloid and Interface Science 1982; 86: 411-421.

104. Furedi-Milhofer H, Sarig S. Interactions between polyelectrolytes and sparingly soluble salts. Progress in Crystal Growth and Characterization 1996; 32: 45-74.

105. Berkovitch-Yellin ZJ, Van Mill J, Addadi L, Idelson M, Lahav M, Leiseowitz L. Crystal morphology engineering by "tailor-made" inhibitors; a new probe to fine intermolecular interactions. American Chemical Society 1985; 107: 3111-3122.

106. Nancollas GH, Budz JA. Analysis of particle size distribution of hydroxyapatite crystallites in the presence of synthetic and natural polymers. Journal of Dental Research 1990; 69: 1678-1685.

107. Brecevic LJ, Hadly V, Furedi-Milhofer H. Influence of gelatin on the precipitation of amorphous calcium phosphate. Colloids and Surfaces 1987; 28: 301-311.

108. Bernardi C. Chromatography of nucleic acids on hydroxyapatite. Nature 1965; 206: 779-783.

109. Termine DJ, Kleinman HK, Whitson SW, Conn KM, McGarvey ML, Martin GR. Osteonectin, a bone-specific protein linking mineral to collagen. Cell 1981; 26: 99-105.

110. Tung, MS, O'Farrell TJ. Effect of ethanol on the formation of calcium phosphates. Colloids and Surfaces, A: Physicochemical and Engineering Aspects 1996; 110(2): 191-198.

111. Lerner E, Azoury R, Sarig S. Rapid precipitation of apatite from ethanol solution. Journal of Crystal Growth 1989; 97 (3-4): 725-730.

112. Larsen MJ, Thorsen A. A comparison of some effects of fluoride on apatite formation in vitro and in vivo. Calcified Tissue International 1984; 36(6): 690-6.

113. Maxian SH, Zawadsky JP, Dunn MG. In vitro evaluation of amorphous calcium phosphate and poorly crystallized hydroxyapatite coatings on titanium implants. Journal of Biomedical Materials Research 1993; 27(1): 111-7.

114. Antonucci JM, Skrtic D, Eanes ED. Bioactive polymeric dental materials based on amorphous calcium phosphate. Polymer Preprints 1994; 35(2): 460-1.

115. Reynolds EC, Cai F, Shen P, Walker GD. Retention in plaque and remineralization of enamel lesions by various forms of calcium in a mouth-rinse or sugar-free chewing gum. Journal of Dental Research 2003; 82(3): 206-211.

116. Shen P, Cai F, Nowicki A, Vincent J, Reynolds EC. Remineralization of enamel subsurface lesions by sugar-free chewing gum containing casein phosphopeptide-amorphous calcium phosphate. Journal of Dental Research 2001; 80(12): 2066-70.

117. Boskey AL. Amorphous calcium phosphate: the contention of bone. Journal of Dental Research 1997; 76(8): 1433-6.

118. Ter Brugge PJ, Wolke JGC, Jansen JA. Effect of calcium phosphate crystallinity and implant surface roughness on differentiation of rat bone marrow cells. Journal of Biomedical Materials Research 2002; 60: 70-78.

119. Nagano M, Nakamura T, Kokubo T, Tanahashi M, and Ogawa M. Differences of bone bonding ability and degradation behavior in vivo between amorphous calcium phosphate and highly crystalline hydroxyapatite coating. Biomaterials 1996; 17: 1771-1777.

120. Simon CG Jr, Antonucci JM, Liu DW, Skrtic D. In vitro cytotoxicity of amorphous calcium phosphate composites. Journal of Bioactive and Compatible Polymers 2005; 20(3): 279-295.

121. Shen WJ, Chung KC, Wang GJ, McLaughlin RE. Mechanical failure of hydroxyapatite and polysulfone coated titanium rods in a weight-bearing canine model. Journal of Arthroplasty 1992; 7: 43-49.

122. Orlovskii VP, Komlev VS, Barinov SM. Hydroxyapatite and hydroxyapatite-based ceramics. Inorganic Materials 2002; 38(10): 973-984.

123. Suchanek W, Yoshimura M. Processing and properties of HA-based biomaterials for use as hard tissue replacement implants. Journal of Materials Research Society 1998; 13(1): 94-103.

124. Bonfield W, Grynaps MD, Tully AE, et al. Hydroxyapatite reinforced polyethylene-a mechanically compatible implant. Biomaterials 1981; 2(1): 137-156.

125. Di silvio L, Dalby M, and Bonfield W. In vitro response of osteoblasts to hydroxyapatite-reinforced polyethylene composites. Journal of Materials Science: Materials in Medicine 1998; 9(12): 845-848.

126. Wang M, Bonfield W, and Joseph R. Hydroxyapatite-reinforced polyethylene composites for bone substitution: effects of ceramic particle size. Biomaterials 1998; 18(24): 2357-2366.

127. Bakos D, Soldan M, and Hernandez-Fuentes I. Hydroxyapatite collagen-hyaluronic acid composite. Biomaterials 1999; 20(2): 191-195.

128. Knepper M, Moricca S, and Milthorpe BK. Stability of hydroxyapatite while processing short fibre reinforced hydroxyapatite ceramics. Biomaterials 1997; 18(23): 1523-1529.

129. Okuno M, and Shikinami Y. Bioresorbable devices made of forged composites of hydroxyapatite (HA) particles and poly-*L*-lactide (PLLA): Part I: basic characteristics. Biomaterials 1999; 19(9): 859-877.

130. Dalby MJ, Di Silvio L, Harper EJ, and Bonfield W. *In vitro* evaluation of new polymethylmethacrylate cement reinforced with hydroxyapatite. Journal of Materials Science: Materials in Medicine 1999; 10(12): 793-796.

131. Watson KE, Tenhuisen KS, and Brown PW. The formation of hydroxyapatite–calcium polyacrylate composites. Journal of Materials Science: Materials in Medicine 1999; 10(4): 205–213.

132. Asai S, Koumoto K, Matsushita Y, et al Advances in nature-guided materials processing. Science and Technology of Advanced Materials 2003; 4: 421-433.

133. Katti KS. Biomaterials in total joint replacement. Colloids and Surfaces B: Biointerfaces 2004; 39: 133-142.

134. Bartl MH, Boettcher SW, Frindell KL, Stucky GD. 3-D Molecular assembly of function in titania-based composite material systems. Accounts of Chemical Research 2005; 38(4): 263-271.

135. Judeinstein P, Sanchez C. Hybrid organic-inorganic materials: a land of multidisciplinary. Journal of Materials Chemistry 1996; 6(4): 511-25.

136. Sanchez C, Lebeau B. Hybrid organic-inorganic materials with second-order optical nonlinearities synthesized via sol-gel chemistry. Pure and Applied Optics 1996; 5(5): 689-699.

137. Forster S, Antonietti M. Amphiphilic block copolymers in structure-controlled nanomaterial hybrids. Advanced Materials 1998; 10(3):195-217.

138. Sanchez C, Lebeau B. Design and properties of hybrid organic-inorganic nanocomposites for photonics. Materials Research Society Bulletin 2001; 26(5): 377-387.

139. Pyun J, Matyjaszewski K. Synthesis of nanocomposite organic/inorganic hybrid materials using controlled/"living" radical polymerization. Chemistry of Materials 2001; 13(10): 3436-3448.

140. Mauritz KA, Mountz DA, Reuschle DA, Blackwell RI. Self-assembled organic/inorganic hybrids as membrane materials. Electrochimica Acta 2004; 50(2-3): 565-569.

141. Kokubo T, Kim H-M, Kawashita M. Novel bioactive materials with different mechanical properties. Biomaterials 2003; 24(13): 2161-75.

142. Kuang M, Wang D, Gao M, Hartmann J, Moehwald H. A bio-inspired route to fabricate submicrometer-sized particles with unusual shapes - mineralization of calcium carbonate within hydrogel spheres. Chemistry of Materials 2005; 17(3): 656-660.

143. Naka K, Chujo Y. Control of crystal nucleation and growth of calcium carbonate by synthetic substrates. Chemistry of Materials 2001; 13: 3245-3259.

144. Kato K, Eika Y, Ikada Y. In situ hydroxyapatite crystallization for the formation of hydroxyapatite/polymer composites. Journal of Materials Science 1997; 32: 5533-43.

145. Dujardin E, Mann S. Bioinspired materials chemistry. Advance Materials 2002; 14: 775-778.

146. Walton AG, Friedman BA, and Schwartz A. Nucleation and mineralization of organic matrices. Journal of Biomedical Materials Research 1967; 1: 337-354.

147. He G, Dahl T, Veis A, George A. Nucleation of apatite crystals in vitro by self-assembled dentin matrix protein 1. Nature Materials 2003; 2: 552-559.

148. Peytcheva A, Antonietti M. "Carving on the nanoscale": polymers for the site specific dissolution of calcium phosphate. Angewandte Chemie- International Edition 2001; 40: 3380.

149. Boskey AL. Phosphoproteins and biomineralization. Phosphorous, Sulfur, and Silicon 1999; 144-146: 189-192.

150. Gorski JP. Acidic phosphoproteins from bone matrix: a structural rationalization of their role in biomineralization. Calcified Tissue International 1992; 50: 391-396.

151. Cuisinier FJG. Bone mineralization. Current Opinions in Solid State and Materials Science 1996; 1: 436-439.

152. Zieba A, Sethurman G, Perez F, Nancollas GH, Cameron D. Influence of organic phosphonates on hydroxyapatite crystal growth kinetics. Langmuir 1996; 12: 2853-2858.

153. Couchourel D, Escoffier C, Rohanizadeh R, Bohic S, Daclusi G, Fortun Y, Padrines M. Effects of fibronectin on hydroxyapatite formation. Journal of Inorganic Biochemistry 1999; 73: 129-136.

154. Koutsopoulos S, Dalas E. The effect of acidic amino acids on hydroxyapatite crystallization. Journal of Crystal Growth 2000; 217: 410-415.

155. Zhang W, Huang Z-L, Liao S-S, and Cui F-Z. Nucleation sites of calcium phosphate crystals during collagen mineralization. Journal of American Ceramic Society 2003; 86(6):1052-1054.

156. Combes C, Rey C, Freche M. In vitro crystallization of octacalcium phosphate on type I collagen: influence of serum albumin. Journal of Materials Science: Materials in Medicine 1999; 10: 153-160.

157. Kikuchi M, Itoh S, Ichinose S, Shinomiya K, Tanaka J. Self-organization mechanism in a bone-like hydroxyapatite/collagen nanocomposite synthesized in vitro and its biological reaction in vivo. Biomaterials 2002; 22: 1705-1711.

158. Shinha A, Nayar S, Agrawal A. Synthesis of nanosized and microporous precipitated hydroxyapatite in synthetic polymers and biopolymers. Journal of American Ceramic Society 2003; 86 (2): 357-59.

159. Liou S-C, Chen S-Y, Liu DM. synthesis and characterization of needlelike apatitic nanocomposite with controlled aspect ratio. Biomaterials 2003; 24(22): 3981-3988.

160. Li Y, Weng W, Cheng K, Du P, Shen G, Wang J. Preparation of amorphous calcium phosphate in the presence of poly(ethylene glycol). Journal of Material Science Letters 2003; 22: 1015-1016.

161. Li H, Chen Y, and Xie Y. Photo-crosslinking polymerization to prepare polyanhydride/needle-like hydroxyapatite biodegradable nanocomposite for orthopedic application. Materials Letters 2003: 2848-2854.

162. Bunker BC, Rieke PC, Tarasevich BJ, Campbell AA, Fryxell GE, Graff GL, Song L, Liu J, Virden JW, McVay GL. Ceramic thin film formation on functionalized interfaces through biomimetic processing. Science 1994; 264 (5155): 48-55.

163. Cima IG, Vacanti C, et al. Tissue engineering by cell transplantation using degradable polymer substrates. Journal of Biomechanical Engineering; 1991; 113: 143.

164. Colton CK. Implantable biohybrid artificial organs. Cell Transplant 1995; 4: 415-436.

165. Sampath TK, Reddi AH. Importance of geometry of the extracellular matrix in endochondral bone differentiation. Journal of Cell Biology 1984; 98(6): 2192-7.

166. Kuboki Y, Saito T, Murata M, Takita H, Mizuno M, Inoue M, Nagai N, Poole AR. Two distinctive BMP-carriers induce zonal chondrogenesis and membranous ossification, respectively; geometrical factors of matrices for cell-differentiation. Connective Tissue Research 1995; 32(1-4): 219-26.

167. Kuboki Y, Takita H, Kobayashi D, Tsuruga E, Inoue M, Murata M, Nagai N, Dohi Y, Ohgushi H. BMP-induced osteogenesis on the surface of hydroxyapatite with geometrically feasible and nonfeasible structures: topology of osteogenesis. Journal of Biomedical Materials Research 1998; 39(2): 190-199.

168. Tsuruga E, Takita H, Itoh H, Wakisaka Y, Kuboki Y. Pore size of porous hydroxyapatite as the cell-substratum controls BMP-induced osteogenesis. Journal of Biochemistry 1997; 121(2): 317-24.

169. Bruder SP, Kraus KH, Goldberg VM, Kadiyala S. The effect of implants loaded with autologous mesenchymal stem cells on the healing of canine segmental bone defects. Journal of bone and joint surgery. American Volume 1998; 80(7): 985-96.

170. Patrick CW, Mikos AG, McIntire LV. Frontiers in tissue engineering. Elsevier Science, New York, 1998.

171. Mikos AG, Bao Y, Cima LG, Ingber DE, Vacanti JP, Langer R. Preparation of poly(glycolic acid) bonded fiber structures for cell attachment and transplantation. Journal of Biomedical Materials Research 1993; 27: 183-189.

172. Lo H, Kadiyala S, Guggino SE, et al. Poly(L-lactic acid) foams with cell seeding and controlled-release capacity. Journal of Biomedical Materials Research 1996; 30: 475-484.

173. Mikos AG, Thorsen AJ, Czerwonka LA, et al. Preparation and characterization of poly(L-lactic acid) foams. Polymer 1994; 35:1068-1077.

174. Mikos AG, Sarakinos; G, Vacanti JP, et al. Biocompatible polymer membranes and methods of preparation of three dimensional membrane structures. U.S. patent No. 5514378, 1996.

175. Thomson RC, Yaszemski MJ, Powers JM, et al. Fabrication of biodegradable polymer scaffolds to engineer trabecular bone. Journal of Biomaterial Science 1995; 7: 23-38.

176. Shastri VP, Martin I, and Langer R. Macroporous polymers foam by hydrocarbon templating. Proceedings of National Academy of Science USA 2000; 97: 1970-1975.

177. Shung A, Timmer MD, Jo S, Engel PS, Mikos A. Kinetics of [poly(propylene fumarate) synthesis by step polymerization of diethyl fumarate and propylene glycol using zinc chloride as a catalyst. Journal of Biomaterials Science Polymer Edition 2002; 13 (1): 95-108.

178. Bao Y, Senos AMR, Almeida M. Rheological behavior of aqueous suspensions of hydroxyapatite (HAP). Journal of Materials Science: Materials in Medicine 2002; 13: 639-643.

179. Pawlik M. Polymeric dispersants for coal-water slurries. Journal of Colloid and Interface Science 2005; 266: 82-90.

180. O'Brien RW, Cannon DW, Rowlands WN. Electroacoustic determination of particle-size and zeta-potential. Journal of Colloid and Interface Science 1995; 173(2): 406-418.

181. Kumar M, Dasarathy H, Riley C. Electrodeposition of brushite coatings and their transformation to hydroxyapatite in aqueous solutions. Journal of Biomedical Materials Research 1998; 45: 302-310.

182. Xie J, Riley C, Chittur K. Effect of albumin on brushite transformation to hydroxyapatite. Journal of Biomedical Materials Research 2001; 57(3): 357-365.

183. Nancollas GH. Phase transformation during precipitation of calcium salts. Life Sciences Research Report 1982; 23(Biol. Miner. Deminer.): 79-99.

184. Socrates G. Infrared characteristic group frequencies. John Wiley and Sons, Toronto, 1980.

185. Termine JD, Posner AS. Infrared analysis of rat bone: Age dependency of amorphous and crystalline mineral fractions. Science 1966; 153 (3743):1523-25.

186. Bienenstock A, Posner AS. Calculation of the X-ray intensities from arrays of small crystallites of hydroxyapatite. Archives of Biochemistry and biophysics 1968; 124: 604-615.

187. Blumenthal NC, Posner AS. Effect of conditions on the properties and transformation of amorphous calcium phosphate. Materials Research Bulletin 1972; 7: 1181-1190.

188. Eanes ED. Amorphous calcium phosphate: thermodynamic and kinetic considerations. Calcium Phosphates in Biological and Industrial Systems 1998; 21-39.

189. Shimabayashi S, Uno T. Crystal growth of calcium phosphates in the presence of polymeric inhibitors. Calcium Phosphates in Biological and Industrial Systems 1998: 193-215.

190. Nancollas GH, Koutsoukos PG. Calcium phosphate nucleation and growth in solution. Progress in Crystal Growth and Characterization 1980; 3(1): 77-102.

191. Shimabayashi S, Hashimoto N, Uno T. Effect of phosphorylated cellulose and bovine serum albumin on crystallization of hydroxyapatite. Phosphorus Research Bulletin 1993; 3: 7-12.

192. Amjad Z. The influence of polyphosphates, phosphonates, and poly(carboxylic acids) on the crystal growth of hydroxyapatite. Langmuir 1987; 3(6):1063-9.

193. Ofir PB-Y, Govrin-Lippman R, Garti N, Furedi-Milhofer H. The influence of polyelectrolytes on the formation and phase development of amorphous calcium phosphate. Crystal Growth and Design 2004; 4(1): 177-183.

194. Howie-Meyers CL, Yu K, Elliott D, Vasudevan T, Aronson MP, Ananthapadmanabhan KP, Somasundaran P. Crystal growth inhibition of hydroxyapatite by polycarboxylates: Role of calcium and polymer molecular weight. Mineral Scale Formation and Inhibition, [Proceedings of an American Chemical Society Symposium on Mineral Scale Formation and Inhibition], Washington, D. C., Aug. 21-26, 1994:169-182.

195. Bunker BC, Rieke PC, Tarasevich BJ, Campbell AA, Fryxell GE, Graff GL, Song L, Liu J, Virden JW, McVay GL. Ceramic thin film formation on functionalized interfaces through biomimetic processing. Science 1994; 264 (5155): 48-55.

196. Amjad Z, Hooley J. Influence of polyelectrolytes on the crystal growth of calcium sulfate dihydrate. Journal of Colloid and Interface Science 1986; 111(2): 496-503.

197. Klepetsanis PG, Kladi A, Koutsoukos PG, Amjad Z. The interaction of water-soluble polymers with solid substrates. Implications on the kinetics of crystal growth. Progress in Colloid & Polymer Science 2000; 115(Trends in Colloid and Interface Science XIV):106-111.

198. Ignjatovic N, Tomic S, Dakic M, Miljkovic M, Plavsic M, Uskokovic D. Synthesis and properties of hydroxyapatite/poly-L-lactide composite biomaterials. Biomaterials 1999; 20: 809-816.

199. Marra KG, Szem JW, Kumta PN, DiMilla PA, Weiss LE. *In vitro* analysis of biodegradable polymer blend/hydroxyapatite composites for bone tissue engineering. Journal of Biomedical Materials Research 1999; 47: 324-335.

200. Liu Q, de Wijn J, van Blitterswijk CA. Composite biomaterials with chemical bonding between hydroxyapatite filler particles and PEG/PBT copolymer matrix. Journal of Biomedical Materials Research 1998; 40: 490-497.

201. Ara M, Watanabe M, Imai Y. Effect of blending calcium compounds on hydrolytic degradation of poly(l-lactic acid-co-glycolic acid). Biomaterials 2002; 23(12): 2479-2483.

202. Ruhe PQ, Hedberg EL, Padron NT, Spauwen PHM, Jansen JA, Mikos AG. rhBMP-2 release from injectable poly(DL-lactic-co-glycolic acid)/calcium-phosphate cement composites. Journal of Bone and Joint Surgery. American Volume 2003; 85-A Suppl: 3 75-81.

203. Peter SJ, Miller ST, Zhu G, Yasko AW, Mikos AG. In vivo degradation of a poly(propylene fumarate)/β -tricalcium phosphate injectable composite scaffold. Journal of Biomedical Materials Research 1998; 41(1): 1-7.

Appendix I

EDX analysis of the calcium phosphate phase observed in the TEM study of the PPF-ACP composite: